Università degli Studi di Milano

Dipartimento di Biotecnologie Mediche e Medicina Traslazionale

Dottorato di Ricerca in Scienze Biochimiche – XXIX Ciclo

Cell Damage Induced by Lysosomal Impairment: Study of the Role of Plasma Membrane Sphingolipids

Supervisore: Prof. Sandro SONNINO

Tutor: Dr. Massimo AURELI

Coordinatore del Dottorato: Prof. Sandro SONNINO

Tesi di Dottorato di:

Maura SAMARANI

Matr. n. R10413

Anno Accademico 2015 - 2016

Table of contents

1. Abstract

Lysosomes are the principal site of the catabolism of sphingolipids, a class of bioactive lipids mainly associated with the external leaflet of cell plasma membrane. Several lines of evidence support a direct correlation between modifications in sphingolipid pattern and the activation of specific signaling pathways, including apoptosis and autophagy. Loss-of-function mutations in genes coding for lysosomal enzymes involved in sphingolipid catabolism result in severe clinical manifestations called sphingolipidoses. These pathologies belong to the group of Lysosomal Storage Diseases and are characterized by the accumulation of undegraded materials leading to lysosomal impairment and consequent cell damage. Until now, the molecular mechanisms by which the perturbation of lysosomal homeostasis affects cell functionality and viability are unknown.

To investigate this issue, I used an artificial *in vitro* model of lysosomal impairment obtained by loading human fibroblasts with 88 mM sucrose for 14 days. In these experimental conditions, the absence of invertase induces sucrose accumulation into lysosomes. I found that sucrose loaded fibroblasts are characterized by a growth slowdown and by the activation of both apoptosis and autophagy. By RNA-sequencing, approximately a thousand of genes were found to be dysregulated after sucrose loading. In particular, 56 cell cycle-related genes are downregulated, whereas 37 lysosomal-related genes are upregulated. Using biochemical approaches, I found that sucrose loading activates lysosomal biogenesis although sucrose storage inhibits lysosomal functionality. In particular, in sucrose loaded cells lipid catabolism is blocked and complex lipids, such as phospholipids, cholesterol, glycosphingolipids, and gangliosides are accumulated. Moreover, I found that sucrose loading induces the nuclear translocation of the Transcription Factor EB (TFEB), a master-gene regulator of lysosomal function, which in turn promotes the increased fusion between lysosomes and the plasma membrane. This last event leads to higher levels of sphingolipid hydrolases at the cell surface resulting in the alteration of the plasma membrane sphingolipid composition and the consequent ectopic production of pro-apoptotic and pro-autophagic ceramide. Interestingly, in sucrose loaded fibroblasts the blocking of glycosphingolipid hydrolysis at the plasma membrane results in a reduction of autophagy and apoptosis.

Similar results were also obtained in response to sphingomyelin accumulation in Niemann-Pick Type A disease (NPA). NPA is a sphingolipidosis caused by acid sphingomyelinase deficiency which leads to sphingomyelin storage. Interestingly, using NPA-derived human fibroblasts loaded with 50 µM exogenous sphingomyelin for 30 days, I found that the lysosomal impairment caused by sphingomyelin accumulation activates the same molecular pathways described in healthy fibroblasts subjected to sucrose loading.

A pathogenic role of TFEB has also been suggested by biochemical analysis on brains from Acid Sphingomyelinase Knockout (ASMKO) mice. In fact, ASMKO mouse brains are characterized by TFEB nuclear translocation, increased lysosomal biogenesis, increased glycohydrolytic activities and onset of apoptosis and autophagy.

Collectively, these data suggest the existence of a cross-talk among lysosomes and the cell plasma membrane. In this context, the lysosomal impairment caused by the accumulation of uncatabolized substrates leads to an altered composition of plasma membrane sphingolipids resulting in the ectopic production of ceramide which in turn is responsible for the onset of cell damage.

2. Introduction

2.1 Lysosomes

2.1.1 Structure

Lysosomes are acidic membrane-bound intracellular organelles described for the first time by Christian de Duve in the 1950s (Appelmans F et al., 1955; De Duve C et al., 1955). Subsequent electron microscopy studies showed that lysosomes appear as cytosolic dense bodies of heterogeneous size and morphology, and are mainly localized in the perinuclear region (Holtzman E, 1989). Lysosomal lumen contains several types of hydrolytic enzymes involved in the intracellular catabolism of different kinds of macromolecules such as: proteins, carbohydrates, lipids and nucleic acids (Saftig P and Klumperman J, 2009). Although for a long time lysosomes have been mainly considered the final destination of degradative pathways, it is now clear that they are also crucial regulators of cell homeostasis (Perera RM and Zoncu R, 2016).

2.1.1.1 Lysosomal membrane

Lysosomes are delimited by a single cholesterol-poor membrane (Schulze H et al., 2009) characterized by a thick glycocalyx due to the presence of highly glycosylated Lysosomal Membrane Proteins (LMPs) localized in the luminal side of the membrane (Schwake M et al., 2013). It is suggested that the glycocalyx could have a protective role against the catabolic action of the lysosomal acid hydrolases. The most abundant LMPs and markers of these organelles are the Lysosomal Associated Membrane Proteins LAMP-1 and LAMP-2 that are characterized by more than 10 glycosylation sites (Schwake M et al., 2013).

The lysosomal membrane is an active mediator of the fusion processes between lysosomes and other membranes, such as endosomes, autophagosomes and the plasma membrane through the action of specific proteins belonging to the family of RAB GTPases and SNAREs (Luzio JP et al., 2007). The lysosomal membrane mediates also the transport of metabolites, ions and soluble substrates from the cytosol into the lysosome and vice versa (Xiong J and Zhu MX, 2016). In particular, it contains the Vacuolar ATPase protons pumps responsible for the acidification of the lysosomal lumen (Mego JL, 1979; Nishi T and Forgac M, 2002). Acidic intra-lysosomal pH is required for proper function of the lysosomal degradative enzymes.

2.1.1.2 Lysosomal enzymes

Lysosomes contain about 60 different acid-hydrolases involved in the catabolism of specific substrates. They are mainly soluble except for those involved in the lipid catabolism which are principally associated with the lysosomal membrane. These enzymes are members of several protein families such as peptidases, glycosidases,

phosphatases, sulphatases, lipases, and nucleases. This variety reflects the capability of the lysosomes to degrade multiple kinds of macro-molecules, including nucleic acids, lipids, proteins, and glycosaminoglycans (Saftig P and Klumperman J, 2009).

Lysosomal enzymes are synthesized in the endoplasmic reticulum and then transported to the Golgi apparatus, where they are glycosylated and tagged with mannose-6-phosphate residues in the terminal position of the oligosaccharide chains (Braulke T and Bonifacino JS, 2009). The mannose-6-phosphate moiety is recognized by specific mannose-6-phosphate receptors (M6PRs) in the trans-Golgi network (Ghosh P et al., 2003). M6PR-enzyme complexes are transferred to lysosomes via the secretory pathway through clathrin-coated vesicles. In the pre-lysosomal compartment, the increased acidity induces the release of enzymes from M6PRs, which are recycled back to the Golgi apparatus. Interestingly, a different transport mechanism mediated by LIMP-2 (Lysosomal Integral Membrane Protein 2) has been recently identified for the lysosomal enzyme β-glucocerebrosidase, responsible for the hydrolysis of the simplest glycosphingolipid glucosyl-ceramide to glucose and ceramide (Reczek D et al., 2007).

2.1.2 Functions

2.1.2.1 Lysosome-mediated catabolism and recycling

Lysosomes play crucial roles in maintaining cell homeostasis (Figure 1). First, lysosomes are the main site of the degradation of intra- and extra-cellular macromolecules (Settembre C et al., 2013). This is possible thanks to the presence of about 60 resident hydrolases, each responsible for the digestion of a specific substrate. The end-products of the catabolic pathways leave the lysosomes and can then be recycled to the biosynthetic pathways (Schulze H et al., 2009).

The substances to be degraded reach the lysosomes by two main processes: endocytosis and autophagy. Endocytosis is the process involved in the internalization of extracellular material as well as in the plasma membrane turnover (Doherty GJ and McMahon HT, 2009). Endocytic pathways include clathrin-dependent and -independent endocytosis. Endosomes that are generated by endocytosis can be recycled back to the plasma membrane or targeted to the endo-lysosomal compartment. In the degradation pathway, endosomes undergo a maturation process characterized by multiple changes including exchange of membrane components, perinuclear localization, and decrease in luminal pH. After that, late endosome fuse with lysosomes and the acquisition of lysosomal components allows the degradation of extracellular material. On the other hand, catabolism of membrane lipids can occur via the formation of intraluminal vesicles. Interestingly, these vesicles are characterized by the presence of the phospholipid

bis(monoacylglycero)-phosphate, also known as lyso-bis-phosphatidic acid that facilitates the recognition between the lipids and their enzymes.

Intracellular material, such as damaged proteins or entire organelles can also be degraded by autophagy. In physiological conditions, autophagy maintains the normal cellular homeostasis mainly by regulating the bioenergetic balance (Kaur J and Debnath J, 2015). In addition, recent lines of evidence indicate that autophagy can also be involved in a novel form of programmed cell death by abnormal degradation of the intracellular compartments (Tsujimoto Y and Shimizu S, 2015).

In mammalian cells three different types of autophagy are described: chaperone-mediated autophagy, microautophagy and macroautophagy. In chaperone-mediated autophagy, proteins to be degraded show specific motifs that are recognized by a chaperone. Then, the chaperone-protein complexes are degraded in lysosomes. Microautophagy is characterized by direct lysosomal engulfment of the cytoplasmic cargo. Cytoplasmic material is catched inside lysosomes by membrane invagination. Macroautophagy, usually referred to autophagy, is the main autophagic pathway characterized by the formation of a double-membrane vesicle, called autophagosome, around the damaged organelle to be destroyed. Then, the fusion of the autophagosome with a lysosome allows the degradation of its content. An important marker of autophagy is the LC3-II protein, the lipidated (phosphatidylethanolamine) form of the cytosolic microtubule-associated protein light chain 3, which is then recruited to autophagosomal membranes (Tanida I et al., 2008).

2.1.2.2 Lysosomal exocytosis

Lysosomal exocytosis, a Ca^{2+}-regulated process (Reddy A et al., 2001), consists in the release of the lysosomal content in the extracellular environment. Lysosomes move from their perinuclear localization to the cell plasma membrane and then fuse with it (Luzio JP et al., 2007). As a direct consequence of lysosomal exocytosis, lysosomal enzymes are released in the extracellular milieu and the luminal region of LAMP-1 as well as the enzymes anchored to the lysosomal membrane appear at the extracellular leaflet of plasma membrane. Initially, exocytosis of secretory lysosomes was thought to be limited to specialized cell types such as hematopoietic cells and melanocytes. However, it is now known to also exist in all cell types, where it plays an important role in several processes such as immune responses, cell signalling and plasma membrane repair. The molecular mechanisms of lysosomal exocytosis, not fully understood until now, involve soluble N-ethylmaleimide-sensitive factor-attachment protein receptors (SNAREs), Ca^{2+} sensors and small Rab GTPase proteins (Rao SK et al., 2004).

2.1.2.3 Calcium storage

Lysosomes can also be considered calcium storage organelles; in fact, their calcium concentration is similar to that found associated with the calcium storage organelle belonging to the endoplasmic reticulum (Appelqvist H et al., 2013). Calcium is important to regulate different processes such as trafficking, recycling and fusion.

2.1.2.4 Cholesterol homeostasis

Cholesterol is an essential structural component of cellular membranes, and the majority of this lipid (80% of its total cellular amount) is found in the cell plasma membrane where it constitutes about 40% of the total lipids (Appelqvist H et al., 2013). Cholesterol is *de novo* synthesized in the endoplasmic reticulum although an important amount can also derive from Low-Density Lipoproteins (LDLs) via receptor-mediated endocytosis. In lysosomes, the action of acid lipase liberates free unesterified cholesterol from LDLs (Goldstein JL et al., 1975). Cholesterol is then transported outside the lysosomes to other cellular sites (such as Golgi apparatus, plasma membrane and endoplasmic reticulum) via two specific binding proteins, Niemann-Pick C1 (NPC1) and NPC2 (Subramanian K and Balch WE, 2008).

2.1.2.5 Lysosomal cell death

Lysosomal-mediated cell death occurs upon lysosomal membrane permeabilization followed by the release of hydrolytic enzymes into the cytosol (Boya P and Kroemer G, 2008). In particular, the enzymes active at neutral pH such as cathepsin B, D and L, are able to activate apoptotic effectors such as mitochondria proteins and/or caspases. The features of lysosomal-mediated cell death (necrotic, apoptotic or apoptosis-like) depend on the extent of the leakage and the cellular conditions.

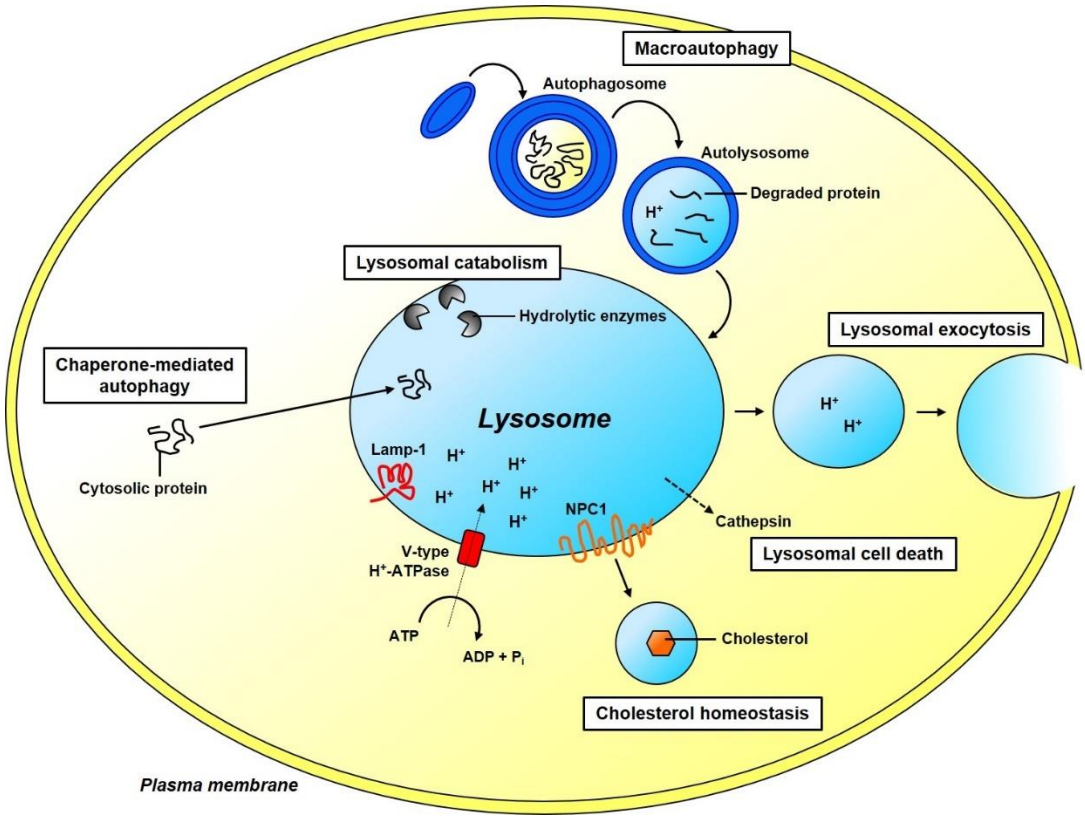

Figure 1 – Lysosomal functions. (adapted from *Saftig P and Klumperman J, Nat. Rev. Mol. Cell Biol., 2009*)

2.2 Transcription Factor EB

2.2.1 MiT family of transcription factors

The Transcription Factor EB (TFEB) belongs to the microphthalmia family of basic/helix-loop-helix/ leucine zipper (bHLH-Zip) transcription factors (MiT family) (Hemesath TJ et al., 1994; Kuiper RP et al., 2004). Four members of the MiT family have been identified: microphthalmia-associated transcription factor (MITF), TFEB, TFE3 and TFEC. All MiT proteins present an identical region responsible for DNA binding (Sardiello M et al., 2009), and highly similar HLH and Zip regions helpful for their dimerization. MiT transcription factors can form both homodimers and heterodimers with any other family member. All MiT members are highly conserved in vertebrates, although only a single MiT ortholog is found in lower organisms, known as Mitf in *Drosophila melanogaster* (Hallsson JH et al. 2004) and HLH-30 in *Caenorhabditis elegans* (Lapierre LR et al., 2013), respectively.

2.2.2 Regulation of TFEB activity

The activity of TFEB is strictly regulated by post-translational modifications, as well as protein-protein interactions and subcellular localization (Figure 2). The main regulation is due to the phosphorylation status of two serine residues, Ser142 and Ser211. The last one is the most important phosphorylation site being the docking site for the chaperone 14-3-3, responsible for the sequestration of TFEB in the cytosol preventing its nuclear translocation (Roczniak-Ferguson A et al., 2012). The main kinases responsible for TFEB phosphorylation are the mechanistic Target Of Rapamycin Complex 1 (mTORC1) (Martina JA et al., 2012) and the Extracellular signal-Regulated Kinase 2 (ERK2, also known as MAPK1) (Settembre C et al., 2011). Interestingly, mTORC1 is activated when associated with the external side of the lysosome membrane. In fact, through a mechanism involving the V-ATPase, in the presence of nutrients, the small Rag GTPases are active and recruit mTORC1 at the lysosomal membrane promoting its activation (Powis K and De Virgilio C, 2016). Moreover, Rag GTPases also bind to TFEB thus helping its recruitment to the lysosomal membrane and its phosphorylation by mTORC1. In case of nutrient starvation or lysosomal stress, for example due to the accumulation of uncatabolized materials, mTORC1 is released from the lysosomal membrane and becomes inactive. In addition, these events also induce calcium release from lysosomes through the Ca^{2+} channel mucolipin 1 (MCOLN1). The increase in cytosolic calcium concentration can activate the phosphatase calcineurin which in turn can dephosphorylate TFEB promoting its nuclear translocation (Medina DL et al., 2015).

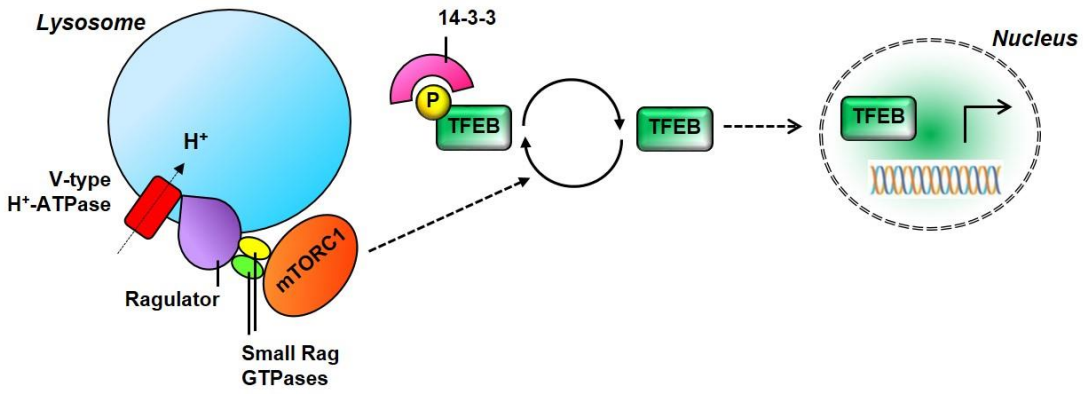

Figure 2 – TFEB regulation.

2.2.3 TFEB as a master regulator of lysosomal function and autophagy

TFEB has been demonstrated to directly bind DNA to a common 10-base E-box-like palindromic sequence called Coordinated Lysosomal Expression And Regulation (CLEAR) motif, which is found as one or more copies in the promoter of several lysosomal genes (namely CLEAR network) (Sardiello M et al., 2009). It has been shown that TFEB positively regulates the transcription of genes belonging to the lysosomal complement (hydrolases, transporters and accessory proteins) and genes contributing to lysosomal function and biogenesis, such as genes encoding subunits of the V-ATPase. In addition, it has been shown that TFEB also promotes the expression of other gene networks involved in autophagy and lysosomal exocytosis (Settembre C et al., 2011; Medina DL et al., 2011). By modulating these processes, TFEB coordinates a transcriptional program able to regulate the principal degradative pathways and to promote intracellular clearance (Settembre C et al., 2013). Notably, TFEB is not responsible for the basal transcription of its targets but it increases their expression in order to respond to cellular needs, like the lack of nutrients. Thus, TFEB represents the first example of a lysosome-to-nucleus signalling mechanism.

2.3 Sphingolipids

2.3.1 Structure and chemical-physical properties

Sphingolipids constitute a class of bioactive lipids which are crucial components of mammalian cells (van Meer G et al., 2008). They are particularly abundant in the cell plasma membrane where they reside asymmetrically mainly in the extracellular leaflet (Ikeda M et al., 2006). Sphingolipids are amphiphilic molecules composed by a hydrophilic portion protruding in the extracellular milieu and by a lipophilic chain inserted in the lipid core of the plasma membrane (Merrill AH Jr, 2011). The lipophilic moiety, called ceramide (Figure 3), is the structural unit common to all sphingolipids. Ceramide is formed by a long chain amino alcohol, 2-amino-1,3-dihydroxy-octadec-4-ene also known as sphingosine, which is linked to a long chain fatty acid through an amide bond. Despite the four possible configurations of sphingosine, only the 2S,3R is present in nature (Carter HE et al., 1947).

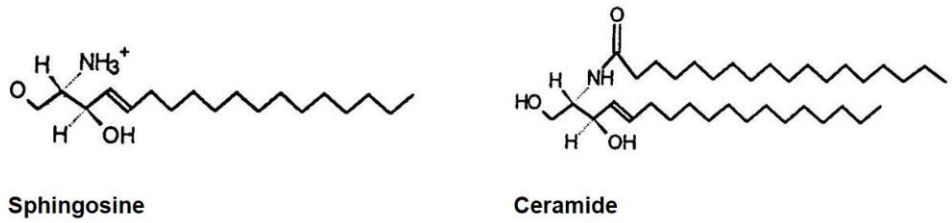

Figure 3 – Chemical structures of Sphingosine and Ceramide.

The presence of ceramide gives specific chemical and physical properties to all sphingolipids. In fact, the amide linkage, characterized by the simultaneous presence of a donor group and an acceptor group of hydrogen bonds (the hydrogen amide and carbonyl oxygen, respectively), allows the establishment of a rich network of hydrogen linkages among sphingolipid molecules at the plasma membrane level (Sonnino S et al., 2007). Notably, these hydrogen bonds stabilize the sphingolipid segregation forming the so-called *lipid rafts* or *sphingolipid-and-cholesterol enriched membrane domains* (Simons K and Ikonen E, 1997; Simons K and Sampaio JL, 2011). With the recruitment of specific proteins, lipid rafts form macromolecular complexes involved in several signalling pathways, such as signal transduction, cellular development and cell-to-cell and cell-to-matrix communication (Simons K and Toomre D, 2000).

2.3.1.1 Classification

The classification of the different classes of sphingolipids is based principally on the nature of the hydrophilic headgroup. In particular, two main groups can be distinguished: phosphosphingolipids and glycosphingolipids.

Phosphosphingolipids

Phosphosphingolipids are characterized by the presence of a phosphate group in the hydrophilic portion linked to ceramide. The phosphosphingolipids of mammals are ceramide-1-phosphate, ceramide phosphoethanolamine and sphingomyelin (Figure 4). The latter is obtained by the addition of a residue of phosphorylcholine and it is the most common sphingolipid in mammalian cells (Ramstedt B and Slotte JP, 2002).

Glycosphingolipids

Glycosphingolipids are divided in several subcategories: first by the carbohydrate attached in β-linkage to ceramide that can be glucose (glucosylceramide) or galactose (galctosylceramide); second by the nature of the additional substituents (for example, sulphated glycosphingolipids are classified as sulphatides) (Merrill AH Jr, 2011). The addition of galactose to glucosylceramide produces lactosylceramide, which is at a branchpoint for the formation of five different families called globo-, isoglobo-, lacto-, neolacto- and ganglio-series. In the latter family, prominent in mammal brains, the core structure Galβ1-3GalNAcβ1-4Galβ1-4GlcβCer can contains one or more residues of sialic acid. Sialic-acid-containing glycosphingolipids are commonly known as gangliosides and are particularly abundant on the cell surface of neuronal cells.

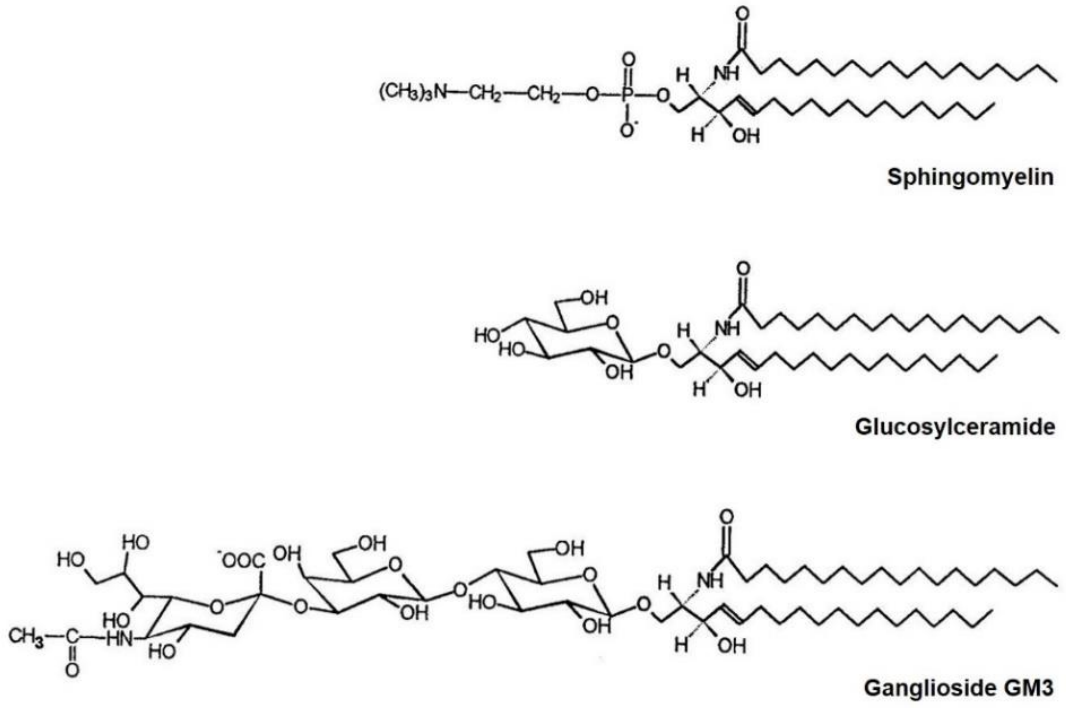

Figure 4 – Chemical structures of Sphingomyelin, Glucosylceramide, and the simplest ganglioside GM3.

2.3.2 Metabolism

2.3.2.1 Biosynthesis

Ceramide biosynthesis

The *de novo* biosynthesis of sphingolipids starts with the production of ceramide at the cytosolic leaflet of the endoplasmic reticulum (Figure 5). The first step of ceramide synthesis consists in the formation of 3-ketosphinganine by condensation of the amino acid L-serine with a fatty acyl-coenzyme A, typically palmitoyl-CoA. This initial reaction is catalysed by serine palmitoyltransferase (Weiss B and Stoffel W, 1997; Hanada K, 2003), then the 3-ketosphinganine obtained is rapidly reduced to produce sphinganine by 3-ketosphinganine reductase in a NADPH-dependent reaction (Stoffel W, 1970). Afterwards, sphinganine is acylated to dihydroceramide by a N-acyltransferase called ceramide synthase. Six different isoforms of ceramide synthase have been identified, each characterized by a selective specificity for the length of the acyl-CoA chain (Levy M and Futerman AH, 2010; Mullen TD et al., 2012). Notably, ceramide synthases can also directly recycle the sphingosine derived from ceramide catabolism. Dihydroceramide is then desaturated to ceramide thanks to the action of dihydroceramide desaturase (Michel C et al., 1997; Geeraert L et al., 1997).

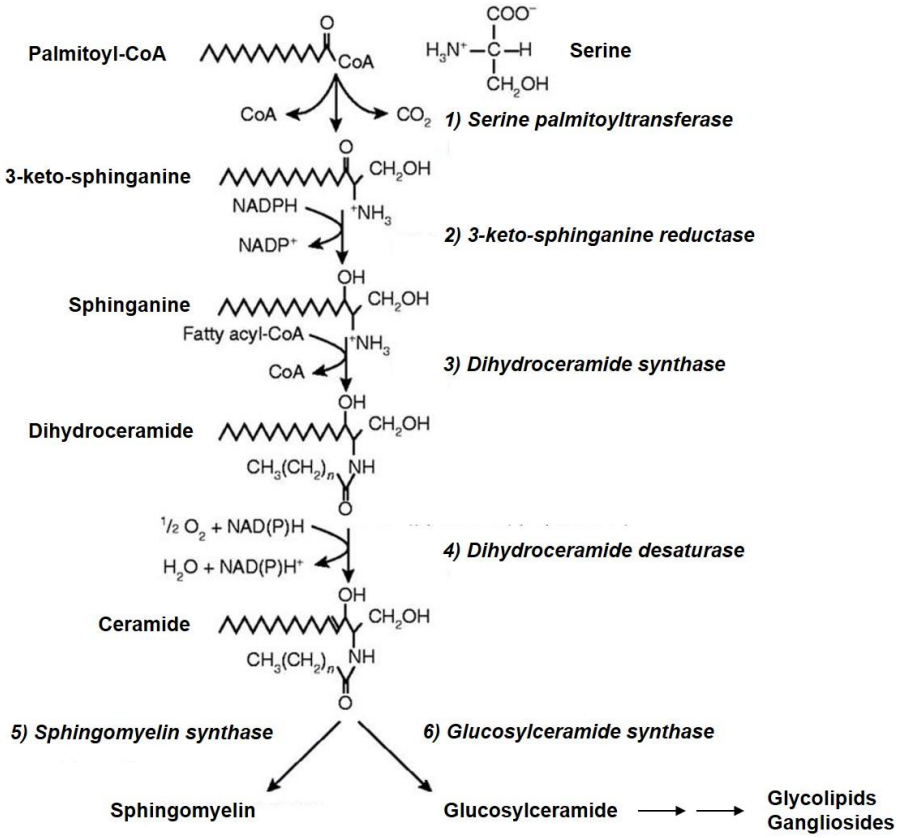

Figure 5 – *De novo* biosynthesis of sphingolipids.

Sphingolipid biosynthesis

The neo-synthesized ceramide can directly reach the plasma membrane or become the precursor for the biosynthesis of complex sphingolipids, such as sphingomyelin and glycosphingolipids. In both cases, ceramide can reach the Golgi apparatus by both a vesicular-dependent and -independent transport mechanisms (Perry RJ and Ridgway ND, 2005). Sphingomyelin synthesis occurs by the addition of a phosphorylcholine residue to the hydroxyl group in position 1 of the sphingoid base. To obtain glycosphingolipids, ceramide is subjected to the sequential addition of sugar residues by the action of specific membrane-bound glycosyltransferases, resulting in the formation of the oligosaccharide chains.

Glucosylceramide is the simplest glycosphingolipid synthesized at the cytosolic leaflet of the early Golgi apparatus by ceramide glucosyltransferase (Ichikawa S and Hirabayashi Y, 1998). Then glucosylceramide can reach the plasma membrane or be translocated to the luminal side of the Golgi apparatus, where it is further glycosylated by other glycosyltransferases to generate more complex glycosphingolipids (Lannert H et al., 1998). Neo-synthesized glycosphingolipids move through the Golgi apparatus to the plasma membrane following the exocytotic vesicular pathway.

The biosynthesis of gangliosides is catalysed by sialyl-transferases in the lumen of the Golgi apparatus starting from the common precursor lactosylceramide (Yu RK et al., 2011) (Figure 6). The gangliosides GM3, GD3 and GT3, are the precursors for the complex gangliosides series o-, a-, b-, and c-. In adult human tissues, gangliosides from the o- and c-series are found only in trace amounts.

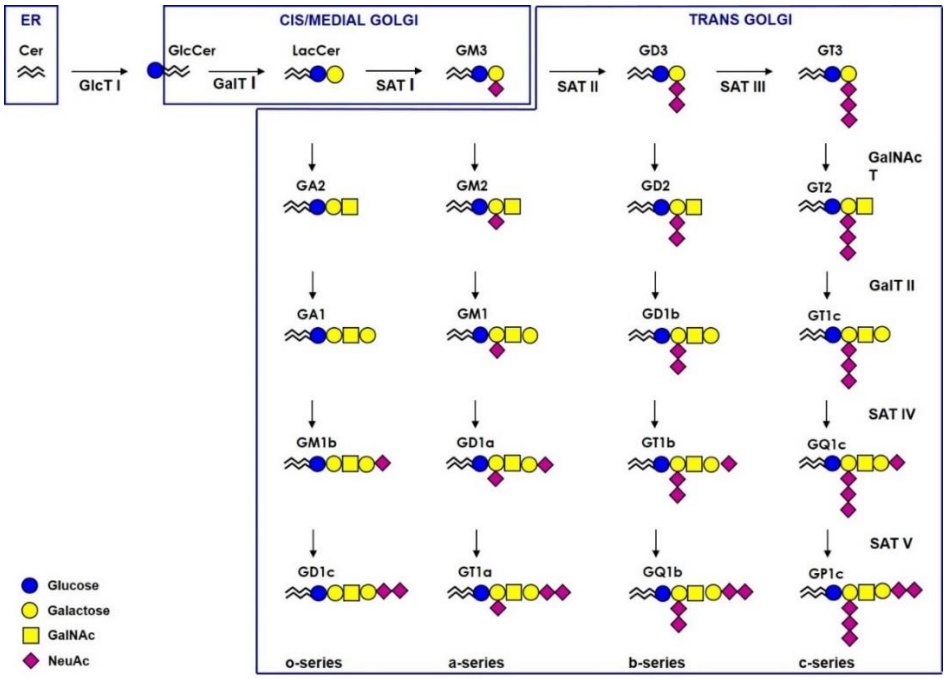

Figure 6 – Biosynthesis of ganglioside series.

2.3.2.2 Catabolism

The catabolism of sphingolipids occurs in lysosomes thanks to the presence of specific hydrolases. Cell plasma membrane sphingolipids reach the lysosomes through the endocytic pathway. In the case of glycosphingolipid catabolism, the lysosomal glycosidases sequentially remove the glycosidic residues from the non-reducing end of the oligosaccharide chains.

Besides the hydrolytic enzymes, for proper glycosphingolipid catabolism is also required the presence of the so-called Sphingolipid Activator Proteins (called also saposins) (Kishimoto Y et al., 1992). For example, in the degradation of ganglioside GM1 (Figure 7), β-galactosidase removes a galactose from GM1 to obtain GM2 thanks to the presence of the GM2-activator protein or saposin B. Ganglioside GM2 is hydrolyzed to ganglioside GM3 and N-acetylgalactosamine by the action of β-hexosaminidases in presence of the GM2-activator protein. The reaction responsible for GM3 degradation to lactosylceramide and sialic acid is mediated by saposin B and sialidases. Lactosylceramide is then cleaved into galactose and glucosylceramide by β-galactosidases and saposins B or C; glucosylceramide is converted to glucose and ceramide by the action of the β-glucosidase GBA1 in presence of saposin C (Sandhoff K and Harzer K, 2013). On the other hand, sphingomyelin is converted to ceramide and phosphoryl-choline by the action of acid sphingomyelinases (Marchesini N and Hannun YA, 2004). Finally, ceramide derived by both glycosphingolipid and sphingomyelin catabolic pathways, is hydrolysed by acid ceramidase and saposin D to sphingosine and fatty acid (Ferlinz K et al., 2001). Acid ceramidase can also hydrolyse the *N*-acyl linkage of several glycosphingolipids to produce the corresponding lyso-derivatives. Lysosphingolipids are typically accumulated in some sphingolipidoses, thus suggesting the involvement of these molecules in the pathogenesis of these lysosomal storage diseases (Spassieva S and Bieberich E, 2016). The end-products of the catabolic process, can leave the lysosomes and be recycled for the biosynthetic pathways (Kitatani K et al., 2008). In particular, sphingosine can be phosphorylated to sphingosine-1-phosphate (Maceyka M et al., 2012) or can be re-acylated to ceramide.

Notably, during the transport of glycosphingolipids from the cell plasma membrane to the lysosomes, some of them can reach different intracellular compartments (presumably the Golgi apparatus) where they can be used as intermediates of the biosynthetic flow (van Meer G and Lisman Q, 2002). It has been suggested that this process may be relevant at least for certain cell types, including neurons, representing an important mechanism for the regulation of the plasma membrane sphingolipid composition.

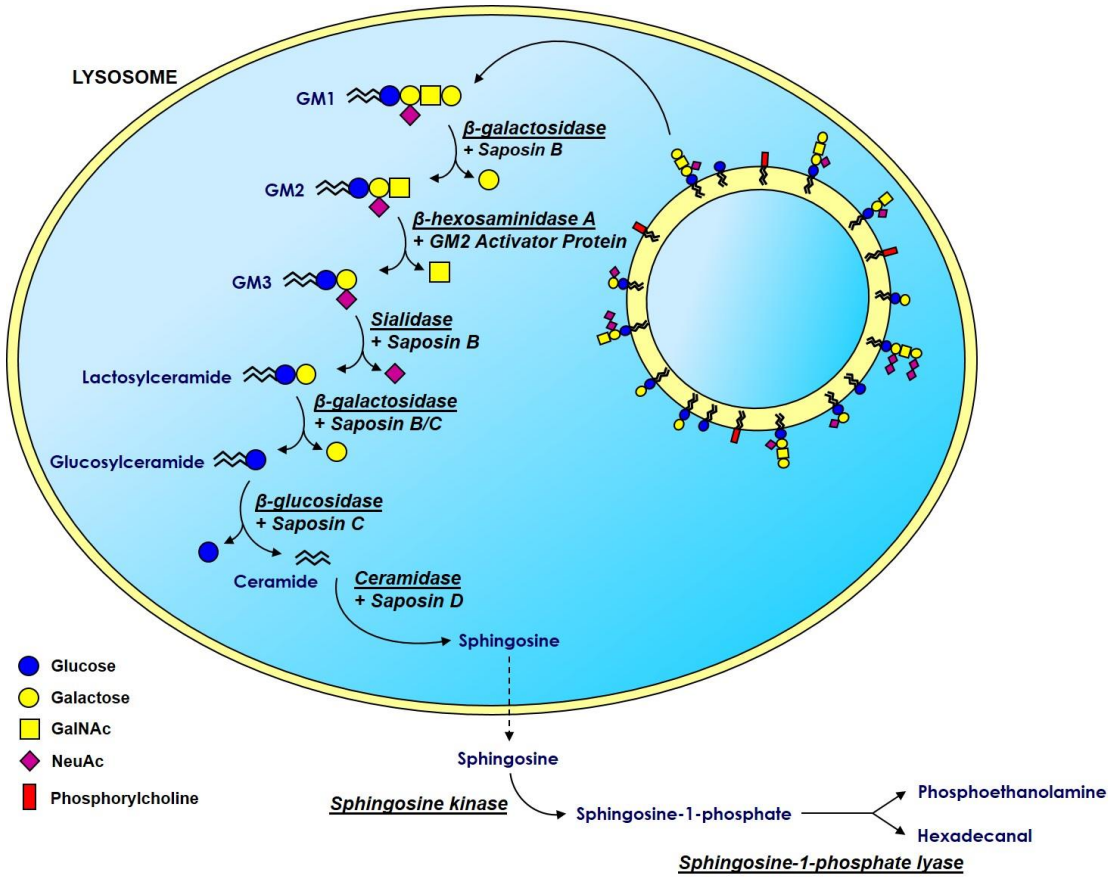

Figure 7 – Lysosomal catabolism of ganglioside GM1.

2.3.2.3 Metabolism at the plasma membrane level

Several enzymes involved in sphingolipid metabolism have been found associated with the external leaflet of the cell plasma membrane: sphingomyelinase, sphingomyelin synthase, sialidase, sialyl transferase, β-hexosaminidase, β-galactosaminyl transferase, β-galactosidase, β-glucosidase, ceramidase and sphingosine kinase (Sonnino S et al., 2010; Aureli M et al., 2011) (Figure 8). Furthermore, it has been demonstrated in live cells that these enzymes can directly work on their substrates at the cell surface. The presence of a series of couples of enzymes catalysing the synthesis and the catabolism of a specific sphingolipid at the plasma membrane level, let to hypothesize that the cell membrane sphingolipid composition can be modified directly at this site, without passing from the intracellular compartments. This fine tuning of sphingolipid membrane composition could rapidly modulate cell functions in response to specific stimuli.

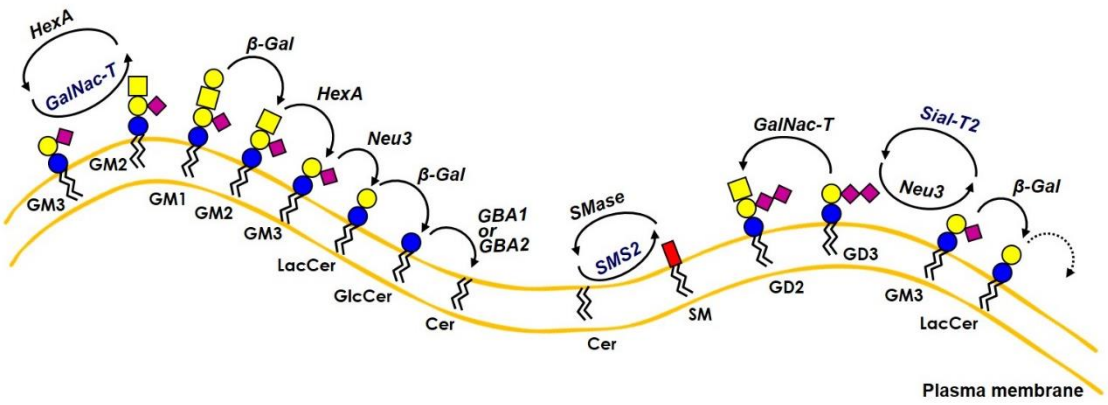

Figure 8 – Sphingolipid catabolism at the plasma membrane level.

Sphingomyelinase/Sphingomyelin synthase

Sphingomyelinases catalyse the hydrolysis of sphingomyelin to ceramide and phosphorylcholine. In eukaryotic cells, three sphingomyelinases have been described: secreted sphingomyelinase, that exerts its activity in the extracellular milieu; acid sphingomyelinase, mainly located in lysosomes but also associated with the cell plasma membrane; and neutral sphingomyelinases that are a family of different enzymes working at a neutral pH (Milhas D et al., 2010). On the other hand, sphingomyelin synthases convert ceramide and phosphatidylcholine in sphingomyelin and diacylglycerol. In mammalian cells, two isoforms have been found: sphingomyelin synthase 1, localized in the Golgi apparatus; and sphingomyelin synthase 2, which is present both in the Golgi and at the plasma membrane (Huitema K et al., 2004). The "sphingomyelin cycle" was the first biosynthetic/catabolic cycle proposed at the plasma membrane level, where probably acid sphingomyelinase and sphingomyelin synthase 2 play the most important role.

Sialidase/Sialyl transferase

Several sialidases located in different subcellular compartments are involved in the hydrolysis of sialic acid containing molecules (Monti E et al., 2010). Neu1 is the lysosomal enzyme; Neu2 is principally located in the cytosol; the two isoforms of Neu4, short and long, are associated with internal membranes and mitochondria, respectively, whereas Neu3 is associated with the plasma membrane. Neu3 can be considered a ubiquitous enzyme that hydrolyses the α2-3 external ketosidic bonds, resulting ineffective on the inner sialic acid residues. The increase of Neu3 activity leads to an important modification of the ganglioside membrane composition, which shifts from polysialylated species to monosialoderivatives, or produces lactosylceramide from ganglioside GM3. These modifications result in significant consequences on neuronal differentiation and apoptosis (Kakugawa Y et al., 2002; Valaperta R et al., 2006;

Valaperta R et al., 2007). Sialyl transferases catalyse the addition of sialic acid to a pre-existing oligosaccharide chain. These enzymes are not only present in the Golgi apparatus but they are also associated with the plasma membrane (Crespo PM et al., 2010).

β-hexosaminidase/β-hexosaminyl transferase

The β-hexosaminidase A found associated with the cell plasma membrane is the same enzyme located in lysosomes (Mencarelli S et al., 2005). It reaches the cell surface after a fusion process between lysosomes and the plasma membrane. Recently, a β-hexosaminyl transferase has also been identified at the cell surface, where it works on exogenous GM3 (Crespo PM et al., 2010). The coexistence at the plasma membrane of β-hexosaminidase and β-hexosaminyl transferase activities corroborates the hypothesis about the existence of a "glycolipid cycle" at the cell surface that could have important biophysical effects on the membrane structure or in events regarding signalling pathways starting at this level.

β-galactosidase

Until now, no data are available about the identity of protein/proteins showing β-galactosidase activity at the cell surface, nevertheless this enzymatic activity has been found in several cell lines (Valaperta R et al., 2007; Aureli M et al., 2011b). On the contrary, no evidence about a β-galactosyl transferase activity at the plasma membrane level is known so far.

β-glucosidase

Three different enzymes with β-glucosidase activity have been described: a β-glucocerebrosidase (GBA1) sensitive to the inhibition of Conduritol B Epoxide (CBE) normally described as a lysosomal enzyme but also found associated with the plasma membrane (Neufeld EF, 1991); a cytosolic β-glucosidase (GBA3) not studied deeply (Daniels LB et al., 1981); and a non-lysosomal β-glucosylceramidase (GBA2) that has been found associated with endosome vesicles and cell surface (Boot RG et al., 2007). GBA2 is insensitive to CBE and is specifically inhibited by N-(5-adamantane-1-yl-methoxy-pentyl)-deoxynojirimycin (AMP-DNM) (Overkleeft HS et al., 1998). Until now, no data are available on the existence of a β-glucosyl transferase activity at the plasma membrane level.

Ceramidase/Sphingosine kinase

Five different genes have been found encoding for: one acid ceramidase, one neutral ceramidase and three different alkaline ceramidases, respectively (Coant N et al., 2016). The neutral ceramidase has been described to play a role in the metabolism of ceramide directly at the cell surface. The sphingosine produced by ceramide catabolism at the

plasma membrane can be released in the extracellular milieu and undergoes different metabolic fates or could be inserted into the inner lipid layer becoming substrate for the sphingosine kinase enzyme which converts the sphingosine to the bioactive lipid sphingosine-1-phosphate (Tani M et al., 2007).

2.3.3 Sphingolipids as regulators of cellular functions

Plasma membrane sphingolipids and cholesterol can spontaneously segregate in the so-called lipid rafts. These membrane domains are characterized by a liquid-ordered phase resulting in a decreased membrane fluidity compared to the overall plasma membrane (Simons K and Sampaio JL, 2011). Numerous studies support the involvement of lipid rafts in signal transduction; in fact, it has been observed that a variety of proteins implicated in cell signalling are associated with the sphingolipid-enriched membrane domains. Several membrane-associated proteins show a strong preference for the association with lipid rafts, for example glycosylphosphatidylinisotol (GPI) anchored proteins or proteins which have a lipid modification (palmitoylation) (Sangiorgio V et al., 2004; Levental I et al., 2010). However, proteins can also be recruited into lipid rafts via interactions with other proteins located in these lipid domains. As mentioned above, it is hypothesized that the seizure of proteins in lipid rafts could influence their functions. Several mechanisms to explain the effect of the lipid environment on the protein functioning have been proposed: *i*) the segregation of proteins in a liquid-ordered phase domain could restrict their lateral motility, thus promoting more stable interactions with other proteins isolated in the same domain; on the contrary, the isolation of a protein into the lipid raft could avoid its interaction with other proteins outside the domain; *ii*) the rigidity characteristic of lipid domains could induce conformational changes in the polypeptide chain resulting in the impairment of protein's functionality; *iii*) lipid raft proteins are more susceptible to interaction with lipid components of the raft themselves. Regarding the last point, glycosphingolipids are good candidates for lateral lipid-protein interactions thanks to their oligosaccharide chain. In fact, the oligosaccharide chain of a glycosphingolipid inserted in the cell plasma membrane could interact with membrane proteins via: a) amino acids of the extracellular loops of the proteins (if the polypeptide chain conformation allows its proximity to the cell surface); b) sugars of glycosylated proteins (also in this case the dynamics of the protein oligosaccharide chain should allow the correct orientation towards the cell surface); c) the hydrophilic portion to the anchor for the GPI anchored proteins.

2.3.3.1 Ganglioside GM3 and Epidermal Growth Factor Receptor (EGFR)

The interaction between ganglioside GM3 and EGF receptor (EGFR) is an example of cellular signalling modulated by a membrane sphingolipid. Direct carbohydrate-

carbohydrate interaction, which takes place between GM3 and the N-acetylglucosamine termini of N-linked glycan of EGFR, has been proven responsible for the GM3 inhibitory action on EGFR (Bremer EG et al., 1986). GM3-EGFR interaction is facilitated by the enrichment of EGFR in lipid rafts where gangliosides as GM3 are also particularly enriched. In addition, other factors, together with GM3, can influence EGFR function. In fact, caveolin-1 protein also contributes to the modulation of EGFR signalling (Pike LJ, 2005). In a keratinocyte derived cell line, GM3 overexpression causes the shift of caveolin-1 in EGFR-enriched membrane regions allowing caveolin-1-EGFR interaction, which in turn results in the inhibition of EGFR tyrosine phosphorylation and the consequent receptor dimerization (Wang XQ et al., 2002).

2.3.3.2 Ganglioside GM3 and Insulin Receptor (IR)

Insulin receptors (IR) localize within caveolae-enriched membrane domains where the β-subunit of IR interacts with a scaffold domain of Caveolin-1 allowing the IR dimerization and function (Couet J et al., 1997). In case of an enrichment of GM3 at the plasma membrane, IR is sequestered by the interaction occurring between a lysine residue (Lys944) and the sialic acid of GM3. The loss of the interaction with Caveolin-1, induced by GM3, does not allow the activation of IR resulting in the onset of insulin resistance (Tagami S et al., 2002).

2.3.3.3 Ganglioside GM1 and Tropomyosin receptor kinase (Trk)

Gangliosides have a significant role in neuronal differentiation processes (Ledeen RW, 1984). Ganglioside GM1, a common ganglioside in neurons, has been described to participate in several pathways including neuronal growth, differentiation and survival (Ledeen RW and Wu G, 2015). Interestingly, in PC12 cells, a cell line derived from a pheochromocytoma of rat adrenal gland, the exogenous administration of GM1 stimulates Tropomyosin receptor kinase (Trk) activity, its dimerization and auto-phosphorylation (Farooqui T et al., 1997). Trk receptors have been found to be associated with lipid rafts suggesting that the receptor localization in these sphingolipid-enriched domains could be relevant for the regulation of their function (Guirland C et al., 2004; Suzuki S et al., 2004). The extracellular portion of Trk receptors is essential for GM1-dependent activation (Rabin SJ et al., 2002). In particular, Trk glycosylation is mandatory for the targeting of Trk into GM1-enriched domains and for the subsequent formation of GM1-Trk complexes (Mutoh T et al., 2000). This suggests that the glycosylation process could be a physiological important mechanism for the regulation of Trk trafficking and function. Thus, also in this case, carbohydrate-carbohydrate interaction (between the oligosaccharide chain of Trk and GM1) may play a regulatory role in the control of the receptor activity at the cell surface.

2.3.3.4 Ceramide as a pro-apoptotic signalling molecule

Several lines of evidence involve the ectopic production of ceramide in the induction of apoptosis (Morales A et al., Apoptosis, 2007). Notably, pro-apoptotic ceramide has been often associated with the hydrolysis of sphingomyelin by the action of sphingomyelinases. Nevertheless, emerging data suggest that also ceramide deriving by the hydrolysis of plasma membrane-glycosphingolipids could have an important pro-apoptotic role (Valaperta et al., The FASEB Journal, 2006; Aureli et al., Glicoconj J, 2012). The molecular mechanisms by which ceramide mediates its possible apoptotic effect are still unknown. However, several targets for ceramide-mediated apoptosis have been identified. For example, ceramide seems to be required for the activation of the Stress Activated Protein Kinase (SAPK)/c-Jun N-terminal Kinases (JNK) signalling pathway (Westwick JK et al., 1995; Verheij M et al., 1996). In addition to the induction of apoptosis, ceramide activation of SAPK pathways causes cell cycle arrest and inhibits cell proliferation (Bourbon NA et al., 2000). Another crucial target of ceramide is the cytosolic serine/threonine (class 2A) phosphoprotein phosphatase Ceramide-Activated Protein Phosphatase (CAPP) (Wolff RA et al., 1994), which induces the downregulation of c-myc resulting in anti-proliferative effects. So, the apoptotic effect of ceramide may be regulated by the activation of the cytotoxic SAPK cascade and, at the same time, by CAPP-mediated inhibition of the cytoprotective MAPK cascade.

Ceramide has been also described play a role in the activation of extrinsic apoptotic pathway mediated by the death receptors Tumor Necrosis Factor 1 (TNFR1) and CD95 (also known as FAS) (Schütze S et al., 2008). In particular, TNFR1 after binding its ligand (TNF) can activate the plasma membrane-associated neutral sphingomyelinase which in turn produce ceramide from the hydrolysis of sphingomyelin; the formed ceramide could then contribute to caspases activation. Moreover, activated-TNFR1 can also be subjected to a clathrin-dependent internalization and, thanks to the interactions with other proteins such as TRADD and FADD, it can activate acid sphingomyelinase within endosomes producing a pool of ceramide responsible for caspases or cathepsin D activation. Regarding CD95-mediated cell death, the first step is the formation of a few FAS-FAS ligand complexes that cause the recruitment of acid sphingomyelinase at the plasma membrane level which results in the increased production of ceramide at this site. The increased ceramide determines its clustering together with CD95 receptors, which in turn are internalized leading to the activation of apoptosis through the cleavage of procaspases.

2.4 Lysosomal Storage Diseases

2.4.1 Pathogenesis

Lysosomal Storage Diseases (LSDs) are a group of more than 50 inherited metabolic disorders characterized by the accumulation of uncatabolized materials within the lysosomes. Typically, LSDs are classified on the base of the accumulated substrate (Filocamo M and Morrone A, 2011). Each of these diseases are rare but considering all LSDs their prevalence in the population is relatively high, approximately 1:6.000 live births. LSDs are monogenic pathologies due to the defective function of a specific lysosomal enzyme (e.g. Gaucher disease is due to the deficiency of the β-glucocerebrosidase and characterized by the accumulation of glucosylceramide) and, in few cases, of non-enzymatic lysosomal proteins (e.g. GM2 gangliosidosis due to the deficit of the GM2 activator protein) or non-lysosomal proteins involved in lysosomal function (I-cell disease, due to mutations in mannose-6-phosphate receptor). Deficit in these proteins determines a lysosomal impairment with the intralysosomal accumulation of undegraded molecules (Platt FM et al., 2012). Interestingly, the primary accumulation is followed by the storage of secondary substrates with a mechanism unknown so far but independent from the genetic defect (Walkley SU, 2004). In addition, a common feature of LSDs is a reduction in the autophagic flux (the rate at which autophagosomes are processes by lysosomes) leading to a prominent dysregulation of the autophagic process (Platt FM et al., 2012). This is confirmed by the increase, in LSDs cells, of autophagic substrates and autophagosome-associated LC3-II. Despite these findings, to date the molecular mechanisms linking the lysosomal impairment to the onset of cellular damage is still unknown.

2.4.1.1 Clinical manifestations

LSDs clinical manifestations involve multiple organs and systems (Wang RY et al., 2011). The principal pathological phenotypes are represented by hepatosplenomegaly, corneal or lenticular opacities, retinal dystrophy, optic nerve atrophy, glaucoma, blindness, bone dysplasia, abnormalities of bone density and osteonecrosis (Parenti G et al., 2015). About two-thirds of patients affected by LSDs also show an important neurological deficiency, which is extremely variable and heterogenous ranging from progressive neurodegeneration and severe cognitive deficit to psychiatric and behavioural disorders (Parenti G et al., 2015). The onset of symptoms can occur before the birth, for the most severe phenotypes, or during the adulthood for the late-onset mild forms. Peculiar is the progress and the evolution of the disease over time. Severity and age of onset in LSDs depend by several factors including: residual enzyme activity, distribution of tissue-specific and cell-specific substrates, cell turnover rate, defective

protein expression, and other mechanisms that influence the life span of affected cells (Jakóbkiewicz-Banecka J et al., 2014). Notably, presence of residual activity can result in mild and late-onset forms.

2.4.1.2 Classifications

Classically, LSDs are classified based on the nature of the accumulated substrate: mucopolysaccharidoses (accumulation of mucopolysaccharides), sphingolipidoses (sphingolipids), oligosaccharidoses also known as glycoproteinoses (oligosaccharides) (Filocamo M and Morrone A, 2011). More recently LSDs have also been classified by the molecular defect, including more pathologies recognized now as LSDs: *i*) non-enzymatic lysosomal defects, *ii*) transmembrane protein defects (transporters and structural proteins), *iii*) lysosomal enzyme protection defects, *iv*) post-translational processing defects of lysosomal enzymes, *v*) trafficking defects in lysosomal enzymes and *vi*) polypeptide degradation defects (Table 1).

2.4.1.3 LSDs etiopathology

In general, LSDs share common features such as secondary storage of toxic metabolites, impaired lipid trafficking, perturbed signalling, enhanced inflammation, disturbed calcium homeostasis in endoplasmic reticulum, and stress and activation of the Unfolded Protein Response (UPR) (Vitner EB et al. 2010). All together these perturbations culminate in dysregulated autophagy and the onset of apoptosis and cell death through still unknown mechanisms. Several processes have been suggested to play a role in the onset of cell damage. For example, the activation of cell death signalling pathways has been speculated to contribute to cellular damage in Krabbe disease, characterized by the deficit of the enzyme galactosylceramidase resulting in the accumulation of its substrate galactosylceramide and of the lysosphingolipid galactosylsphingosine (also known as psychosine) (Giri S et al., 2006). The aberrant storage of these molecules can alter the activation of receptors or enzymes that are involved in signalling cascades. Also, the alteration of lipid content could play an important role in the pathobiology of LSDs because it can affect receptor responses and subsequent signalling events (Spector AA and Yorek MA, 1985).

Disease	*Defective protein*	*Main storage materials*
Mucopolysaccharidoses (MPS)		
MPS I (Hurler, Scheie, Hurler/Scheie)	α-Iduronidase	Dermatan sulphate, heparan sulphate
MPS II (Hunter)	Iduronate sulphatase	Dermatan sulphate, heparan sulphate
MPS III A (Sanfilippo A)	Heparan sulphamidase	Heparan sulphate
MPS III B (Sanfilippo B)	Acetyl α-glucosaminidase	Heparan sulphate
MPS III C (Sanfilippo C)	Acetyl CoA: α-glucosaminide N-acetyltransferase	Heparan sulphate
MPS III D (Sanfilippo D)	N-acetyl glucosamine-6-sulphatase	Heparan sulphate
MPS IV A (Morquio A)	Acetyl galactosamine-6-sulphatase	Keratan sulphate, chondroiotin 6-sulphate
MPS IV B (Morquio B)	β-Galactosidase	Keratan sulphate
MPS VI (Maroteaux-Lamy)	Arylsulphatase B	Dermatan sulphate
MPS VII (Sly)	β-Glucuronidase	Dermatan sulphate, heparan sulphate, chondroiotin 6-sulphate
MPS IX (Natowicz)	Hyaluronidase	Hyluronan
Sphingolipidoses		
Fabry	α-Galactosidase A	Globotriasylceramide
Farber	Acid ceramidase	Ceramide
Gangliosidosis GM1 (Types I, II, III)	GM1 β-galactosidase	GM1 ganglioside, Keratan sulphate, oligosaccharides, glycolipids
Gangliosidosis GM2 (Tay-Sachs)	β-Hexosaminidase A	GM2 ganglioside, oligosaccharides, glycolipids
Gangliosidosis GM2 (Sandhoff)	β-Hexosaminidase A + B	GM2 ganglioside, oligosaccharides, glycolipids
Gaucher (Types I, II, III)	Glucosylceramidase	Glucosylceramide
Krabbe	β-Galactosylceramidase	Galactosylceramide
Metachromatic leucodystrophy	Arylsulphatase A	Sulphatides
Niemann-Pick (Types A, B)	Sphingomyelinase	Sphingomyelin
Oligosaccharidoses (Glycoproteinoses)		
Aspartylglicosaminuria	Glycosylasparaginase	Aspartylglucosamine
Fucosidosis	α-Fucosidase	Glycoproteins, glycolipids, fucoside-rich oligosaccharides
α-Mannosidosis	α-Mannosidase	Mannose-rich oligosaccharides
β-Mannosidosis	β-Mannosidase	Man(β1→4)GlnNAc
Schindler	N-acetylgalactosaminidase	Sialylated/asialoglycopeptides, glycolipids
Sialidosis	Neuraminidase	Oligosaccharides, glycopeptides
Glycogenoses		
Glycogenosis II/ Pompe	Acid maltase	Glycogen
Lipidoses		
Wolman/CESD	Acid lipase	Cholesterol esters

Table 1 – Lysosomal Storage Diseases

Disease	*Defective protein*	*Main storage materials*
Non-enzymatic lysosomal protein defect		
Gangliosidosis GM2, activator defect	GM2 activator protein	GM2 ganglioside, oligosaccharides
Metachromatic leucodystrophy	Saposin B	Sulphatides
Krabbe	Saposin A	Galactosylceramide
Gaucher	Saposin C	Glucosylceramide
Transmembrane protein defect		
Transporters		
Sialic acid storage disease; infantile form (ISSD) and adult form (Salla)	Sialin	Sialic acid
Cystinosis	Cystinosin	Cystine
Niemann–Pick Type C1	Niemann–Pick type 1 (NPC1)	Cholesterol and sphingolipids
Niemann–Pick, Type C2	Niemann–Pick type 2 (NPC2)	Cholesterol and sphingolipids
Structural Proteins		
Danon	Lysosome-associated membrane protein 2	Cytoplasmatic debris and glycogen
Mucolipidosis IV	Mucolipin	Lipids
Lysosomal enzyme protection defect		
Galactosialidosis	Protective protein cathepsin A	Sialyloligosaccharides
Post-translational processing defect		
Multiple sulphatase deficiency	Multiple sulphatase	Sulphatides, glycolipids, GAGs
Trafficking defect in lysosomal enzymes		
Mucolipidosis IIα/β, IIIα/β	GlcNAc-1-P transferase	Oligosaccharides, GAGs, lipids
Mucolipidosis IIIγ	GlcNAc-1-P transferase	Oligosaccharides, GAGs, lipids
Polypeptide degradation defect		
Pycnodysostosis	Cathepsin K	Bone proteins
Neuronal ceroid lipofuscinoses (NCLs)		
NCL 1	Palmitoyl protein thioesterase	Saposins A and D
NCL 2	Tripeptidyl peptidase 1	Subunit c of ATP synthase
NCL 3	CLN3, lysosomal transmembrane protein	Subunit c of ATP synthase
NCL 5	CLN5, soluble lysosomal protein	Subunit c of ATP synthase
NCL 6	CLN6, transmembrane protein of ER	Subunit c of ATP synthase
NCL 7	CLC7, lysosomal chloride channel	Subunit c of ATP synthase
NCL 8	CLN8, transmembrane protein of ER	Subunit c of ATP synthase
NCL 10	Cathepsin D	Saposins A and D

Table 1 – Lysosomal Storage Diseases (continued)

2.4.2 Sphingolipidoses

Sphingolipidoses are the first LSDs to be described and are caused by defects in the degradation of sphingolipids, resulting in their accumulation within the lysosomes (Sandhoff K, 1974). All sphingolipidoses are inherited autosomal recessive disorders, except Fabry disease, an X-linked recessive LSD (Schiffmann R, 2015). Lysosomal accumulation of undegraded sphingolipids occurs mainly in cells characterized by high levels of sphingolipids. The amount of residual activity of the defective enzyme is one of the factors contributing to the pathogenesis and severity of the disease. In fact, according to the threshold theory first postulated by Conzelmann and Sandhoff (Conzelmann E and Sandhoff K, 1983-1984), a correlation between the level of the residual catabolic activity and the progression of the lipid storage disease has been confirmed in several clinical forms of sphingolipidoses such as GM2-gangliosidosis (Leinekugel P et al., 1992), metachromatic leukodystrophy (Tan MA et al., 2010), Gaucher disease (Gieselmann V, 2005) and Niemann-Pick type A and B diseases (Ferlinz K et al., 1995).

2.4.2.1 GM1-gangliosidosis

GM1-gangliosidosis is due to the deficit of the lysosomal enzyme GM1-β-galactosidase (Brunetti-Pierri N and Scaglia F, 2008). Together with GM2-activator protein or Saposin B, GM1-β-galactosidase hydrolyses the terminal β-galactose residue from ganglioside GM1 generating GM2. Three clinical forms can be distinguished: type I, the infantile and most severe form characterized by progressive impairment of the nervous system in the early infancy; type II, the late infantile/juvenile form showing progressive neurological symptoms in childrens; and type III, the adult/chronic form.

2.4.2.2 GM2-gangliosidoses

GM2-gangliosidoses are a group of three sphingolipidoses resulting from defects in degradation of ganglioside GM2 and related glycolipids (Kolter T and Sandhoff K, 1998). Three lysosomal β-hexosaminidases have been described which differ in the combination of their two subunits (α and β). β-hexosaminidase A (α+β) cleaves the terminal β-glycosidic bond between N-acetylglucosamine or N-acetylgalactosamine residues and the negatively charged and uncharged glycoconjugates. β-hexosaminidase B (β+β) cleaves the terminal N-acetylhexosamine residues from uncharged substrates such as oligosaccharides. β-hexosaminidase S (α+α) participates in the degradation of glycosaminoglycans and sulphated glycolipids.

The B-variant of GM2-gangliosidosis (Tay-Sachs disease is the infantile form) is characterized by α-chain deficiency resulting in the deficit of hexosaminidase A and S, but the activity of hexosaminidase B is normal. The 0-variant (Sandhoff disease)

presents the deficiency of both hexosaminidase A and B. The AB-variant shows normal β-hexosaminidase A, B and S activities but the deficit of GM2 activator protein.

2.4.2.3 Fabry disease

Fabry disease is caused by α-galactosidase A deficiency resulting in the accumulation of several neutral glycolipids, expecially globotriaosylceramide (Schiffmann R, 2015). Since Fabry disease has an X-linked inheritance mode, the most severe forms affect hemizygous males. The pathology is characterized by a progressive course and premature death because of renal failure, stroke and cardiac disease; these organs are also the main sites of globotriaosylceramide accumulation.

2.4.2.4 Gaucher disease

Gaucher disease is caused by mutations in the gene coding for the lysosomal enzyme β-glucocerebrosidase leading to the accumulation of its substrate glucosylceramide (Nagral A, 2014). Gaucher disease type I, the non-neuronopathic form, is the most common sphingolipidosis with a frequency of 1:50.000-200.000 live births, that is higher in the Ashkenazi Jewish population (1:1.000). Thanks to the Enzyme Replace Therapy the life expectancy of these patients is up to 80 years. The neuronopathic forms are the type II, the most severe one characterized by the involvement of the central nervous system with an early onset and a life expectancy of less than two years, and the type III, an intermediate variant of the other two types.

2.4.2.5 Krabbe disease

Krabbe disease is also known as globoid cell leukodystrophy and it is caused by the deficiency of β-galactocerebrosidase (Bongarzone ER et al., 2016). This enzyme is responsible for the hydrolysis of galactosylceramide and lactosylceramide. Since galactosylceramide is mainly localized in oligodendrocytes, its accumulation together with the formation of the lyso-derivative galactosphingosine induce a progressive de-myelinisation in the affected patients.

2.4.2.6 Metachromatic leukodystrophy

Metachromatic leukodystrophy is caused by the deficiency of arylsulphatase A enzyme, resulting in the accumulation of sulfatides mainly present in myelin sheaths in the white matter of the brain and in the peripheral nervous system (van Rappard DF et al. 2015). This pathology can be classified in three forms: late infantile, juvenile and adult, correlating with increasing residual activity.

2.4.2.7 Farber disease

Farber disease is characterized by the deficit of lysosomal acid ceramidase that catalyses the degradation of ceramide into sphingosine and a fatty acid resulting in

ceramide accumulation (Ehlert K et al., 2007). This disease shows a broad spectrum of clinical signs ranging from the classical articular and laryngeal symptoms to the respiratory and neurological involvement in the most severe phenotypes.

2.4.2.8 Niemann-Pick diseases

Niemann-Pick diseases include three sphingolipidoses: Type A, B and C. The first two types, A and B, are caused by mutations in the sphingomyelin phosphodiesterase 1 gene (SMPD1) coding for the lysosomal enzyme acid sphingomyelinase (Schuchman EH and Wasserstein MP, 2016). Acid sphingomyelinase is responsible for catalysing the breakdown of sphingomyelin to ceramide and phosphorylcholine and its deficiency leads to the accumulation of the undegraded substrate sphingomyelin. The Niemann-Pick Type A is the most severe form characterized by a rapid progressive neurodegenerative course; it is a fatal disorder of infancy caused by an almost complete deficiency of acid sphingomyelinase. In contrast, Type B is the late-onset form characterized by a higher residual catabolic activity with little or no involvement of nervous system but severe and progressive visceral organ abnormalities. Type C disease presents similar clinical manifestations but is caused by impaired cholesterol transport (Vanier MT, 2010).

The first patient with Niemann-Pick disease Type A (NPA) was described in 1914 by the German paediatrician Albert Niemann. A few years later, in the 1930s, the primary lipid accumulating in these patients was identified as sphingomyelin (Crocker AC, 1961). Now, it is known that NPA, like others LSDs, is characterized by secondary accumulation of lipids, including cholesterol, glucosylceramide, lactosylceramide and gangliosides, especially ganglioside GM2 (Walkley SU and Vanier MT, 2009). Cells accumulating sphingomyelin, and other undegraded molecules, are present in several organs of NPA affected patients such as liver, spleen, lymph nodes, lung, bone marrow and brain. Sphingomyelin storage is also observed in multiple types of skin cells including dermal fibroblasts, macrophages and vascular endothelial cells (Schuchman EH and Wasserstein MP, 2015).

Sphingomyelin is a major component of cell membranes and normally the function of acid sphingomyelinase is essential to maintain sphingolipid homeostasis. In NPA cells, the storage of sphingomyelin and other lipids, and the consequent impaired sphingolipid metabolism, could lead to the alteration of the plasma membrane lipid composition, which in turn could affect several signalling pathways.

An important model for the study of NPA pathogenesis is represented by the Acid Sphingomyelinase Knock-Out (ASMKO) mice, developed in the mid-1990s (Horinouchi K et al. 1995). The ASMKO mice show progressive lipid storage, particularly in

reticuloendothelial organs as well as in the brain. The ASMKO mice present neurological symptoms starting from two months after birth and die within 6-8 months.

3. Aim

Lysosomal Storage Diseases (LSDs) are rare inherited metabolic disorders caused by defects in lysosomal proteins leading to the accumulation of undegraded materials into lysosomes and the consequent lysosomal impairment and onset of cell damage. Until now, the molecular mechanisms linking lysosomal dysfunction with the onset of cell injury are unknown.

Lysosomes are the principal site of the catabolism of sphingolipids, a class of bioactive lipids mainly associated with the external leaflet of cell plasma membranes (PM). Interestingly, in LSDs, when the primary storage reaches high levels, also other lysosomal catabolic enzymes which are not genetically deficient may be inhibited leading to secondary substrate accumulations, including sphingolipids. For example, Niemann-Pick Type A disease (NPA), a neurodegenerative sphingolipidosis caused by deficit of the lysosomal enzyme acid sphingomyelinase resulting in primary sphingomyelin storage, is characterized by secondary accumulations of both gangliosides GM2 and GM3. Several lines of evidence support a direct correlation between modifications in sphingolipid pattern and content and the activation of specific signalling pathways, including apoptosis and autophagy. Alteration of cell PM sphingolipid composition could also occur *in situ* by the action of PM-associated sphingolipid-hydrolases. Several lines of evidence indicate that the ectopic production of ceramide from sphingolipid catabolism can promote signalling death pathways, such as autophagy and apoptosis.

The cellular response to such accumulation is to promote the nuclear translocation of Transcription Factor EB (TFEB) which in turn causes: i) an enhanced expression of lysosomal genes; ii) the increase of lysosomal biogenesis; iii) autophagy and iv) fusion between lysosomes and PM (lysosomal exocytosis). These processes can be potentially involved in changes of sphingolipid PM composition resulting in the production of pro-apoptotic ceramide.

Based on these findings, my PhD Thesis was aimed to verify the hypothesis of the existence of a positive loop occurring in LSDs cells which could explain the onset of cell damage. The loop is triggered by the aberrant lysosomal storage of uncatabolized molecules. The massive accumulation of the undegraded substrates into lysosomes causes a general impairment of lysosomal catabolism leading to abnormal storage of other uncatabolized molecules, including complex sphingolipids. This lysosomal impairment causes TFEB nuclear translocation and, therefore, an increased lysosomal biogenesis as well as an enhanced fusion between lysosomes and PM. This last event is related to two different subsequent effects: alteration of PM sphingolipid composition, with the enrichment of sphingolipids undegraded into lysosomes, and increase of sphingolipid-hydrolases at the cell surface. In this way, the coexistence at the PM level of sphingolipid substrates and the enzymatic cascade, composed by β-hexosaminidase,

sialidase, β-galactosidases and β-glucosidases, could result in the ectopic production of ceramide which in turn leads to apoptosis and autophagy.

4. Materials and Methods

4.1 Cell cultures

Healthy and pathological human fibroblasts were obtained by skin biopsy. Niemann-Pick Type A disease (NPA) fibroblasts (code number FFF0841985) were derived from the "*Cell line and DNA Biobank from patients affected by Genetic Diseases*" of the Istituto G. Gaslini (Genova, Italy). According to ethical and legal recommendations, the samples have been taken for analysis and biobanking after written donor informed consent, approved by the local Ethics Committee.

Fibroblasts were cultured and propagated in RPMI-1640 medium which was supplemented with 10% FBS, 2 mM L-glutamine, 100 U/ml penicillin and 100 µg/ml streptomycin. The cells were cultured as monolayer in a humidified atmosphere at 37°C, 5% CO_2.

4.1.1 Sucrose loading

Healthy fibroblasts were cultured for 14 days in complete growth medium supplemented with 88 mM sucrose (Sigma-Aldrich). The proper amount of sucrose was solubilized in RPMI-1640 medium, the solution was then filtered and supplemented with serum, glutamine and antibiotics. In parallel, control healthy fibroblasts were cultured with the same culture medium without sucrose. Fibroblasts were plated in T75 flasks at a density of 3,000 cells/cm^2. Sucrose loading was started the day after plating and culture media were changed after 7 days from plating.

4.1.2 Sphingomyelin loading

NPA fibroblasts were cultured for 30 days in complete growth medium supplemented with 50 µM sphingomyelin (SM) (Avanti Polar Lipids). SM was solubilized according to the following experimental conditions for the preparation of 100 ml culture medium (Levade T et al., 1995). An aliquot corresponding to 5 µmoles of SM was taken from a solution of 25 mg/ml SM solubilized in chloroform/methanol 2:1 (v/v), transferred in a sterile tube and dried under nitrogen flow. 10 ml of heat-inactivated FBS supplemented with antibiotics were added to SM. The mixture consisting of SM-FBS-antibiotics was stirred, sonicated using an ultrasonic bath for three times (1 minute per time) and incubated at 37°C overnight. The day after, the mixture was added to the culture medium containing glutamine. In parallel, control NPA fibroblasts were cultured with the same culture medium without SM. NPA fibroblasts control and loaded with SM were plated in T75 flasks at a density of 3,000 cells/cm^2. SM loading was started the day after plating and culture media were changed every 7 days from plating.

4.2 Evaluation of cell proliferation

Healthy fibroblasts were plated in T25 flasks at a density of 3,000 cells/cm^2 and sucrose loading was started the day after plating. After 1, 2, 3, 7, 10 and 14 days of sucrose loading both control and loaded cells were detached with Trypsin-EDTA solution. An aliquot of cell suspension was used to evaluate the cell number by Trypan blue exclusion assay and counted using a Bürker chamber. Data are expressed as number of live cells for cm^2 of growth area.

4.3 Cell treatment with Bafilomycin A1

Healthy fibroblasts loaded or not with 88 mM sucrose for 7 days were plated in T25 flasks at a density of 10,000 cells/cm^2 and sucrose loading was maintained for other 7 days. At the end of 14 days of loading, both control and loaded cells were treated with Bafilomycin A1 (Sigma-Aldrich) at the final concentration of 100 nM for 6 hours at 37°C, 5% CO_2. As control, cells loaded or not with sucrose were cultured in the same support at the same concentration and were treated with only the vehicle (ethanol). At the end of incubation, cells were harvested and processed for immunoblot analysis.

4.4 Cell treatment with Conduritol B epoxide (CBE) and AMP-DNM

Healthy fibroblasts loaded or not with 88 mM sucrose for 7 days were plated in T25 flasks at a density of 10,000 cells/cm^2 and sucrose loading was maintained for other 7 days. At 12 days of loading, loaded cells were treated with 500 µM CBE (Calbiochem), inhibitor of β-glucocerebrosidase GBA1, and 20 nM AMP-DNM (kindly given by Professor JMFG Aerts, Leiden University, Netherlands), inhibitor of the non-lysosomal β-glucosylceramidase GBA2, directly diluted in culture medium for 48 hours at 37°C, 5% CO_2. In parallel, as control, other sucrose loaded cells were maintained in culture without the inhibitors of β-glucosidases. At the end of incubation, cells were harvested and processed for immunoblot analysis.

4.5 Transient transfection of TFEB-GFP lentiviral vector in fibroblasts

4.5.1 Lentiviral vector packaging

Lentiviral vector packaging was performed using Lenti-vpak Lentiviral Packaging Kit (OriGene). Briefly, 2.5 x 10^6 HEK-293 cells (DMEM High Glucose, 10% heat-inactivated FBS, 2 mM L-glutamine, 100 U/ml penicillin and 100 µg/ml streptomycin) were plated in

a Petri dish 100mm (day 1). The day after (day 2), 5 µg of pLenti-ORF clone of TFEB-GFP (RC230141L2, OriGene) and 6 µg of packaging plasmids were mixed with 500 µl of Opti-MEM (tube 1). In a different tube (tube 2), 44 µl of MegaTran transfection reagent were mixed with 500 µl of Opti-MEM. Then, DNA solution was transferred from tube 1 to tube 2 and the mixture was incubated for 30 minutes at room temperature (RT). At the end of incubation, the mixture was added directly to the HEK-293 cells medium without antibiotics. After overnight incubation (day 3), the culture medium was changed. At day 4, the culture medium was harvested and centrifuged at 450 x g for 5 minutes at RT. The viral supernatant was filtered through a 0.45 µm filter to remove cellular debris and stored in aliquots at -80°C.

4.5.2 Transient transfection

Healthy fibroblasts were plated in 6-well plates on a coverslip of 24 mm of diameter at a density of 5,000 cells/cm^2. The day after, cells were infected with 300 µl of viral supernatant containing lentiviral vector coding for TFEB-GFP. After 72 hours from the infection, cell medium was changed and 88 mM sucrose loading was started. At different times of sucrose loading (12, 48, 96 hours and 14 days), cells were washed three times with PBS and fixed in 4% paraformaldehyde for 20 minutes at RT. Coverslip was mounted on a glass slide with Dako fluorescent mounting medium. Images were acquired with Olympus BX50 Upright Fluorescence Microscope equipped with a mercury burner lamp. Objective used was UPlanApo 100X/1.35 Oli Iris.

4.6 RNA-sequencing

Healthy fibroblasts were plated in Petri dish 100mm at a density of 3,000 cells/cm^2 and sucrose loading was started the day after plating. After 14 days of sucrose loading, total RNA from 3 sucrose-treated and 3 untreated Petri dishes was extracted using the EuroGold TriFast reagent (Euroclone, Wetherby, UK), following the manufacturer's instructions. RNA concentration was determined using the NanoDrop ND-1000 spectrophotometer and the RNA integrity was assessed on a LabChip GX Touch (Perkin Elmer). Subsequently, 500 ng of RNA for each sample were used to generate paired-end sequencing libraries with a Illumina TruSeq Stranded mRNA Sample LS Preparation kit (Illumina), according to the manufacturer's protocol. Sequencing was performed on a NextSeq500 platform at the Humanitas Genomic Facility (Illumina). After quality filtering according to the Illumina pipeline, 76 bp paired-end reads were mapped to the hg19 reference genome and to the Homo sapiens transcriptome (Illumina's iGenomes reference annotation downloaded from UCSC http://support.illumina.com/sequencing/sequencing_software/igenome.html) using

STAR v2.3.1s (Dobin A et al., 2013) . Differential expression analysis between treated and untreated samples was evaluated with an exact test for the negative binomially distributed counts using DeSeq2 (Bioconductor package) (Love MI et al., 2014). Differentially expressed genes were selected using an FDR (false discovery rate) ≤ 0.01 and FC (fold change) >=1.

4.7 Electron microscopy of cell monolayers

Healthy fibroblasts loaded or not with 88 mM sucrose for 7 days and NPA fibroblasts loaded or not with 50 µM SM for 23 days were plated in 6-well plate at a density of 10,000 cells/cm^2. Cells were processed for electron microscopy after other 7 days of culturing in the same conditions (at 14 days of sucrose loading and at 30 days of SM loading, respectively). Cells monolayer were fixed in a mixture of 4% paraformaldehyde and 2% glutaraldehyde in cacodylate buffer (0.12 M, pH 7.4) for 4 hours at 4°C. Then, cells were extensively washed with cacodylate buffer and subsequently post-fixed for 1 hour on ice in a mixture of 1% osmium tetroxide and 1.5% potassium ferrocyanide in cacodylate buffer. After several washes with ultrapure water, samples were "en bloc" stained with 0.5% uranyl acetate in water overnight at 4°C. Finally, samples were dehydrated in a graded ethanol series, then infiltrated for 2 hours in a mixture 1:1 (v/v) of ethanol and Epon and subsequently in 100% Epon, twice for 1 hour. Then polymerization was performed for 24 hours in an oven at 60°C. Ultra-thin sections (80 nm) were prepared using a ultramicrotome (Leica Ultracut; Leica Microsystems GmBH, Wien, Austria), collected on nickel grids and stained with saturated uranyl acetate for 5 minutes, washed and then stained with 3 mM lead citrate for 5 minutes. Finally, the sections were photographed using a transmission electron microscope LEO 912AB (Advanced Light and Electron Microscopy BioImaging Center - San Raffaele Scientific Institute).

4.8 LysoTracker staining

LysoTracker Red DND-99 (Molecular Probes) is a red-fluorescent dye for labelling and tracking acidic organelles in live cells. Healthy fibroblasts loaded or not with 88 mM sucrose for 14 days and NPA fibroblasts loaded or not with 50 µM sphingomyelin for 30 days were plated in 6-well plate at a density of 14,000 cells/cm^2 (approximately 70% of confluence). The day after, cells were incubated with LysoTracker diluted directly in the cell media at a final concentration of 50 nM (1 hour, 37°C, 5% CO_2). After one wash in PBS, Images were acquired with Olympus IX50 Inverted Fluorescence Microscope equipped with a halogen lamp. Objective used was LCAch 20X/0.40 PhC directly on live cells.

4.9 Immunofluorescence experiments

Cells for immunofluorescence staining were plated at sub-confluence in 6-well plates on a coverslip of 24 mm of diameter. Healthy fibroblasts were plated after 7 days of sucrose loading whereas NPA fibroblasts were plated after 23 days of sphingomyelin loading; the immunofluorescence staining was performed after other 7 days of culturing in the same conditions (at 14 days of sucrose loading and at 30 days of SM loading, respectively). Cells were washed three times with PBS and fixed in 4% paraformaldehyde for 20 minutes at room temperature (RT).

4.9.1 Lamp-1

Cells were blocked and permeabilized with 5% donkey serum/1% Bovine Serum Albumin (BSA) fatty acid free/0.2% Triton X-100/PBS for 1 hour at RT. Cells were then washed three times with PBS and incubated with mouse anti-Lamp-1 H4A3 (Developmental Studies Hybridoma Bank) overnight at 4°C. The primary antibody was diluted in 1.25% donkey serum/0.25% BSA fatty acid free/0.05% Triton X-100/PBS at the final concentration of 3 µg/ml. The day after, cells were washed three times in 0.05% Triton X-100/PBS and then incubated with anti-mouse AlexaFluor594 (Life Technologies) for 1 hour at RT. The secondary antibody was diluted 1:2,500 in 1.25% donkey serum/0.25% BSA fatty acid free/0.05% Triton X-100/PBS. After three washing with 0.05% Triton X-100/PBS, coverslip was mounted on a glass slide with Dako fluorescent mounting medium. Images were acquired with Olympus BX50 Upright Fluorescence Microscope equipped with a mercury burner lamp. Objective used was UPlanApo 100X/1.35 Oli Iris.

4.9.2 Lamp-1 – nonpermeabilizing conditions

For the immunofluorescence staining of the only Lamp-1 associated with cell plasma membrane, cells were processed as described above without the use of Triton X-100 in all the solutions.

4.9.3 LC3

Cells were blocked and permeabilized in a solution containing 10% donkey serum/0.2% Triton X-100/PBS for 30 minutes at RT. Cells were then washed three times with PBS and incubated with rabbit anti-LC3B (Sigma-Aldrich) for 2 hours at RT. The primary antibody was diluted in 1% donkey serum/0.1% Triton X-100/PBS at a final concentration of 5 µg/ml. After three washing with PBS, cells were incubated with anti-rabbit AlexaFluor488 (Life Technologies) for 1 hour at RT. The secondary antibody was diluted 1:600 in 1% donkey serum/0.1% Triton X-100/PBS. Cells were then washed three times with PBS and coverslip was mounted on a glass slide with Dako fluorescent mounting

medium. Images were acquired with Olympus BX50 Upright Fluorescence Microscope equipped with a mercury burner lamp. Objective used was UPlanApo 100X/1.35 Oli Iris.

4.9.4 Lysenin

Cells were permeabilized with digitonin (Sigma-Aldrich) diluted in PBS at the final concentration of 50 µg/ml for 10 minutes at RT. Cells were then washed three times with PBS and blocked with a solution containing 2% BSA fatty acid free/PBS for 15 minutes at RT. After three washing with PBS, cells were incubated with Lysenin (Sigma-Aldrich) for 2 hours at RT. Lysenin was diluted in 2% BSA fatty acid free/PBS at a final concentration of 1 µg/ml. Cells were then washed three times with PBS and incubated for 1 hour at RT with rabbit Lysenin antiserum (Peptides International) diluted 1:500 in 2% BSA fatty acid free/PBS. After three washing with PBS, cells were incubated with anti-rabbit AlexaFluor488 (Life Technologies) for 45 minutes at RT. The secondary antibody was diluted 1:600 in 2% BSA fatty acid free/PBS. Cells were then washed three times with PBS and coverslip was mounted on a glass slide with Dako fluorescent mounting medium. Images were acquired with Olympus BX50 Upright Fluorescence Microscope equipped with a mercury burner lamp. Objective used was UPlanApo 100X/1.35 Oli Iris.

4.10 Nuclear extraction from cells

Nuclear extraction was performed as previously described (Settembre C and Medina DL 2015). Briefly, cells deriving from a confluent T75 flask were lysed with 0.5 ml of lysis buffer (50 mM Tris-HCl at pH 7.5, 0.5% Triton X-100, 137.5 mM NaCl, 10% glycerol, 5 mM EDTA) supplemented with Protease Inhibitor Cocktail (Sigma-Aldrich) and 1 mM Na_3VO_4, for 15 minutes in ice under gentle shaking. Lysates were then transferred in Eppendorf tubes and centrifuged at 15,700 x g for 15 minutes at 4°C. The supernatant was discarded and the nuclear pellet was rinsed three times with 0.5 ml of lysis buffer. Then, nuclear pellet was resuspended in 0.1 ml of lysis buffer supplemented with 0.5% sodium dodecyl sulfate (SDS), and sonicated in ice three times for 3 seconds at low output to shear genomic DNA. After centrifugation at 15,700 x g for 15 minutes at 4°C, the supernatant (nuclear extract) was transferred to a new tube. The protein concentration of nuclear extracts was determined by DC Protein Assay (Biorad), accordingly to manufacturer's instruction.

4.11 Nuclear extraction from mouse brain tissue

Wild type and Acid Sphingomyelinase Knockout (ASMKO) mice (kindly given by Professor EH Schuchman, Icahn School of Medicine at Mount Sinai, New York) were

sacrificed and brains were collected and weighed. After mechanical homogenization in ice, brain tissue was resuspended in lysis buffer (10 mM HEPES at pH 7.9, 1.5 mM $MgCl_2$, 10 mM KCl, 0.2 mM EDTA) supplemented with 0.32 M sucrose, 1 mM DTT, 1 mM NaF, 1 mM Na_3VO_4 and Protease Inhibitor Cocktail (Sigma-Aldrich) with a ratio of 0.1 g tissue/0.9 ml lysis buffer. Brain tissue was then homogenized in a Teflon pestle PYREX Potter-Elvehjem tissue grinder and centrifuged at 850 x g for 10 minutes at 4°C. The supernatant was removed and the pellet was resuspended in lysis buffer supplemented with 1 mM DTT and Protease Inhibitor Cocktail, corresponding to ½ of the tissue homogenate volume. The protein concentration of tissue homogenates was determined by DC Protein Assay (Biorad), accordingly to manufacturer's instruction. Aliquots of tissue homogenates were further processed for nuclear extraction. In particular, they were centrifugated at 850 x g for 10 minutes at 4°C. Cell pellet was resuspended in extraction buffer (20 mM HEPES at pH 7.9, 1.5 mM $MgCl_2$, 0.42 M NaCl, 0.2 mM EDTA, 25% v/v glycerol) supplemented with 1 mM DTT and Protease Inhibitor Cocktail, corresponding to ½ of the pellet volume. After Dounce homogenization (10 hits with tight pestle and 10 hits with loose pestle), the suspension obtained was maintained in gently shaking for 45 minutes at 4°C. Then, the suspension was centrifuged at 20,000 x g for 20 minutes at 4°C. The supernatant (nuclear extract) was dialyzed versus 50 volumes of dialysis buffer (20 mM HEPES at pH 7.9, 1.5 mM $MgCl_2$, 10 mM KCl, 0.2 mM EDTA, 20% v/v glycerol) supplemented with 1 mM DTT and Protease Inhibitor Cocktail for 3 hours (buffer change after 1.5 h). The protein concentration of nuclear extracts was determined by DC Protein Assay (Biorad), accordingly to manufacturer's instruction.

4.12 Immunoblotting

4.12.1 Samples preparation

Cells were harvested in PBS by mechanical scraping. After centrifugation at 450 x g for 10 minutes at 4°C, cell pellet was lysed in an appropriate volume of Milli-Q water supplemented with Protease Inhibitor Cocktail (Sigma-Aldrich) using an ultrasonic homogenizer. The protein concentration of cell lysates was determined by DC Protein Assay (Biorad), accordingly to manufacturer's instruction.

Brain tissue homogenates were prepared as described above (see Chapter "*Nuclear extraction from brain mouse tissue*").

4.12.2 SDS-PAGE and Western-Blotting

Cell lysates, brain tissue homogenates and nuclear extracts from cells or brain tissues were denatured with Laemmli buffer and subsequent heating (100°C for 10 minutes); then they were analyzed by SDS-PAGE. Equivalent amounts of proteins were separated

on polyacrylamide (AA) gels (15% AA for Caspase-3 and LC3; 10% AA for GBA1 and Lamp-1; 12.5% AA for TFEB) and then transferred to PVDF membranes by electroblotting. Membranes were washed with TBS-T (10 mM Tris-HCl, 150 mM NaCl, 0.05% Tween-20 at pH 8) and then blocked with 5% non-fat dry milk in TBS-T (blocking solution) for 1 hour at room temperature (RT). PVDFs were incubated with primary antibody diluted in blocking solution overnight at 4°C. The day after, PVDFs were washed with TBS-T three times for 5 minutes. Then membranes were incubated with the appropriate horseradish peroxidase conjugated (HRP) secondary antibody for 1 hour at RT. After washing PVDFs with TBS-T three times for 5 minutes, signals were visualized using a chemiluminescent kit (WESTAR ηC, Cyanagen). Digital images were obtained by the chemiluminescence system Alliance Mini HD9 (UVItec).
Differently, immunoblotting of Lamp-1 was performed using 1% non-fat dry milk in PBS-0.1% Tween-20 for blocking and dilution of the primary antibody.

4.12.3 Antibodies

Primary antibodies: rabbit anti-Caspase-3, 1:1000 (Cell Signaling); rabbit anti-LC3B, 1 µg/ml (Sigma-Aldrich); rabbit anti-GBA1, 1.125 µg/ml (Abcam); mouse anti-Lamp-1 H4A3, 0.37 µg/ml (Developmental Studies Hybridoma Bank); rat anti-Lamp-1 1D4B, 0.325 µg/ml (Developmental Studies Hybridoma Bank); rabbit anti-TFEB, 0.33 µg/ml (Bethyl Laboratories); rabbit anti-GAPDH, 0.14 µg/ml (Sigma-Aldrich); mouse anti-α-tubulin, 1:20,000 (Sigma-Aldrich); rabbit anti-Histone H3, 1:2,000 (Cell Signaling).
Secondary HRP-linked antibodies: goat anti-rabbit, 1:2,000 (Cell Signaling); goat anti-mouse, 1:40,000 (ThermoFisher Scientific); goat anti-rat, 1:5,000 (Santa Cruz).

4.13 Evaluation of enzymatic activities in cell lysates and tissue homogenates

4.13.1 Samples preparation

Cells were harvested in PBS by mechanical scraping. After centrifugation at 450 x g for 10 minutes at 4°C, cell pellet was lysed in an appropriate volume of Milli-Q water supplemented with Protease Inhibitor Cocktail (Sigma-Aldrich) using an ultrasonic homogenizer. The protein concentration was determined by DC Protein Assay (Biorad), accordingly to manufacturer's instruction.
Wild type and Acid Sphingomyelinase Knockout (ASMKO) mice were sacrificed and brains were collected and weighed. After washing in PBS, brains were mechanically homogenized and then resuspended in 10 volumes (respect to their weight) of McIlvaine buffer (0.1 acid citric/0.2 Na_2HPO_4) at pH 6. After homogenization with a Potter homogenizer at 4°C, 50 µl of Complete Protease Inhibitor Cocktail Tablets (Roche) and

5 µl of PMSF 1 mM were added to the homogenate. After sonication and centrifugation at 300 x g for 10 minutes at 4°C, supernatants were collected for determination of protein concentration by DC Protein Assay (Biorad), accordingly to manufacturer's instruction.

4.13.2 Substrates

The enzymatic activities associated with total cell lysates and brain homogenates were determined using a method previously described (Aureli M et al., 2011b). The fluorogenic substrates used were purchased by Glycosynth: 4-Methylumbelliferyl β-D-glucopyranoside (MUB-β-Gluc) for β-glucocerebrosidase GBA1 and non-lysosomal β-glucosylceramidase GBA2, 4-Methylumbelliferyl β-D-galactopyranoside (MUB-β-Gal) for β-galactosidase, 4-Methylumbelliferyl N-acetyl-β-D-glucuronide (MUG) for β-hexosaminidase, 4-Methylumbelliferyl α-D-mannopyranoside (MUB-α-Man) for α-mannosidase, 4-Methylumbelliferyl β-D-mannopyranoside (MUB-β-Man) for β-mannosidase. 6-hexadecanoylamino 4-MU-phosphoryl-choline (HMU-PC) (Moscerdam Substrates) was used for measuring sphingomyelinase activity.

4.13.3 GBA1 and GBA2

Aliquots of cell lysates or brain homogenates were pre-incubated for 30 minutes at room temperature in a 96-well microplate with a reaction mixture composed by: 25 µl of McIlvaine buffer 4X (0.4 M citric acid /0.8 M Na_2HPO_4) pH 6, the specific inhibitors and water to a final volume of 75 µl. In particular, AMP-DNM (Adamantane–pentyl-dNM;N-(5-adamantane-1-yl-methoxy-pentyl)-Deoxynojirimycin) at the final concentration of 5 nM was used to inhibit GBA2; whereas Conduritol B epoxide (CBE) at the final concentration of 1 mM to inhibit GBA1. At the end of pre-incubation, the reaction was started by the addition of 25 µl of MUB-β-Gluc at the final concentration of 6 mM.

4.13.4 β-galactosidase, β-hexosaminidase, α-mannosidase, β-mannosidase and sphingomyelinase

Aliquots of cell lysates or brain tissue homogenates were incubated in a 96-well microplate with 25 µl of McIlvaine buffer 4X (0.4 M citric acid /0.8 M Na_2HPO_4) pH 5.2 containing the specific fluorogenic substrates (MUB-β-Gal, MUG, MUB-α-Man and MUB-β-Man at the final concentration of 500 µM and 250 µM for HMU-PC. Then water was added to reach the final volume of 100 µl.

4.13.5 Enzymatic assay

The reaction mixtures were incubated at 37°C under gentle shaking. At different time points 10 µl of the reaction mixtures was transferred in a black microplate (Black, 96-well, OptiPlate- 96 F, Perkin Elmer) and 190 µl of 0.25 M glycine pH 10.7 were added. For sphingomyelinase assay (HMU-PC), 190 µl of 0.25 M glycine pH 10.7 containing

0.3% Triton X-100 were added. The fluorescence was detected by a Victor microplate reader (Perkin Elmer). Data were expressed as nmoles of converted substrate/mg cellular proteins x hour and are the averages ± standard deviation of three independent experiments.

4.14 Evaluation of enzymatic activities at the cell surface of live cells

Cells were plated in a 96-well plate at a density of 70,000 cells/cm^2. The day after, plasma membrane-associated GBA1, GBA2, β-galactosidase and β-hexosaminidase activities were determined using a method previously described (Aureli M et al., 2011b). The artificial fluorogenic substrates MUB-β-Gluc, MUB-β-Gal and MUG solubilized in DMEM/F-12 without phenol red at the final concentrations of 6 mM, 0.25 mM and 1 mM, respectively; the pH of medium was adjusted at pH 6. Cell medium was removed and cells were washed twice with DMEM/F-12. For GBA1 and GBA2 assays cells were pre-incubated for 30 minutes at room temperature with 5 nM AMP-DNM and 1 mM CBE diluted in DMEM/F-12 pH 6, respectively. The specific substrates where then added to the cell monolayers and the incubation was performed at 37°C under very gently shaking. At different time points, aliquots of the medium were transferred in a black microplate (Black, 96-well, OptiPlate- 96 F, Perkin Elmer) and 20 volumes of 0.25 M glycine pH 10.7 were added. The fluorescence was evaluated using a Victor microplate reader (Perkin Elmer). Data were expressed as nmoles of converted substrate/10^6 cells x hour and are the averages ± standard deviation of three independent experiments. (Aureli M et al., 2011b).

4.15 Lipid analysis

Cells were harvested in PBS by mechanical scraping and collected. After centrifugation at 450 x g for 10 minutes at 4°C, cell pellet was lysed in an appropriate volume of Milli-Q water supplemented with Protease Inhibitor Cocktail (Sigma-Aldrich) using an ultrasonic homogenizer. The protein concentration was determined by DC Protein Assay (Biorad), accordingly to manufacturer's instruction. For NPA fibroblasts loaded or not with sphingomyelin (SM) for 30 days, before harvesting, cells were subjected to a specific treatment aimed to remove the exogenous SM fraction weakly associated with the cell plasma membranes. In details, fibroblasts were washed three times with culture medium supplemented with 10% FBS (RPMI-FBS). Then, cells were incubated in mild agitation for 1 minute with 3 ml of PBS containing 0.1% trypsin; immediately trypsin was blocked by the addition of 10 ml RPMI-FBS.

Cells lysates were lyophilized and subjected to lipid extraction with chloroform/methanol/water 2:1:0.1 (v/v/v). The total lipid extracts were then subjected to a two-phase partitioning, resulting in the separation of an aqueous phase containing gangliosides and in an organic phase containing all other lipids (Folch J et al., 1957). Briefly: to obtain the phase separation 20% in volume of water was added to the total lipid extract. The mixture was centrifuged at 5,000 x g for 5 minutes, obtaining the separation of the two phases. The aqueous phase (upper phase) was transferred in another tube and an identical volume of chloroform/methanol/water 3:48:47 (v/v/v) was added to the organic phase (lower phase). The mixture was centrifuged as described above and the second aqueous phase was combined to the first one. The organic phases and the aqueous phases were then dried under nitrogen flow.

The dried aqueous phases were resuspended in 100 µl of water and then dialyzed against water for 48 hours at 4°C (water change every 12 hours). This procedure allows to remove salts from aqueous phases. At the end of dialysis, the samples were lyophilised and resuspended in a known volume of chloroform/methanol 2:1 (v/v).

Aliquots of the organic phases were dried and resuspended in 800 µl of chloroform and 800 µl of 0.5 M NaOH in methanol; the mixture was then incubated overnight at 37°C. This alkaline treatment allows to remove glycerophospholipids from the organic phases, breaking their ester bonds and preserving the amide bonds of sphingolipids. At the end of incubation, the reaction was blocked by adding 50 µl of 0.5 M HCl in methanol. The samples were then dried under nitrogen flow and subjected again to the two-phase partitioning as described above to obtain the new alkali-stable organic phases resuspended in a known volume of chloroform/methanol 2:1 (v/v).

The dialyzed aqueous phases, the organic phases and the alkali-stable organic phases obtained were then separated by mono-dimensional High Performance Thin Layer Chromatography (HPTLC) carried out with the following solvent systems: chloroform/methanol/acetic acid/water 30:20:2:1 (v/v/v/v) for the analysis of phospholipids; hexane/ethyl acetate 3:2 (v/v) for cholesterol; chloroform/methanol/water 110:40:6 (v/v/v) for neutral glycolipids; hexane/chloroform/acetone/acetic acid 20:70:20:4 (v/v/v/v) for ceramide; chloroform/methanol 9:1 (v/v) followed by chloroform/methanol/0.2% aqueous $CaCl_2$ 50:42:11 (v/v/v) for gangliosides. Identification of lipids after separation was assessed by co-migration with lipid standards. Phospholipids were detected by spraying the HPTLC with a molybdate reagent (Vaskovsky et al. 1968); cholesterol, neutral glycolipids and ceramide were visualized by spraying the HPTLC with anisaldehyde; gangliosides were detected by spraying the HPTLC with Ehrlich's reagent. The relative amounts of lipids were determined by densitometry using ImageJ software.

4.16 Treatment of cell cultures with [3-^{3}H(sphingosine)]GM3

Healthy fibroblasts loaded or not with sucrose for 13 days were plated in Petri dishes 100mm at a density of 9,500 cells/cm^{2}. The day after, isotopically labelled [3-^{3}H(sphingosine)]GM3 was administered to both control and sucrose loaded cells. [3-^{3}H(sphingosine)]GM3 dissolved in propanol/water 7:3 (v/v) was transferred in a sterile glass tube and dried under nitrogen flow. The residue was solubilised in the cell culture medium without serum at the final concentration of $4.5x10^{-6}$ M. To follow the catabolism of [3-^{3}H(sphingosine)]GM3 both in the lysosomes and at the plasma membrane level, dedicated cells were pre-incubated with 100 µM chloroquine for 1 hour in cell medium without serum. After removal of the medium and rapid washing of cells, 5 ml of the medium containing the radioactive lipid were added to each dish and the cells were incubated at 37°C in the presence or not of 100 µM chloroquine for 4 hours. At the end of incubation, cells were washed three times with complete cell culture medium and incubated in the same medium for 30 minutes. Finally, cells were harvested with PBS and processed for lipid analysis as described above. The radioactivity associated with lipid extracts was determined by liquid scintillation counting. Total lipid extracts were then separated by HPTLC carried out with the solvent system chloroform/methanol/water 110:40:6 (v/v/v). Radioactive lipids were detected and quantified by radioactivity imaging performed with a Beta-Imager 2000 instrument (BioSpace) using an acquisition time of about 48 hours. Identification of lipids after separation was assessed by co-migration with radioactive lipid standards. The radioactivity associated with individual lipids was determined with M3Vision software.

4.17 Statistics

All the experiments have been performed in triplicate and repeated three times. Data are presented as the mean values ± standard deviation and were tested for significance employing Student's t-test analysis (GraphPad Prism software). The level of significance was set at $p<0.05$.

5. Results

5.1 Sucrose loading in human fibroblasts

5.1.1 Sucrose loading induces cell damage in human fibroblasts

Lysosomal Storage Diseases (LSDs) are characterized by lysosomal dysfunction leading to the accumulation of uncatabolized molecules within lysosomes. In LSDs cells, the lysosomal accumulation of undigested materials is associated with the onset of cell damage. Nevertheless, the molecular mechanisms linking these two events are still unknown.

To investigate this issue, I used an artificial *in vitro* model of lysosomal impairment represented by human healthy fibroblasts loaded with 88 mM sucrose for 14 days in culture (Kato T et al., 1981). Sucrose is rapidly taken up by the cells and stored into lysosomes due to the absence of invertase, the enzyme responsible for its hydrolysis. Importantly, at this concentration, sucrose was previously assessed not to induce osmotic stress in fibroblasts (Karageorgos LE et al., 1997). As control cells I used the same fibroblasts cultured in the identical medium without sucrose.

Since one of the main feature of LSDs is the onset of cell damage, to validate this cellular model I first evaluated the effect of sucrose loading on cellular proliferation. Interestingly, as shown in Figure 9, I found that fibroblasts loaded with sucrose are characterized by a significant growth slowdown. If compared to control cells, the reduction in cell growth is about 30% starting at day 3 after sucrose loading until 14 days in culture (Figure 9).

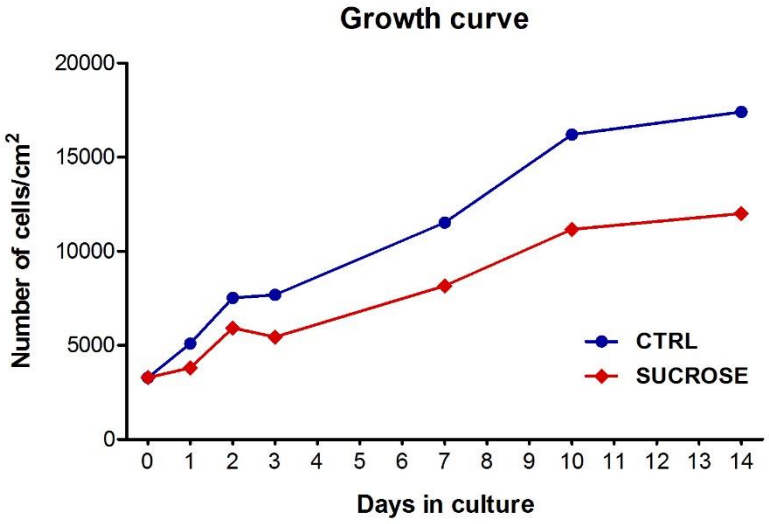

Figure 9 – Sucrose loading causes growth slowdown in human fibroblasts. Human fibroblasts were loaded with 88 mM sucrose for 14 days and cell counting was performed at 1, 2, 3, 7, 10, 14 days after sucrose loading by Trypan blue exclusion assay. Data are expressed as number of live cells for cm^2 of growth area. Each value represents the average of three independent experiments. CTRL: control cells; SUCROSE: sucrose loaded cells.

I investigated the main cell death pathways such as apoptosis and autophagy. First, I analysed one of the most important final effectors of apoptosis: Caspase-3, which is activated both by extrinsic and intrinsic apoptotic pathways. As shown in Figure 10 (panel A), sucrose loaded cells are characterized by the activation of apoptosis as indicated by the presence of the cleaved form of Caspase-3. Furthermore, sucrose loaded cells show a strong increase of the autophagic marker LC3-II compared to control cells (Figure 10, panel B and C) suggesting the possible activation of autophagy.

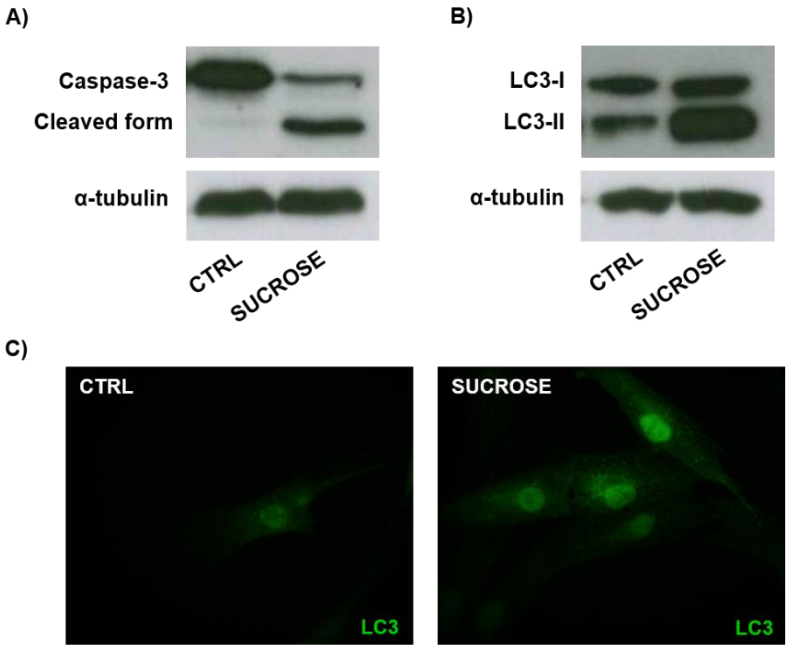

Figure 10 – Sucrose loading induces the activation of both apoptosis and autophagy in human fibroblasts. A) Representative Western Blot image showing Caspase-3 (procaspase) and the cleaved form protein expression; α-tubulin was used as loading control. B) Representative Western Blot image showing LC3-I and LC3-II protein expression; α-tubulin was used as loading control. C) Representative indirect immunofluorescence images of LC3; cells were permeabilized with Triton X-100 before staining. CTRL: control cells; SUCROSE: 14-day sucrose loaded cells.

To elucidate if the increase of the autophagic marker LC3-II after sucrose loading was due to autophagy activation or rather to a blockage of autophagosomes degradation, I treated cells with Bafilomycin A1. Bafilomycin A1 blocks the lysosomal functionality via the inhibition of the lysosomal proton pump V-ATPase resulting in autophagosomes and LC3-II accumulation. As shown in Figure 11, control cells treated with Bafilomycin A1 show an increased LC3-II protein expression with respect to untreated control cells. I performed the same experiment in sucrose loaded cells and I found that Bafilomycin A1 treatment induces a further increase of LC3-II level compared to untreated sucrose loaded cells. Since the amount of LC3-II further accumulates in the presence of a lysosomal function's inhibitor, this result suggests that sucrose loading activates the autophagic flux.

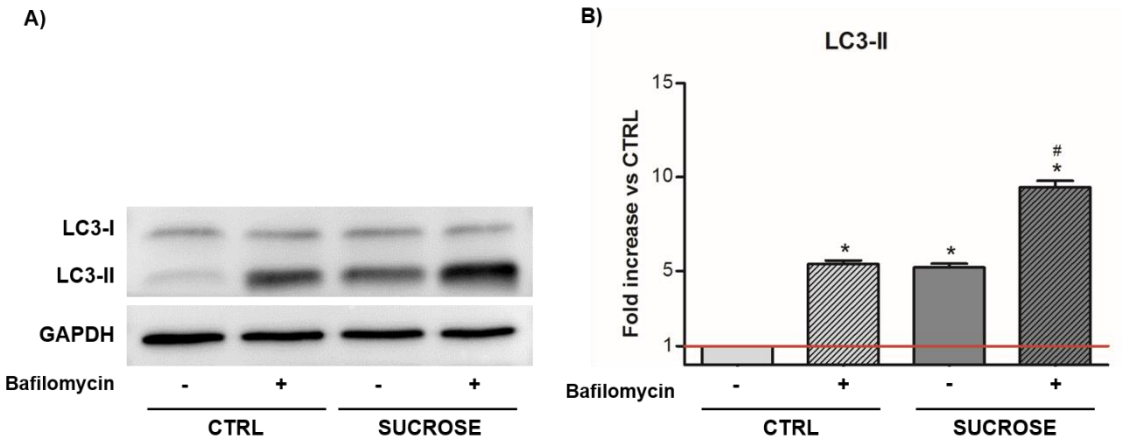

Figure 11 – Sucrose loading enhances the autophagic flux in human fibroblasts. Cells were treated with Bafilomycin A1 (100 nM) for 6 hours at 37°C, 5% CO_2. A) Representative Western Blot image showing LC3-I and LC3-II protein expression; GAPDH was used as loading control. B) Semi-quantitative graph of normalized LC3-II/GAPDH; *p<0.05 vs CTRL (-), #p<0.05 vs SUCROSE (-). CTRL: control cells; SUCROSE: 14-day sucrose loaded cells; (-) untreated cells; (+) Bafilomycin A1-treated cells.

As well known, several factors could contribute to induce cell growth slowdown. To deeply investigate this aspect, thanks to a collaboration with Professor Duga's laboratory from Humanitas University (Milano, Italy), we performed a Next-Generation RNA Sequencing (Illumina platform). Transcriptomes of control and 14-day sucrose loaded cells derived from three independent experiments were evaluated and data were analysed with DeSeq2 (Bioconductor). We found that approximately a thousand of genes are deregulated after sucrose loading. Among these, 56 genes encoding for proteins involved in cell cycle regulation are downregulated (Figure 12; Table 2): 3 genes coding for proteins working on DNA replication and repair processes; 9 for proteins responsible for cytokinesis; 18 for proteins playing a role in the mitotic spindle formation; 24 for other proteins contributing in the regulation of cell cycle and 2 for proteins involved in the inhibition of apoptosis.

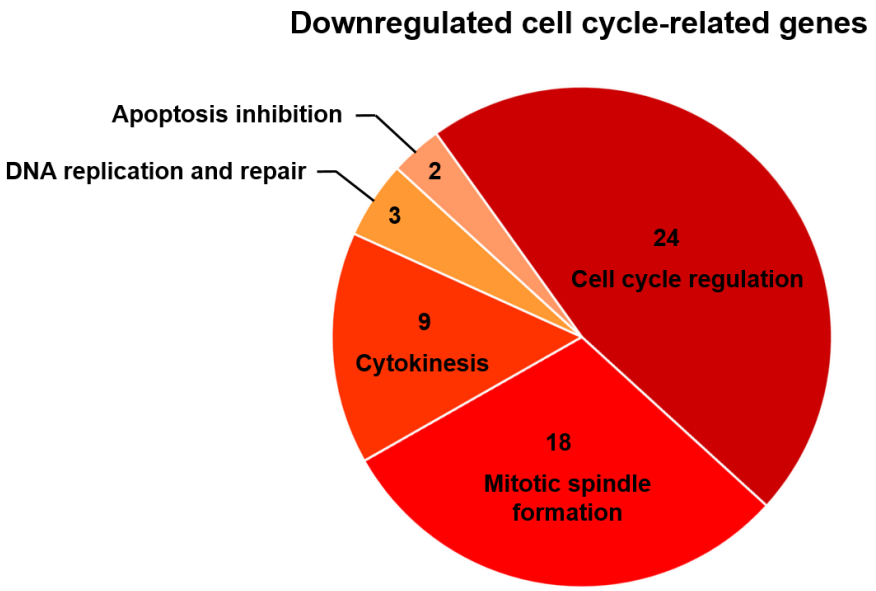

Figure 12 – Cell cycle-related genes downregulated in 14-day sucrose loaded fibroblasts. RNA sequencing analysis was performed by Illumina platform; differential expression analysis between treated and untreated samples was evaluated using DeSeq2 (Bioconductor).

Collectively, these results indicate that fibroblasts loaded with sucrose represented an artificial *in vitro* model of lysosomal storage characterized by the onset of cell damage. In particular, in these cells I observed: cell growth slowdown, downregulation of cell cycle-related genes and the activation of both apoptosis and autophagy. Therefore, I proved that sucrose loaded fibroblasts represent a valid model to further study the possible molecular mechanisms linking lysosomal storage to the onset of cell damage.

Downregulated cell cycle-related genes	
Cell cycle regulation	
BUB1	BUB1 Mitotic Checkpoint Serine/Threonine Kinase
BUB1B	BUB1 Mitotic Checkpoint Serine/Threonine Kinase B
CCNB2	Cyclin B2
CCNE2	Cyclin E2
CDK1	Cyclin-Dependent Kinase 1
CYP26B1	Cytochrome P450 Family 26 Subfamily B Member 1
ESCO2	Establishment of Sister Chromatid Cohesion N-Acetyltransferase 2
E2F2	E2F Transcription Factor 2
E2F8	E2F Transcription Factor 8
FBXO5	F-Box Protein 5
GAS7	Growth Arrest Specific 7
GTSE1	G2 and S-Phase Expressed 1
HJURP	Holliday Junction Recognition Protein
ID4	Inhibitor Of DNA Binding 4, HLH Protein
KIFC1	Kinesin Family Member C1
KIF15	Kinesin Family Member 15
KIF20B	Kinesin Family Member 20B
MKI67	Marker Of Proliferation Ki-67
NEK2	NIMA Related Kinase 2
NUSAP1	Nucleolar and Spindle Associated Protein 1
PBK	PDZ Binding Kinase
PLK1	Polo Like Kinase 1
PTTG1	Pituitary Tumor-Transforming 1
UBE2C	Ubiquitin Conjugating Enzyme E2 C
Mitotic spindle formation	
ASPM	Abnormal Spindle Microtubule Assembly
AURKB	Aurora Kinase B
CENPA	Centromere Protein A
CENPF	Centromere Protein F
CEP55	Centrosomal Protein 55
KIF2C	Kinesin Family Member 2C
KIF11	Kinesin Family Member 11
NCAPG	Non-SMC Condensin I Complex Subunit G
NCAPH	Non-SMC Condensin I Complex Subunit H
NDC80	NDC80 Kinetochore Complex Component
NUF2	NDC80 Kinetochore Complex Component NUF2
SGOL1 or SGO1	Shugoshin 1
SKA1	Spindle and Kinetochore Associated Complex Subunit 1
SKA3	Spindle and Kinetochore Associated Complex Subunit 3
SPAG5	Sperm Associated Antigen 5
SPC25	Kinetochore-associated Ndc80 Complex Subunit SPC25
TACC3	Transforming Acidic Coiled-Coil Containing Protein 3
TTK	TTK Protein Kinase
Cytokinesis	
ANLN	Anillin Actin Binding Protein
CDCA2	Cell Division Cycle Associated 2
CDCA3	Cell Division Cycle Associated 3
CDCA8	Cell Division Cycle Associated 8
CDC20	Cell Division Cycle 20
CDC25C	Cell Division Cycle 25C
CDC45	Cell Division Cycle 45
CIT	Citron Rho-Interacting Serine/Threonine Kinase
PRC1	Protein Regulator of Cytokinesis 1
DNA replication and repair	
CLSPN	Claspin
EXO1	Exonuclease 1
RAD54L	RAD54-Like (S. Cerevisiae)
Apoptosis inhibition	
BIRC5	Baculoviral IAP Repeat Containing 5
C11ORF82	known also as DDIAS (DNA Damage Induced Apoptosis Suppressor)

Table 2 - Downregulated cell cycle-related genes in human fibroblasts loaded with 88 mM sucrose for 14 days.

5.1.2 Sucrose loading induces lysosomal impairment

Morphologically, sucrose loaded fibroblasts are characterized by the presence of intracellular translucent vesicles that are absent in control cells (Figure 13).

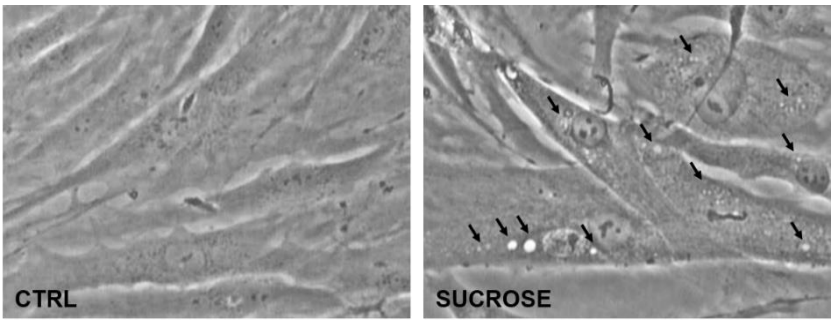

Figure 13 – Phase contrast microscopy images of human fibroblasts loaded or not with sucrose. Black arrows indicate sucrose loaded intracellular vesicles. CTRL: control cells; SUCROSE: 14-day sucrose loaded cells.

To better characterize the morphology of these intracellular structures, thanks to a collaboration with Dr. Zucca from Istituto di Tecnologie Biomediche – Consiglio Nazionale delle Ricerche (Milano, Italy) we performed an ultrastructural analysis by Transmission Electron Microscopy (TEM). Normally, lysosomes measure approximately 500 nm in diameter and in TEM appear like electron-dense vesicles due to the reaction between osmium tetroxide and lipids, of which lysosomes are particularly rich (Figure 14B and 14C, white arrows). As shown in Figure 14D, sucrose loaded cells are characterized by a large amount of non-electron-dense white intracellular bodies. These structures are apparently lysosomes which have accumulated sucrose. These non-electron-dense vesicles show a larger size compared to normal lysosomes, with an average of approximately 1 µm in diameter (Figure 14F, black arrow).

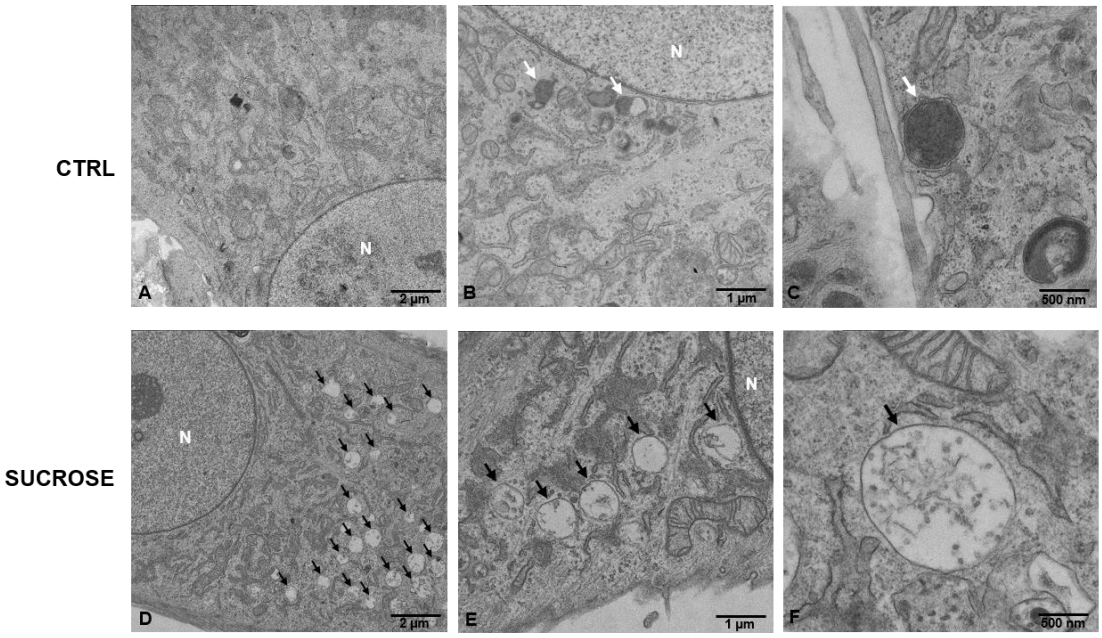

Figure 14 – Electron micrographs of human fibroblasts loaded or not with sucrose. (N) Nucleus; white arrows: normal electron-dense lysosomes, black arrows: not electron-dense bodies. A, B, C: control cells; D, E, F: 14-day sucrose loaded cells. Scale bars are shown: 2 µm for A and D; 1 µm for B and E; 500 nm for C and F.

From the data obtained by RNA sequencing, we found that 37 genes encoding for lysosomal proteins are upregulated in sucrose loaded fibroblasts compared to control cells. These genes include: 6 genes encoding for lysosomal structural proteins; 6 for lysosomal membrane transporters; 6 for other proteins contributing in the regulation of lysosomal function and 19 for enzymes involved in the degradation of several kinds of macromolecules (Figure 15; Table 3).

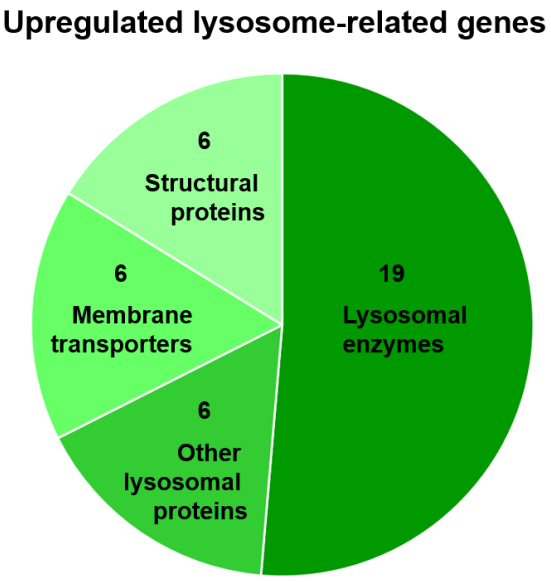

Figure 15 – Lysosome-related genes upregulated in 14-day sucrose loaded fibroblasts. RNA sequencing analysis was performed by Illumina platform; differential expression analysis between treated and untreated samples was evaluated using DeSeq2 (Bioconductor).

Upregulated lysosome-related genes	
Lysosomal enzymes	
ACP5	Acid Phosphatase 5, Tartrate Resistant
ADA	Adenosine Deaminase
ARSB	Arylsulfatase B
ASAH1	Acid Ceramidase
CTSA	Cathepsin A
CTSH	Cathepsin H
CTSK	Cathepsin K
DNASE2	Lysosomal Deoxyribonuclease II
FUCA1	Fucosidase, Alpha-L- 1
GBA	β-glucocerebrosidase
GNS	Glucosamine (N-Acetyl)-6-Sulfatase
HEXA	α-subunit of the β-hexosaminidase
HEXB	β-subunit of the β-hexosaminidase
MANBA	β-mannosidase
NEU1	Neuraminidase 1
PLA2G15	Phospholipase A2 Group XV
PNPLA7	Patatin Like Phospholipase Domain Containing 7
SMPD1	Sphingomyelin Phosphodiesterase 1
TPP1	Tripeptidyl Peptidase 1
Membrane transporters	
CTNS	Cystinosin
MCOLN1	Mucolipin 1
NPC1	NPC intracellular cholesterol transporter 1
NPC2	NPC intracellular cholesterol transporter 2
SLC17A5	Solute Carrier Family 17 Member 5
SLC36A1	Solute Carrier Family 36 Member 1
Structural proteins	
CLN3	Ceroid-Lipofuscinosis, Neuronal 3
COL4A3BP	Collagen Type IV Alpha 3 Binding Protein
C1ORF85	Lysosomal Protein NCU-G1
EPDR1	Ependymin Related 1
LITAF	Lipopolysaccharide-induced TNF-α factor
TMEM192	Transmembrane Protein 192
Other lysosomal proteins	
GM2A	GM2 Ganglioside Activator
IGF2R	Insulin Like Growth Factor 2 Receptor
MARCH9	Membrane Associated Ring-CH-Type Finger 9
PCSK9	Proprotein Convertase Subtilisin/Kexin Type 9
P2RX7	Purinergic Receptor P2X 7
STX3	Syntaxin 3

Table 3 - Upregulated lysosome-related genes in human fibroblasts loaded with 88 mM sucrose for 14 days.

The results obtained by RNA sequencing suggest that fibroblasts are characterized by an increased lysosomal function and biogenesis after sucrose loading. To further investigate this hypothesis, I used the fluorescent probe LysoTracker® Red DND-99 wich allows to selectively label intracellular acidic organells in live cells.

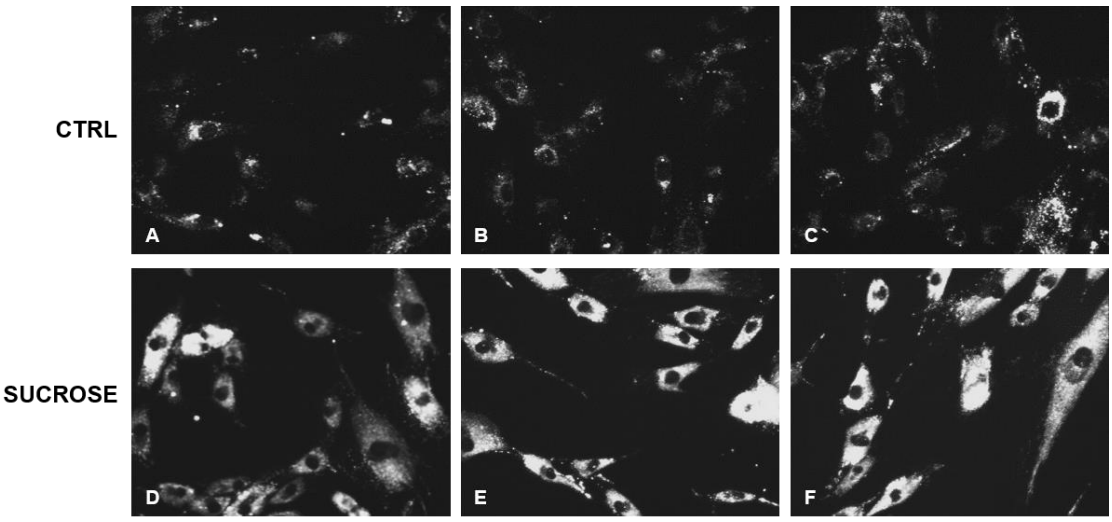

Figure 16 –LysoTracker® Red DND-99 staining of human fibroblasts loaded or not with sucrose. The staining was performed on live cells. A, B, C: control cells; D, E, F: 14-day sucrose loaded cells.

As shown in Figure 16, sucrose loaded fibroblasts are characterized by an increased LysoTracker® Red DND-99 staining with respect to control cells, which is evaluated as fluorescence intensity. This result suggests that sucrose loading induces an increase in the volume of acidic intracellular compartments. To better identify these acidic intracellular compartments, I performed indirect immunofluorescence experiments in permeabilized fibroblasts using a primary antibody against the lysosomal marker “Lysosomal associated membrane protein 1” (Lamp-1). As shown in Figure 17, sucrose loaded cells show a higher immunofluoresce intensity associated with Lamp-1 compared to control cells, suggesting that sucrose loading induces an increased lysosomal biogenesis.

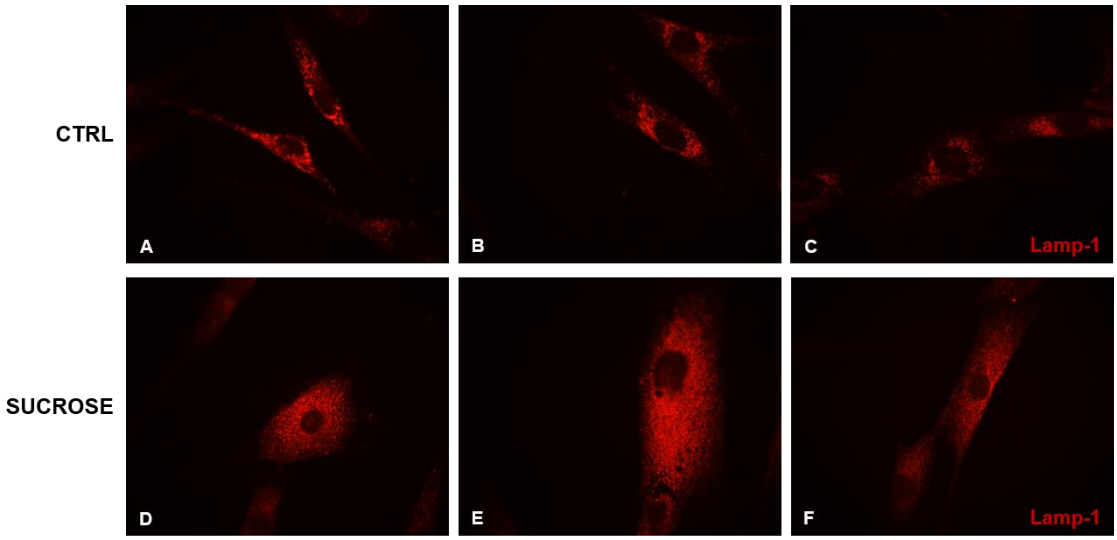

Figure 17 – Indirect immunofluorescence staining of Lamp-1 in human fibroblasts loaded or not with sucrose. Cells were permeabilized with Triton X-100 before staining. A, B, C: control cells; D, E, F: 14-day sucrose loaded cells.

These data were also confirmed by Western Blot analysis (Figure 18), showing that the increase in Lamp-1 protein expression is more than 2 fold in sucrose loaded fibroblasts with respect to control cells.

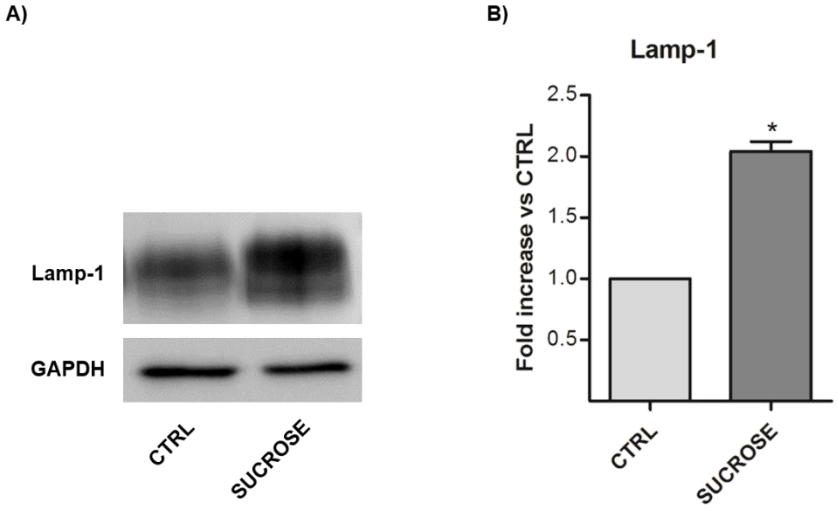

Figure 18 – Western Blot analysis of Lamp-1 in human fibroblasts loaded or not with sucrose. A) Representative Western Blot image showing Lamp-1 protein expression; GAPDH was used as loading control. B) Semi-quantitative graph of normalized Lamp-1/GAPDH; *p<0.05 vs CTRL. CTRL: control cells; SUCROSE: 14-day sucrose loaded cells.

Moreover, by *in vitro* fluorimetric assays, I measured the activity of the main lysosomal enzymes such as: β-glucocerebrosidase GBA1, β-galactosidase, β-hexosaminidase, α-mannosidase, β-mannosidase and sphingomyelinase. As shown in Figure 19, all the activities are increased in sucrose loaded fibroblasts with respect to control cells. In particular, GBA1 activity is 2.8 fold higher in sucrose loaded fibroblasts compared to control cells (21.00 ± 1.46 nmoles/mg proteins/h vs 7.60 ± 0.55 nmoles/mg proteins/h,

respectively); β-galactosidase activity increases 1.9 fold (347.71 ± 24.05 nmoles/mg proteins/h vs 186.76 ± 9.64 nmoles/mg proteins/h); β-hexosaminidase 1.7 fold (1,746.19 ± 95.93 nmoles/mg proteins/h vs 1,009.07 ± 47.75 nmoles/mg proteins/h); α-mannosidase 3.8 fold (24.47 ± 0.69 nmoles/mg proteins/h vs 6.41 ± 0.35 nmoles/mg proteins/h); β-mannosidase 2.4 fold (30.65 ± 3.66 nmoles/mg proteins/h vs 12.72 ± 0.41 nmoles/mg proteins/h); sphingomyelinase 2.7 fold (3.34 ± 0.37 nmoles/mg proteins/h vs 1.26 ± 0.13 nmoles/mg proteins/h).

Interestingly, the increase in the activities of β-glucocerebrosidase GBA1, β-hexosaminidase and sphingomyelinase, that are three of the principal enzymes involved in sphingolipid catabolism, positively correlates with the upregulation of their respective genes (GBA, HEXA, HEXB and SMPD1) as found by RNA sequencing analysis.

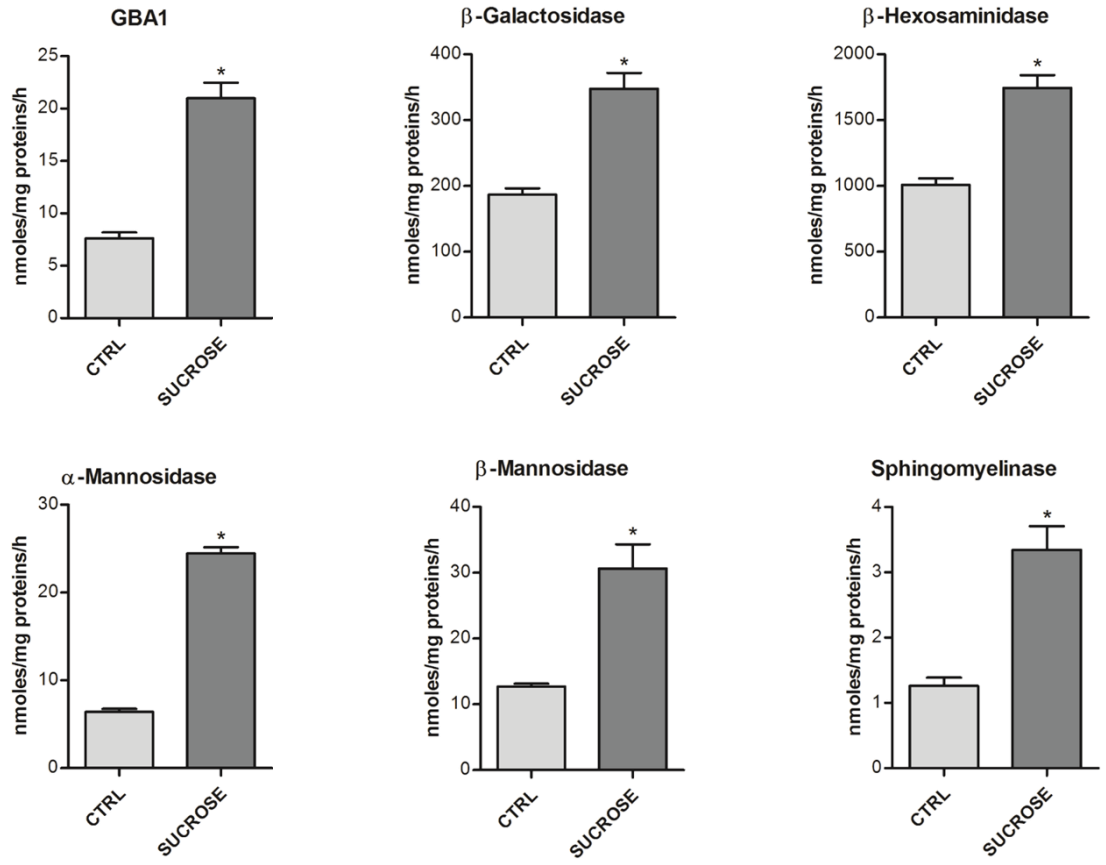

Figure 19 – Sucrose loading induces increased activity of the main lysosomal hydrolases. Graphs represent the enzymatic activities of β-glucocerebrosidase GBA1, β-galactosidase, β-hexosaminidase, α-mannosidase, β-mannosidase and sphingomyelinase measured in total cell lysates of human fibroblasts loaded or not with sucrose. Average value of triplicate analyses is expressed as nmoles/mg proteins/h. *p<0.05 vs CTRL. CTRL: control cells; SUCROSE: 14-day sucrose loaded cells.

GBA1 increase was also confirmed by Western Blot analysis (Figure 20), showing that GBA1 protein expression is 1.4 fold higher in sucrose loaded fibroblasts with respect to control cells.

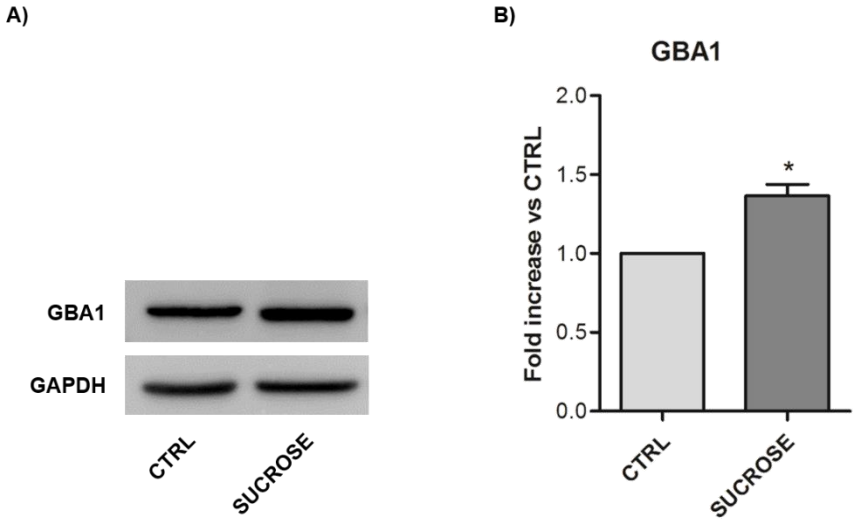

Figure 20 – Western Blot analysis of GBA1 in human fibroblasts loaded or not with sucrose. A) Representative Western Blot image showing GBA1 protein expression; GAPDH was used as loading control. B) Semi-quantitative graph of normalized GBA1/GAPDH; *p<0.05 vs CTRL. CTRL: control cells; SUCROSE: 14-day sucrose loaded cells.

Taken together, these results suggest that sucrose loading induces an increased biogenesis of mature lysosomes enhancing the catabolic flow.

In order to follow the lysosomal catabolism in live cells, I fed fibroblasts loaded or not with sucrose with the ganglioside GM3 tritium-labeled at position 3 of sphingosine ([3-^{3}H(sphingosine)]GM3). [^{3}H(sphingosine)]GM3 was solubilized in cell culture medium without FBS and then administered to the cells. After 4 hours of incubation, cells were harvested and then radioactive lipids were extracted and analysed. I found that cells have incorporated the same amount of GM3 independently from the sucrose loading. The digital autoradiography reported in Figure 21 shows that [3-^{3}H(sphingosine)]GM3 catabolism is strongly reduced in sucrose loaded fibroblasts with respect to control cells. In fact, the percentage of radioactivity associated with GM3 catabolites (lactosylceramide, glucosylceramide and ceramide) is reduced for all sphingolipid species in sucrose loaded cells compared to control ones. In particular, a 1.8, 3.7 and 4.3 fold decrease of lactosylceramide, glucosylceramide and ceramide respectively was observed in sucrose loaded cells.

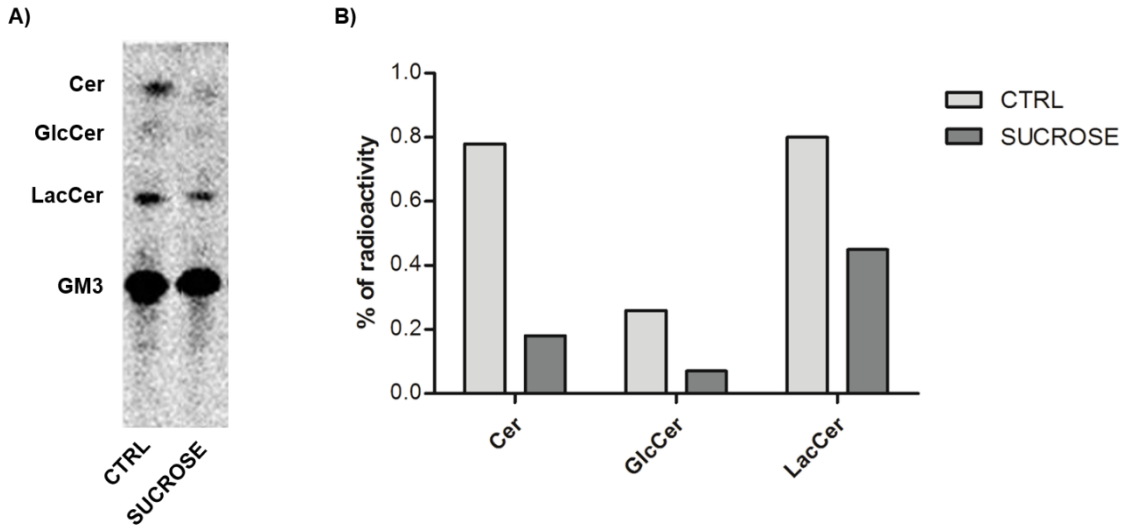

Figure 21 – Sucrose loading reduces lysosomal catabolism of radioactive ganglioside GM3 in live cells. A) Digital autoradiography of HPTLC performed using the solvent system chloroform/methanol/water 110:40:6 (v/v/v); 1000 dpm of total lipid extracts were applied per lane. B) Radioactivity quantification of GM3 catabolites: lactosylceramide (LacCer), glucosylceramide (GlcCer) and ceramide (Cer); data are expressed as percentage of radioactivity with respect to the total radioactivity associated with lipid extracts. CTRL: control cells; SUCROSE: 14-day sucrose loaded cells.

These results indicate that after sucrose loading the lysosomal catabolism is impaired. Therefore, in sucrose loaded fibroblasts the increased biogenesis of lysosomes is not related to an enhancement of their catabolic function.

5.1.3 Sucrose loading cells show an altered lipid composition

Fibroblasts loaded or not with sucrose were subjected to lipid extraction to evaluate their lipid content. Total lipid extracts were subjected to a two-phase partitioning to separate gangliosides from the other lipids.

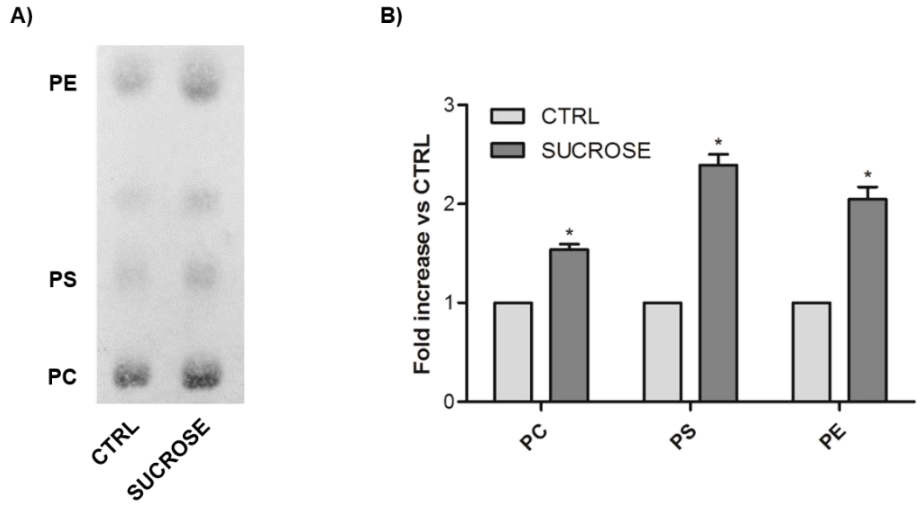

Figure 22 – Phospholipid analysis in human fibroblasts loaded or not with sucrose. A) Representative HPTLC performed using the solvent system chloroform/methanol/acetic acid/water 30:20:2:1 (v/v/v/v); aliquots of the organic phases corresponding to 120 µg of cellular proteins were applied per lane. B) Densitometric quantification of phosphatidylcholine (PC); phosphatidylserine (PS) and phosphatidylethalamine (PE); graph shows the fold increase in sucrose loaded cells with respect to control cells; each value is the average of three independent experiments. *p<0.05 vs CTRL. CTRL: control cells; SUCROSE: 14-day sucrose loaded cells.

The organic phases obtained after partitioning were first analyzed for the phospholipid pattern and content. As shown in Figure 22, all the phospholipid species identified including phosphatidylcholine (PC), phosphatidylserine (PS) and phosphatidylethalamine (PE) are increased in sucrose loaded fibroblasts with respect to control cells. In particular, PC increases 1.53, PS 2.39 fold and PE 2.19 fold.

Afterwards, the organic phases were subjected to an alkaline treatment to remove glycerophospholipids thus allowing the analyses of neutral glycosphingolipids and cholesterol.

As shown in Figure 23, cholesterol content increases 1.8 fold in sucrose loaded cells compared to control cells.

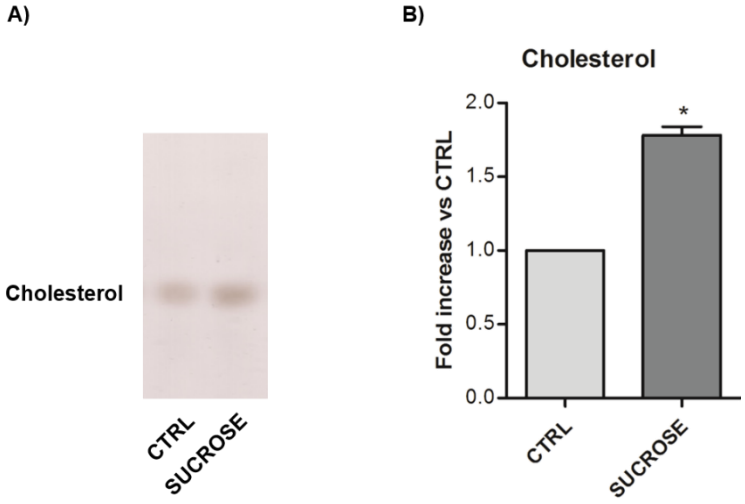

Figure 23 – Cholesterol analysis in human fibroblasts loaded or not with sucrose. A) Representative HPTLC performed using the solvent system hexane/ethyl acetate 3:2 (v/v); aliquots of the alkali-stable organic phases corresponding to 100 µg of cellular proteins were applied per lane. B) Densitometric quantification of cholesterol; graph shows the fold increase in sucrose loaded cells with respect to control cells; the value is the average of three independent experiments. *p<0.05 vs CTRL. CTRL: control cells; SUCROSE: 14-day sucrose loaded cells.

The analysis of neutral lipids show an increase in the main sphingolipids after sucrose loading. In particular, compared to control cells, sphingomyelin (SM) increases 1.75 fold, globotriaosylceramide (Gb3) 1.87 fold, lactosylceramide (LacCer) 10 fold and glucosylceramide (GlcCer) 4.6 fold (Figure 24).

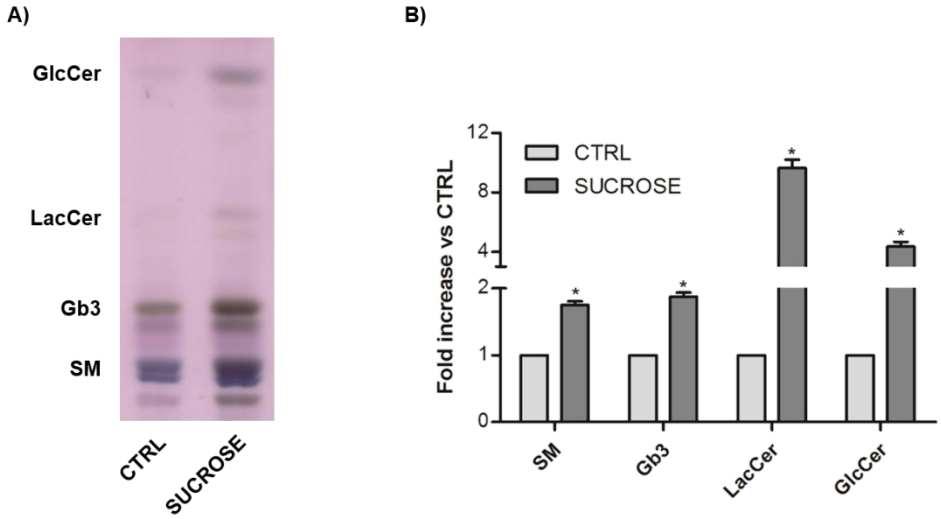

Figure 24 – Analysis of neutral glycosphingolipids in human fibroblasts loaded or not with sucrose. A) Representative HPTLC performed using the solvent system chloroform/methanol/water 110:40:6 (v/v/v); aliquots of the alkali-stable organic phases corresponding to 500 µg of cellular proteins were applied per lane. B) Densitometric quantification of sphingomyelin (SM); globotriaosylceramide (Gb3); lactosylceramide (LacCer); glucosylceramide (GlcCer); graph shows the fold increase in sucrose loaded cells with respect to control cells; each value is the average of three independent experiments. *p<0.05 vs CTRL. CTRL: control cells; SUCROSE: 14-day sucrose loaded cells.

Ceramide was analysed separately using a specific solvent system and, as shown in Figure 25, its content is increased about 1.7 fold in sucrose loaded cells with respect to control cells.

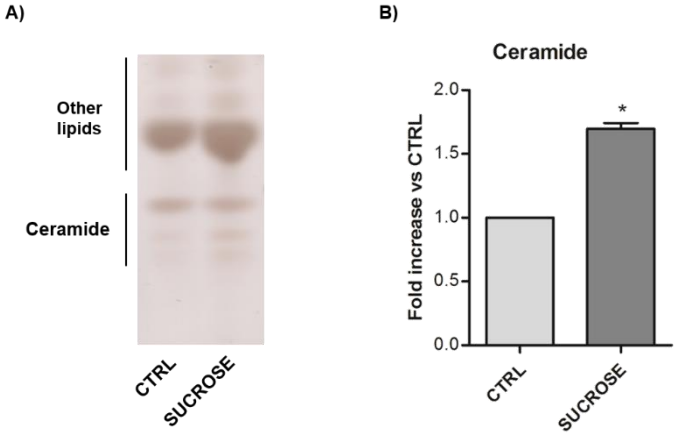

Figure 25 – Ceramide analysis in human fibroblasts loaded or not with sucrose. A) Representative HPTLC performed using the solvent system hexane/chloroform/acetone/acetic acid 20:70:20:4 (v/v/v/v); aliquots of the alkali-stable organic phases corresponding to 1.2 mg of cellular proteins were applied per lane. B) Densitometric quantification of ceramide; graph shows the fold increase in sucrose loaded cells with respect to control cells; the value is the average of three independent experiments. *p<0.05 vs CTRL. CTRL: control cells; SUCROSE: 14-day sucrose loaded cells.

Subsequently, I analysed ganglioside content and pattern in the aqueous phases obtained after partitioning. As shown in Figure 26, ganglioside levels are also increased after sucrose loading. In particular, a 12.2 fold increase for ganglioside GD1a, a 2.1 fold increase for GD3, and 2.8 and 3.7 fold increase respectively for GM2 and GM3 compared to control cells.

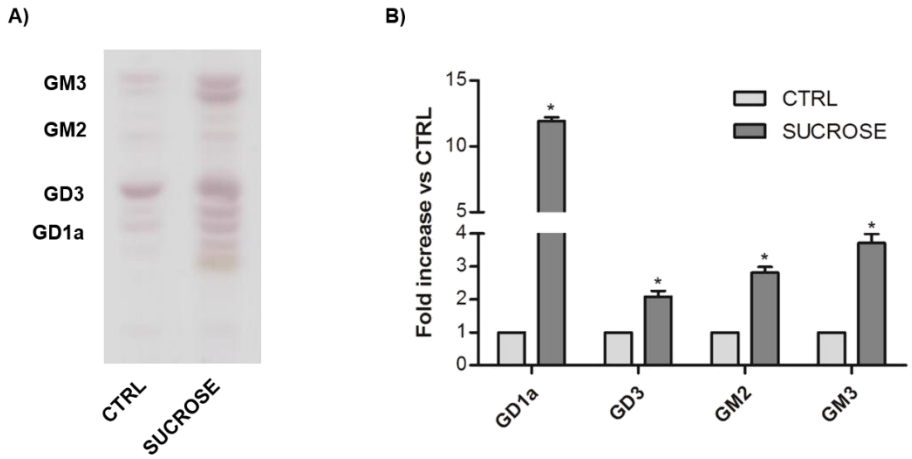

Figure 26 – Ganglioside analysis in human fibroblasts loaded or not with sucrose. A) Representative HPTLC performed using the solvent system chloroform/methanol 9:1 (v/v) followed by chloroform/methanol/0.2% aqueous $CaCl_2$ 50:42:11 (v/v/v); aliquots of the aqueous phases corresponding to 1.5 mg of cellular proteins were applied per lane. B) Densitometric quantification of GD1a, GD3, GM2 and GM3; graph shows the fold increase in sucrose loaded cells with respect to control cells; each value is the average of three independent experiments. *p<0.05 vs CTRL. CTRL: control cells; SUCROSE: 14-day sucrose loaded cells.

Collectively, these results indicate that sucrose loaded fibroblasts show a higher content of the principal phospholipid and sphingolipid species. This condition could be explained as the consequence of the impairment of intralysosomal catabolism resulting in the accumulation of secondary undegraded molecules, such as complex lipids.

5.1.4 Lysosomal impairment leads to the production of pro-apoptotic ceramide through the hydrolysis of cell surface glycosphingolipids

Recent lines of evidence support the role of the Transcription Factor EB (TFEB) in the regulation of lysosomal function. TFEB is normally localized into cytosol but under cellular stress conditions, such as lack of nutrients or lysosomal dysfunction, TFEB rapidly translocates to the nucleus and upregulates several set of genes involved in lysosomal function and biogenesis. I performed a transient transfection of TFEB tagged with the Green Fluorescent Protein (GFP) to monitor its intracellular localization during the 14 days of sucrose loading.

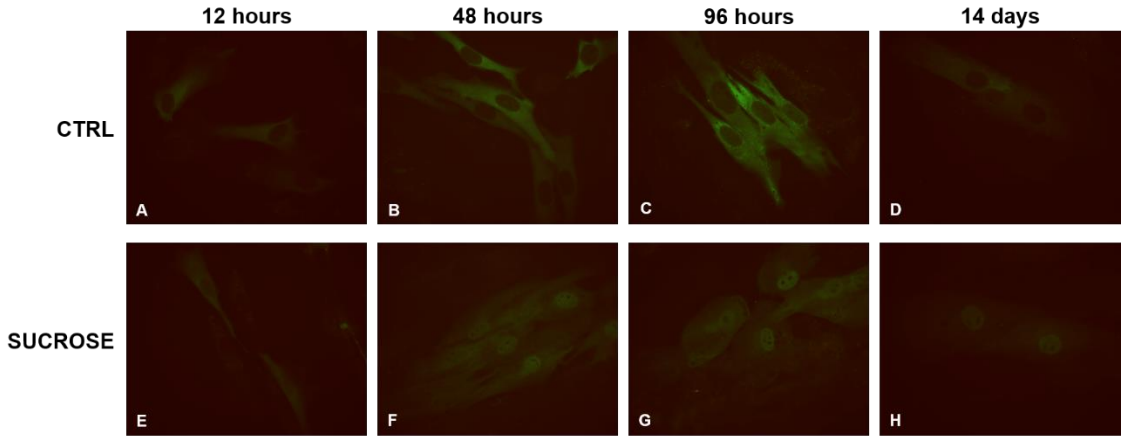

Figure 27 – Transient transfection of human fibroblasts loaded or not with sucrose with lenti-TFEB-GFP at different time points (12, 48, 96 hours and 14 days). Representative images obtained with Olympus BX50 Upright Fluorescence Microscope.

As shown in Figure 27, TFEB nuclear translocation occurs in sucrose loaded fibroblasts starting at 48 hours after sucrose loading; TFEB reaches an almost complete nuclear translocation at 14 days. On the contrary, in control cells, TFEB localization was mostly cytosolic at all the times investigated.

Endogenous TFEB nuclear localization was also confirmed in sucrose loaded cells after 14 days of sucrose loading by Western Blot analysis (Figure 28). In particular, a 1.8 fold increase of TFEB levels was detected in the nuclear extracts of sucrose loaded fibroblasts compared to control cells.

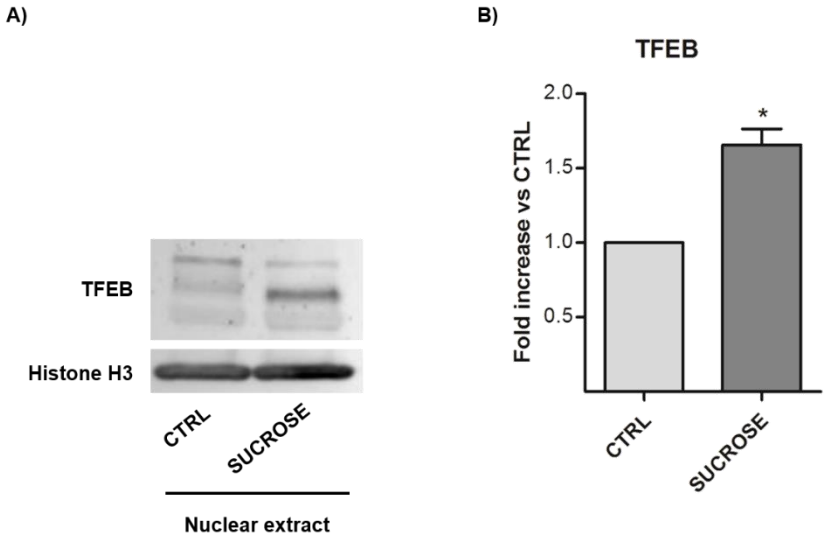

Figure 28 – Western Blot analysis of TFEB in human fibroblasts loaded or not with sucrose. A) Representative Western Blot image showing TFEB protein expression; Histone H3 was used as loading control. B) Semi-quantitative graph of normalized TFEB/Histone H3; *p<0.05 vs CTRL. CTRL: control cells; SUCROSE: 14-day sucrose loaded cells.

Recent findings from the literature suggest a role of TFEB in the promotion of lysosomal exocytosis. For this reason, I decided to study this aspect in the sucrose loading *in vitro* model. To this purpose, I evaluated the cell surface expression of Lamp-1 by indirect immunofluorescence experiments in nonpermeabilizing conditions. In fact, following the fusion between lysosomes and the cell surface, the luminal portion of Lamp-1 is localized at the extracellular leaflet of the plasma membrane. As shown in Figure 29, sucrose loaded fibroblasts are characterized by a greater staining of Lamp-1 at the plasma membrane level compared to control cells.

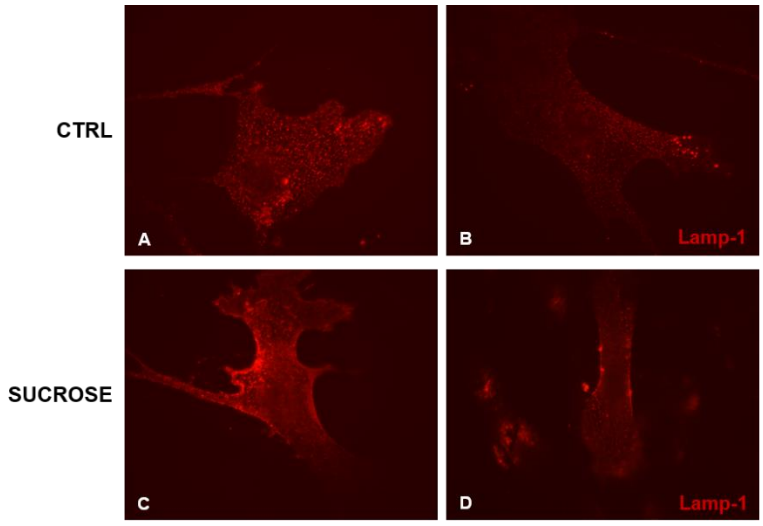

Figure 29 – Indirect immunofluorescence staining of Lamp-1 at the plasma membrane level in human fibroblasts loaded or not with sucrose. Staining was performed in nonpermeabilizing conditions. A, B: control cells; C, D: 14-day sucrose loaded cells.

To further support this evidence suggesting an increased lysosomal exocytosis in sucrose loaded fibroblasts, I decided to measure the activity of the main glycohydrolases associated with the cell plasma membrane in live cells. Among the evaluated enzymes, the lysosomal β-glucocerebrosidase GBA1, β-galactosidase and β-hexosaminidase can reach the cell surface after the fusion between lysosomes and the plasma membrane. As shown in Figure 30, all these enzymatic activities are increased in sucrose loaded cells with respect to control cells. Remarkably, the activity of GBA2, which is the non-lysosomal β-glucosylceramidase mainly associated with the cell surface, is also augmented after sucrose loading. In particular, a 6.4 fold increase for GBA1 activity (19.54 ± 0.21 nmoles/10^6 cells/h vs 3.06 ± 0.14 nmoles/10^6 cells/h, respectively sucrose loaded vs control cells), 1.8 fold increase for GBA2 (0.97 ± 0.03 nmoles/10^6 cells/h vs 0.54 ± 0.07 nmoles/10^6 cells/h), 12.6 fold for β-galactosidase (8.16 ± 1.09 nmoles/10^6 cells/h vs 0.65 ± 0.13 nmoles/10^6 cells/h) and 18.8 fold for β-hexosaminidase (259.27 ± 10.56 nmoles/10^6 cells/h vs 13.82 ± 5.13 nmoles/10^6 cells/h).

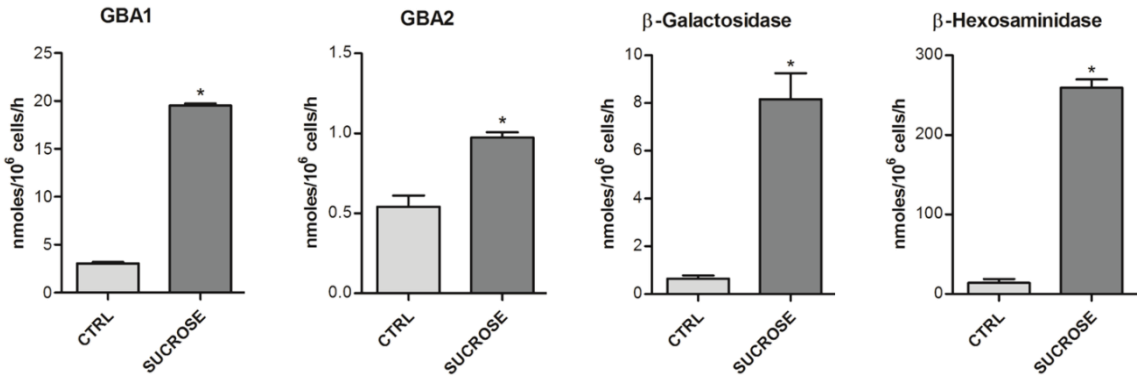

Figure 30 – Sucrose loading induces increased activity of plasma membrane-associated glycohydrolases. Graphs represent the enzymatic activities of plasma membrane-associated β-glucocerebrosidase GBA1, non-lysosomal β-glucosylceramidase GBA2, β-galactosidase and β-hexosaminidase measured in live human fibroblasts loaded or not with sucrose. Average value of triplicate analyses is expressed as nmoles/10^6 cells/h. *p<0.05 vs CTRL. CTRL: control cells; SUCROSE: 14-day sucrose loaded cells.

These results, obtained using artificial substrates, were validated using a natural substrate, such as ganglioside GM3. For this purpose, I fed fibroblasts loaded or not with sucrose with [3-^{3}H(sphingosine)]GM3 as previously described. Differently, in this case cells were pre-treated with chloroquine, a compound able to block the lysosomal function. Therefore, in this condition, [3-^{3}H(sphingosine)]GM3 can only be catabolized at the cell surface through the action of plasma membrane associated-hydrolases. After 4 hours of incubation, cells were harvested and then radioactive lipids were extracted and analysed. I found that cells have incorporated the same amount of GM3 independently from the sucrose loading. The digital autoradiography reported in Figure 31 shows that [3-^{3}H(sphingosine)]GM3 catabolism at the plasma membrane level is increased in

sucrose loaded fibroblasts with respect to control cells. In fact, the percentage of radioactivity associated with GM3 catabolites (lactosylceramide, glucosylceramide and ceramide) is augmented for all sphingolipid species in sucrose loaded cells compared to control ones. In particular, 1.6, 5.3, and 11.5 fold increase respectively of lactosylceramide, glucosylceramide and ceramide.

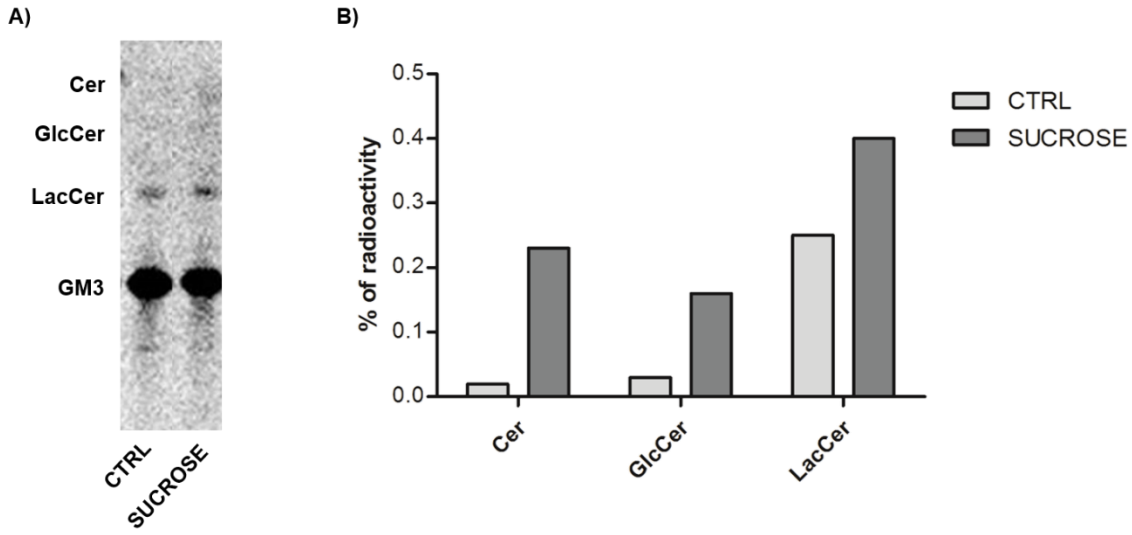

Figure 31 – Sucrose loading leads to increased catabolism of radioactive ganglioside GM3 at the plasma membrane. Cells were pre-treated with chloroquine to block lysosomal function. A) Digital autoradiography of HPTLC performed using the solvent system chloroform/methanol/water 110:40:6 (v/v/v); 1000 dpm of total lipid extracts were applied per lane. B) Radioactivity quantification of GM3 catabolites: lactosylceramide (LacCer), glucosylceramide (GlcCer) and ceramide (Cer); data are expressed as percentage of radioactivity with respect to the total radioactivity associated with the lipid extracts. CTRL: control cells; SUCROSE: 14-day sucrose loaded cells.

Taken together these results strongly suggest that sucrose loading induces an increased fusion between lysosomes and the cell plasma membrane. Consequently, the augmented lysosomal exocytosis could alter the lipid composition at the cell surface. In fact, the coexistence at the plasma membrane level of lysosomal glycohydrolytic enzymes and their substrates leads to an ectopic production of pro-apoptotic ceramide at this site. To verify this hypothesis, in sucrose loaded fibroblasts I performed an experiment aimed to block the production of ceramide at the cell surface by inhibiting the plasma membrane-associated β-glucosidases GBA1 and GBA2; these enzymes catalyse the last step of glycosphingolipid catabolism leading to ceramide production. For this reason, at 12 days after sucrose loading, fibroblasts were treated for 48 hours with CBE and AMP-DNM, inhibitors of GBA1 and GBA2 respectively. At the end of incubation, both treated and untreated sucrose loaded cells were harvested and the level of Caspase-3 and LC3 was detected by Western Blot analysis. As shown in Figure 32, I found that sucrose loaded cells treated with β-glucosidases inhibitors are characterized by a reduction in the cleaved active form of Caspase-3 and LC3-II levels compared to

the corresponding untreated cells. In particular, 13.4 fold decrease of the cleaved form of Caspase-3 and 1.46 fold decrease of LC3-II. These results suggest that the cell damage caused by sucrose loading could be reverted by blocking the production of ceramide at the plasma membrane level. Therefore, these findings corroborate the hypothesis that the ectopic ceramide produced at the cell surface could be responsible for the activation of downstream signalling pathways leading to the onset of cell damage.

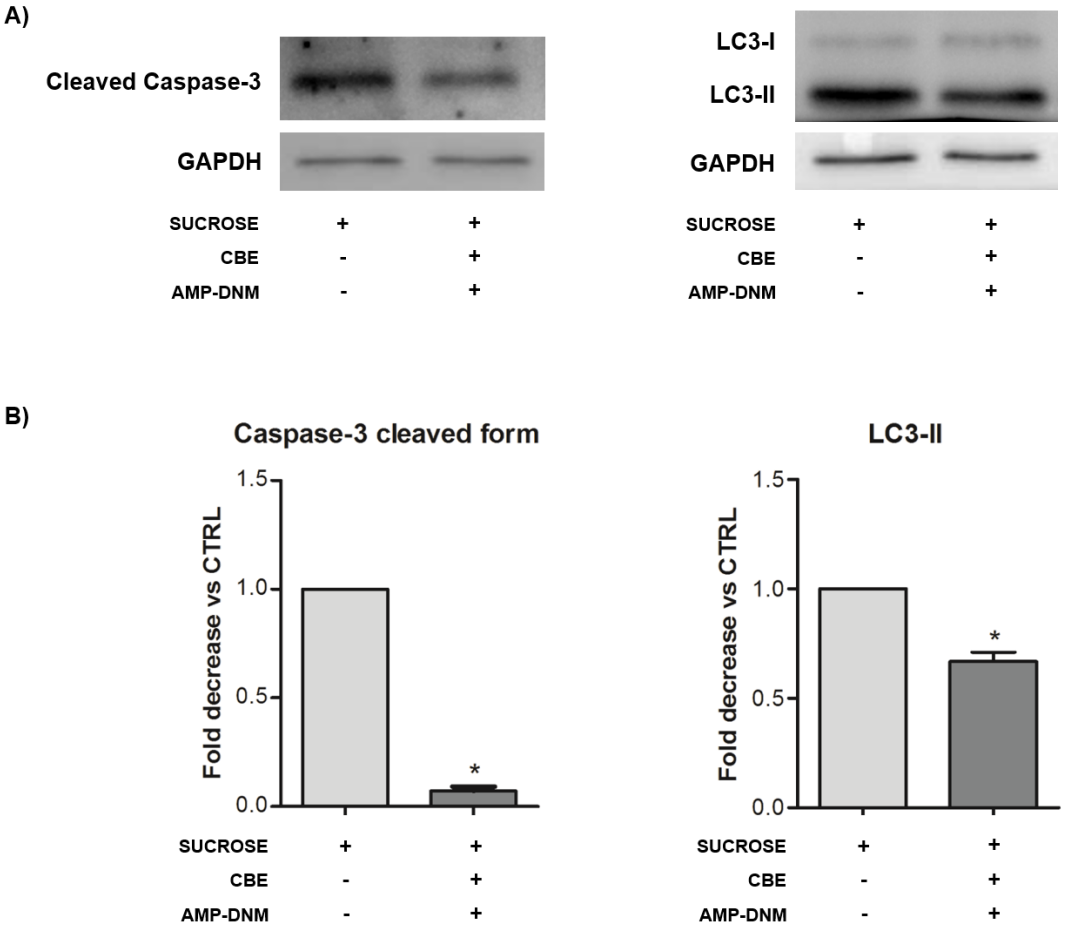

Figure 32 – Cell treatment with CBE and AMP-DNM reduces the cleaved form of Caspase-3 and LC3-II levels in 14-day sucrose loaded fibroblasts. A) Representative Western Blot images showing the cleaved form of Caspase-3 and LC3-II protein expression; GAPDH was used as loading control. B) Semi-quantitative graphs of normalized cleaved Caspase-3/GAPDH and LC3-II/GAPDH; *p<0.05 vs untreated sucrose loaded cells. CBE: inhibitor of β-glucocerebrosidase GBA1; AMP-DNM: inhibitor of non-lysosomal β-glucosylceramidase GBA2.

5.2 Sphingomyelin loading in human Niemann-Pick Type A fibroblasts

5.2.1 Sphingomyelin accumulation induces cell damage in human fibroblasts from a Niemann-Pick Type A disease patient

Niemann-Pick Type A disease (NPA) is a sphingolipidosis belonging to the group of Lysosomal Storage Diseases; NPA is caused by mutations in the gene coding for the acid sphingomyelinase. SM storage occurs primarily in the lysosomes of neurons and reticuloendothelial cells, although it has been demonstrated in other cell types such as hepatocytes, Schwann cells, and dermal fibroblasts (Bhuvaneswaran C et al., Eur. J. Cell Biol., 1985; Schuchman EH et al., Best Pract. Res. Clin. Endocrinol. Metab., 2014). To date, the molecular mechanisms by which SM accumulation leads to cell damage and cell death are still unknown. To investigate the possible molecular mechanism, I developed an *in vitro* model able to accumulate an amount of SM similar to that observed in the more compromised NPA cells. The NPA fibroblasts used in this study have a residual acid sphingomyelinase activity less than 2% corresponding to a 3.5 fold increase in SM content compared to healthy fibroblasts (Figure 34). Since this level of SM is insufficient to cause cell damage, I exogenously administered 50 μM SM to NPA fibroblasts for different time points in order to increase its lysosomal accumulation. The amount of administered SM is approximately 10 fold higher with respect to its concentration in serum (Chigorno V et al., 2005).

As shown in Figure 33 (panel A), 30-day SM loaded NPA fibroblasts (+SM) are characterized by the activation of apoptosis as demonstrated by the increase of the cleaved form of Caspase-3. Moreover, SM loaded cells show a strong increase of the autophagic marker LC3-II with respect to control cells (Figure 33, panel B and C) suggesting also autophagy activation. Activation of both apoptosis and autophagy was not observed after 14 days of SM loading (data not shown); for this reason, 30-days of SM loading were used for the following experiments.

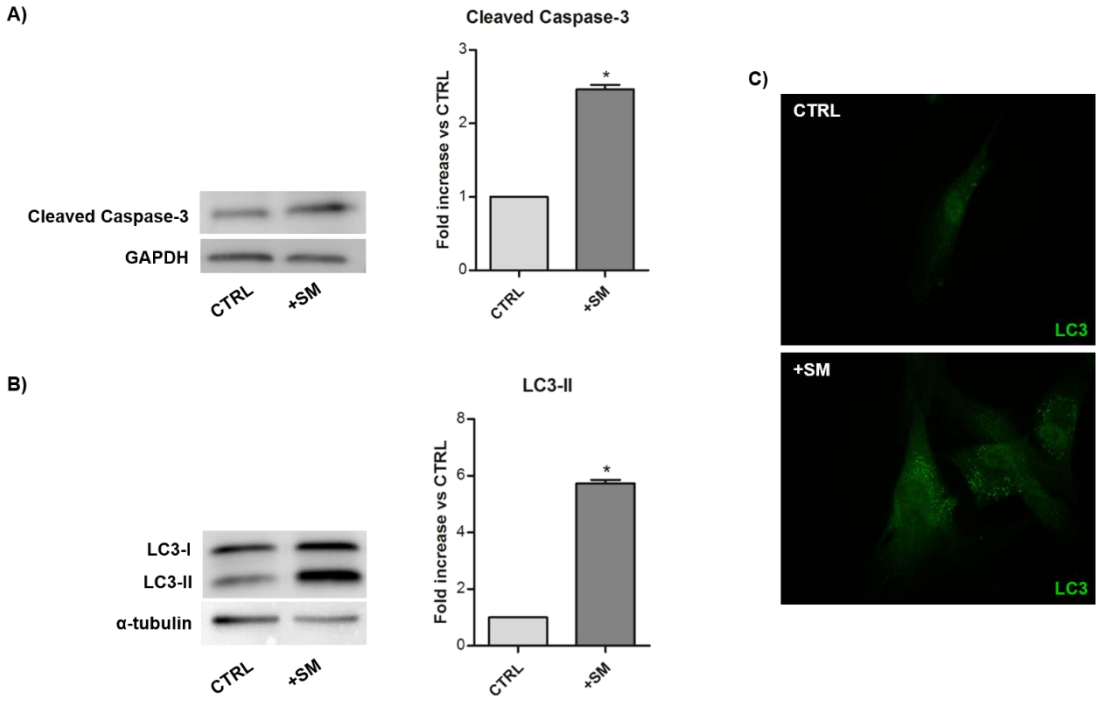

Figure 33 – Sphingomyelin (SM) loading in Niemann-Pick Type A human fibroblasts induces the activation of both apoptosis and autophagy. A) Representative Western Blot image showing the cleaved form of Caspase-3 protein expression, GAPDH was used as loading control; semi-quantitative graph of normalized cleaved Caspase-3/GAPDH, *p<0.05 vs CTRL. B) Representative Western Blot image showing LC3-I and LC3-II protein expression, α-tubulin was used as loading control; semi-quantitative graph of normalized LC3-II/α-tubulin, *p<0.05 vs CTRL. C) Representative indirect immunofluorescence images of LC3; cells were permeabilized with Triton X-100 before staining. CTRL: control cells; +SM: 30-day SM loaded cells.

I analysed SM in healthy fibroblasts and NPA fibroblasts loaded or not with SM. To this purpose, cell lysates were subjected to lipid extraction followed by a two-phase partitioning and then the organic phases were analysed by HPTLC. As shown in Figure 34, NPA fibroblasts (NPA CTRL) are characterized by a 3.5 fold increase in SM content with respect to healthy fibroblasts (Healthy) (80 ± 5.3 nmoles/mg cellular proteins vs 23 ± 2.4 nmoles/mg cellular proteins). Interestingly, NPA cells loaded for 30 days with exogenous SM (NPA +SM) show a 22 fold increase of SM content compared to healthy cells (760 ± 40.2 nmoles/mg cellular proteins).

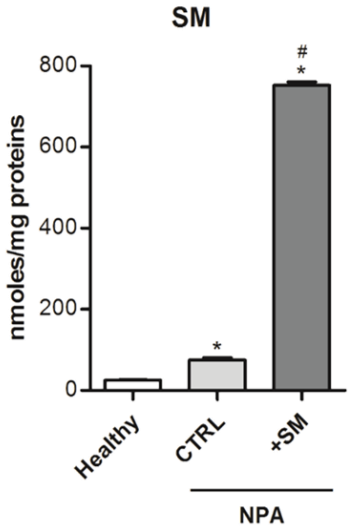

Figure 34 – Sphingomyelin (SM) content in healthy human fibroblasts and Niemann-Pick Type A (NPA) human fibroblasts loaded or not with 50 µM SM. Quantification of HPTLC performed using the solvent system chloroform/methanol/acetic acid/water 30:20:2:1 (v/v/v/v) was obtained by comparison with known amounts of SM standard applied in the same HPTLC; aliquots of the organic phases corresponding to 120 µg of cellular proteins were applied per lane. Graph shows the SM cellular content; average value of triplicate analyses is expressed as nmoles SM/mg cellular proteins. *p<0.05 vs Healthy; #p<0.05 vs NPA CTRL. Healthy: healthy cells; NPA CTRL: NPA control cells; NPA +SM: NPA 30-day SM loaded cells.

I evaluated the cellular localization of accumulated SM by indirect immunofluorescence experiments using Lysenin, a SM-binding protein; as shown in Figure 35, NPA fibroblasts (NPA CTRL) are characterized by a higher perinuclear fluorescence intensity with respect to healthy cells (Healthy). Remarkably, NPA cells loaded for 30 days with exogenous SM (NPA +SM) show a further increase of fluorescence intensity compared to NPA control cells. The perinuclear localization of SM suggests that its accumulation mainly occurs into lysosomes.

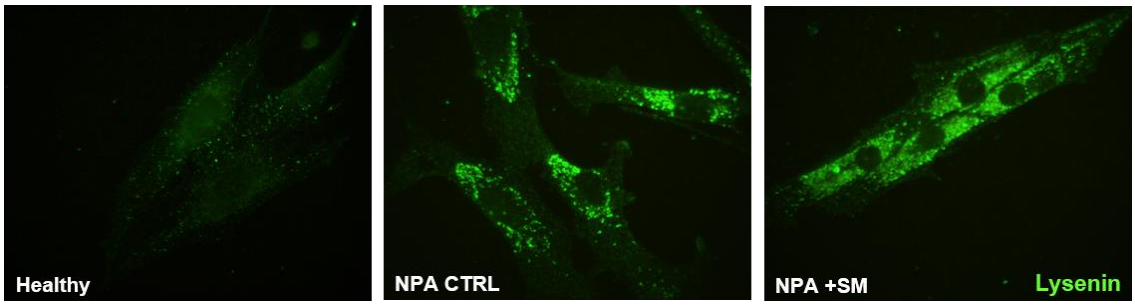

Figure 35 - Indirect immunofluorescence staining of sphingomyelin (SM) using the specific SM-binding protein Lysenin in healthy human fibroblasts and Niemann-Pick Type A (NPA) human fibroblasts loaded or not with 50 µM SM. Cells were permeabilized with Digitonin before staining. Healthy: healthy cells; NPA CTRL: NPA control cells; NPA +SM: NPA 30-day SM loaded cells.

Thanks to a collaboration with Dr. Zucca from Istituto di Tecnologie Biomediche – Consiglio Nazionale delle Ricerche (Milano, Italy) we performed an ultrastructural analysis by Transmission Electron Microscopy (TEM) on NPA fibroblasts loaded or not with SM.

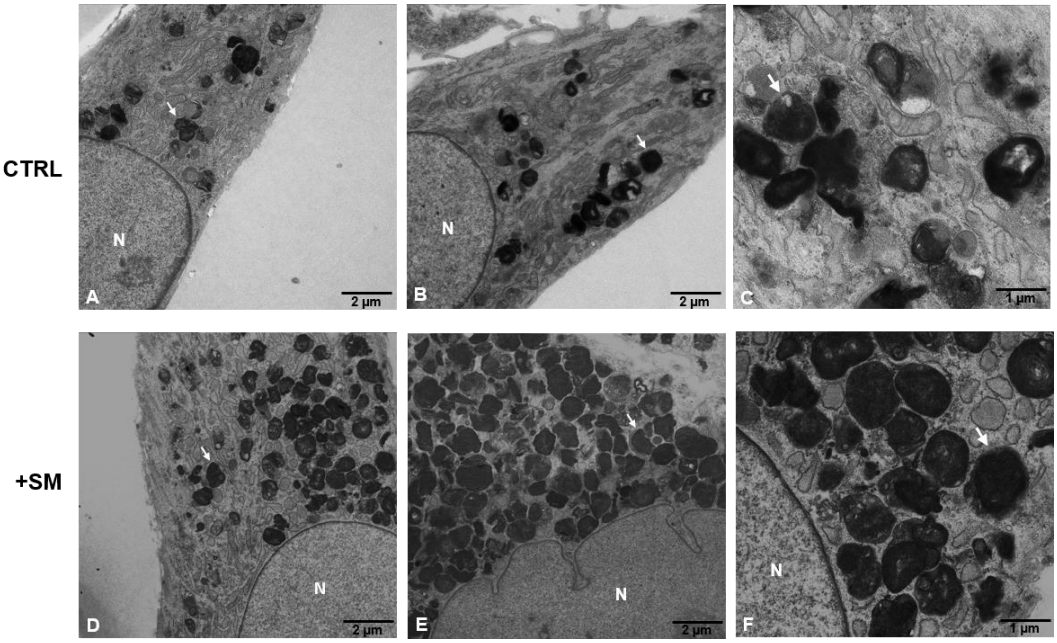

Figure 36 – Electron micrographs of Niemann-Pick Type A human fibroblasts loaded or not with 50 µM sphingomyelin (SM). (N) Nucleus; white arrows: SM accumulating organelles. A, B, C: control cells; D, E, F: 30-day SM loaded cells. Scale bars are shown: 2 µm for A, B, D, E; 1 µm for C and F.

As shown in Figure 36 (A-C), NPA control cells are characterized by electron-dense intracellular organelles (white arrows) which are lysosomes storing SM. These vacuoles appear like dark intracellular bodies due to the reaction between the lipid SM and osmium tetroxide used for sample preparation. Interestingly, NPA SM loaded cells show a greater number of dark intracellular bodies (Figures 36D-36F) compared to control cells, suggesting that SM loading induces an increased lysosomal biogenesis.

To verify this hypothesis, I performed a staining with LysoTracker® Red DND-99 to selectively label intracellular acidic organelles in live cells.

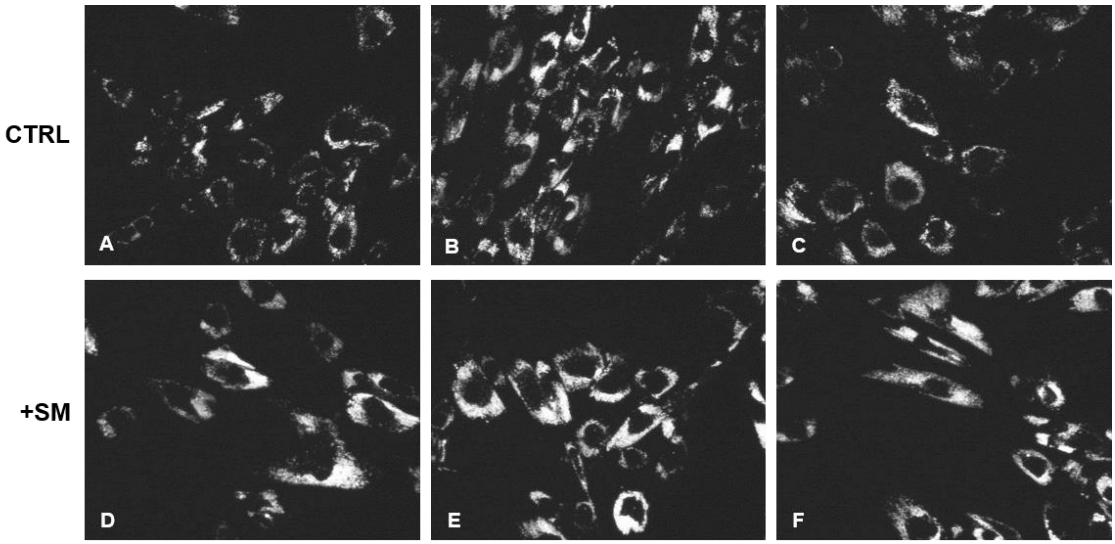

Figure 37 – LysoTracker® Red DND-99 staining of Niemann-Pick Type A human fibroblasts loaded or not with 50 μM sphingomyelin (SM). The staining was performed on live cells. A, B, C: control cells; D, E, F: 30-day SM loaded cells.

As shown in Figure 37, NPA +SM fibroblasts are characterized by an increased LysoTracker® Red DND-99 staining with respect to control cells, which is evaluated as fluorescence intensity. This result indicates that SM loading causes an increased relative volume of acidic intracellular compartments. To better classify these acidic intracellular vesicles, I performed indirect immunofluorescence experiments in permeabilized NPA fibroblasts using a primary antibody against the lysosomal marker "Lysosomal associated membrane protein 1" (Lamp-1). As shown in Figure 38, NPA +SM cells exhibit a higher immunofluorescence intensity compared to control cells, indicating that SM loading determines an increased lysosomal biogenesis.

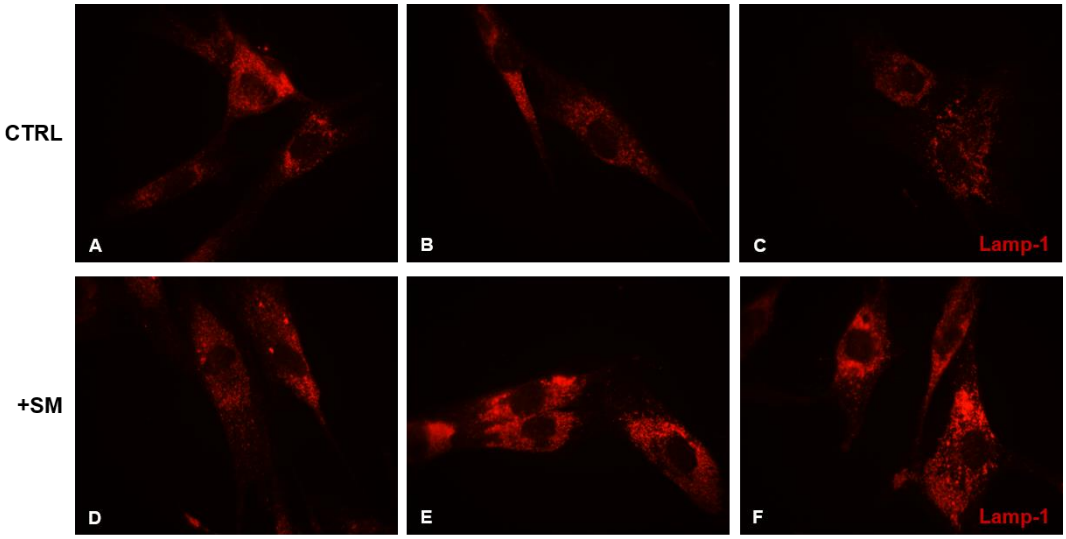

Figure 38 – Indirect immunofluorescence staining of Lamp-1 in Niemann-Pick Type A human fibroblasts loaded or not with 50 μM sphingomyelin (SM). Cells were permeabilized with Triton X-100 before staining. A, B, C: control cells; D, E, F: 30-day SM loaded cells.

These results were also confirmed by Western Blot analysis (Figure 39) showing a 8 fold increase in Lamp-1 protein expression in NPA SM loaded fibroblasts with respect to control cells.

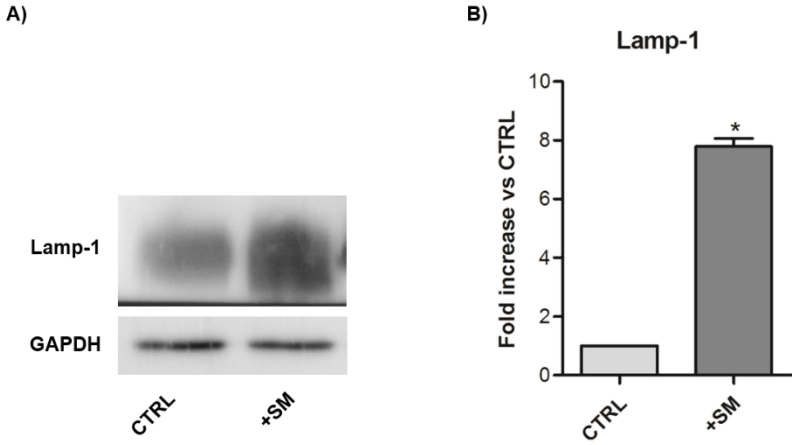

Figure 39 – Western Blot analysis of Lamp-1 in Niemann-Pick Type A human fibroblasts loaded or not with 50 μM sphingomyelin (SM). A) Representative Western Blot image showing Lamp-1 protein expression; GAPDH was used as loading control. B) Semi-quantitative graph of normalized Lamp-1/GAPDH; *p<0.05 vs CTRL. CTRL: control cells; +SM: 30-day SM loaded cells.

5.2.2 Sphingomyelin loading cells show an altered lipid composition

NPA fibroblasts loaded or not with SM were subjected to lipid extraction to evaluate their lipid content and pattern. Total lipid extracts were subjected to a two-phase partitioning to separate gangliosides from the other lipids.

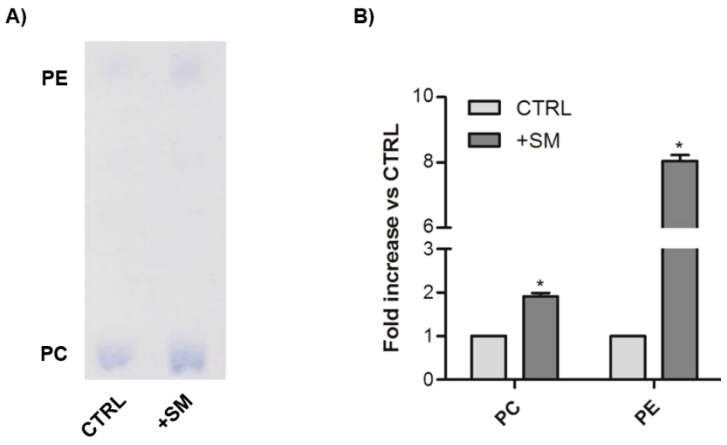

Figure 40 – Phospholipid analysis in Niemann-Pick Type A human fibroblasts loaded or not with 50 µM sphingomyelin (SM). A) Representative HPTLC performed using the solvent system chloroform/methanol/acetic acid/water 30:20:2:1 (v/v/v/v); aliquots of the organic phases corresponding to 120 µg of cellular proteins were applied per lane. B) Densitometric quantification of phosphatidylcholine (PC) and phosphatidylethalamine (PE); graph shows the fold increase of SM loaded cells with respect to control cells; each value is the average of three independent experiments. *p<0.05 vs CTRL. CTRL: control cells; +SM: 30-day SM loaded cells.

The organic phases obtained after partitioning were first analysed for the phospholipid pattern and content. As shown in Figure 40, phosphatidylcholine (PC) and phosphatidylethanolamine (PE) are increased in NPA SM loaded fibroblasts with respect to control cells. In particular, a 1.9 and 8.3 fold increase in PC and PE levels respectively. Afterwards, the organic phases were subjected to an alkaline treatment to remove glycerophospholipids in order to analyse neutral glycosphingolipids and cholesterol.

As shown in Figure 41, cholesterol content increases 1.7 fold in SM loaded cells compared to control cells.

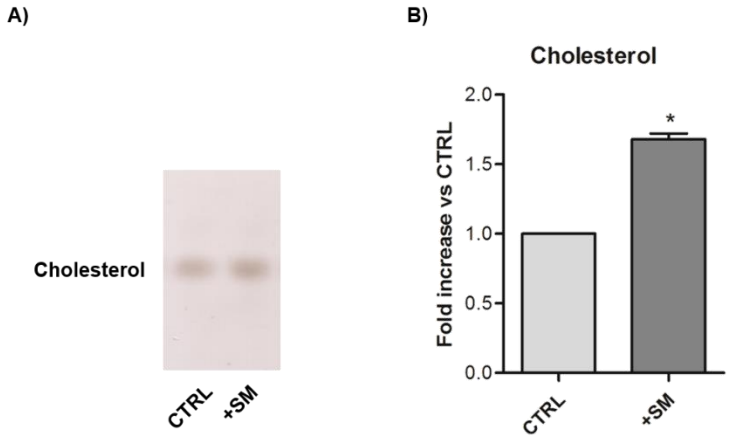

Figure 41 – Cholesterol analysis in Niemann-Pick Type A human fibroblasts loaded or not with 50 µM sphingomyelin (SM). A) Representative HPTLC performed using the solvent system hexane/ethyl acetate 3:2 (v/v); aliquots of alkali-stable organic phases corresponding to 100 µg of cellular proteins were applied per lane. B) Densitometric quantification of cholesterol; graph shows the fold increase of SM loaded cells with respect to control cells; the value is the average of three independent experiments. *p<0.05 vs CTRL. CTRL: control cells; +SM: 30-day SM loaded cells.

The analysis of neutral glycolipids shows an increase in the main glycosphingolipids after SM loading. In fact, a 1.6, 2.2 and 2.1 fold increase for globotriaosylceramide (Gb3), lactosylceramide (LacCer) and glucosylceramide (GlcCer) respectively are observed in NPA SM loaded fibroblasts with respect to control cells (Figure 42).

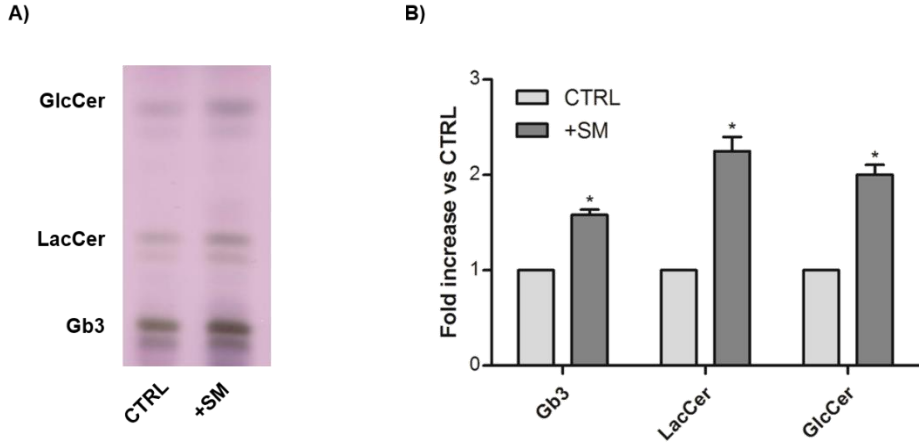

Figure 42 – Neutral glycosphingolipid analysis in Niemann-Pick Type A human fibroblasts loaded or not with 50 µM sphingomyelin (SM). A) Representative HPTLC performed using the solvent system chloroform/methanol/water 110:40:6 (v/v/v); aliquots of the alkali-stable organic phases corresponding to 500 µg of cellular proteins were applied per lane. B) Densitometric quantification of globotriaosylceramide (Gb3); lactosylceramide (LacCer); glucosylceramide (GlcCer); graph shows the fold increase of SM loaded cells with respect to control cells; each value is the average of three independent experiments. *p<0.05 vs CTRL. CTRL: control cells; +SM: 30-day SM loaded cells.

Ceramide was analysed separately using a specific solvent and, as shown in Figure 43, its content is increased in sucrose loaded cells of about 1.3 fold with respect to control cells.

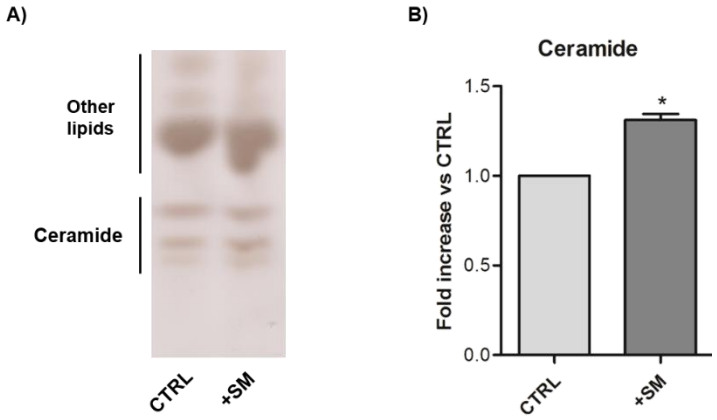

Figure 43 – Ceramide analysis in Niemann-Pick Type A human fibroblasts loaded or not with 50 μM sphingomyelin (SM). A) Representative HPTLC performed using the solvent system hexane/chloroform/acetone/acetic acid 20:70:20:4 (v/v/v/v); aliquots of the alkali-stable organic phases corresponding to 1.2 mg of cellular proteins were applied per lane. B) Densitometric quantification of ceramide; graph shows the fold increase of SM loaded cells with respect to control cells; the value is the average of three independent experiments. *p<0.05 vs CTRL. CTRL: control cells; +SM: 30-day SM loaded cells.

Then, I analysed ganglioside content and pattern in the aqueous phases obtained after partitioning. As shown in Figure 44, ganglioside content is also increased after SM loading. In particular, higher levels of ganglioside GD1a (2.1 fold), GD3 (1.4 fold), GM2 (4.1 fold) and GM3 (1.6 fold) are detectable in NPA SM loaded fibroblasts with respect to control cells.

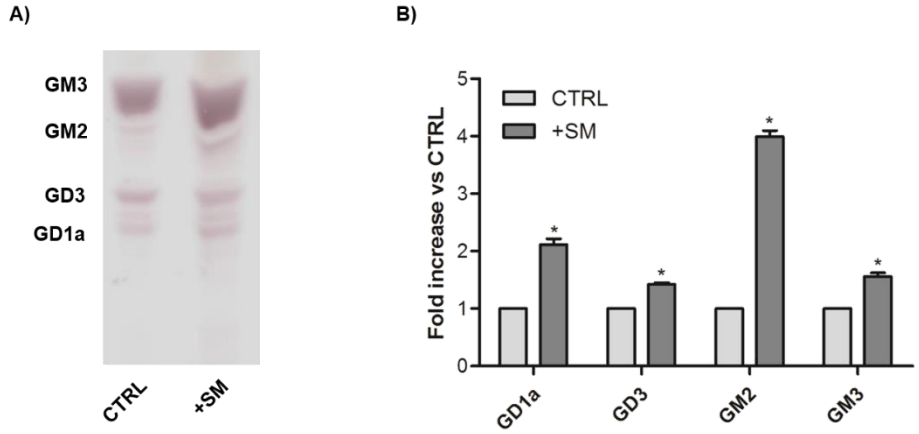

Figure 44 – Ganglioside analysis in Niemann-Pick Type A human fibroblasts loaded or not with 50 μM sphingomyelin (SM). A) Representative HPTLC performed using the solvent system chloroform/methanol 9:1 (v/v) followed by chloroform/methanol/0.2% aqueous $CaCl_2$ 50:42:11 (v/v/v); aliquots of the aqueous phases corresponding to 1.5 mg of cellular proteins were applied per lane. B) Densitometric quantification of GD1a, GD3, GM2 and GM3; graph shows the fold increase of SM loaded cells with respect to control cells; each value is the average of three independent experiments. *p<0.05 vs CTRL. CTRL: control cells; +SM: 30-day SM loaded cells.

These results indicate that NPA SM loaded fibroblasts show a higher content of the main phospholipid and sphingolipid species. This condition could be explained as the consequence of the impaired catabolism into lysosomes resulting in the accumulation of secondary undegraded molecules, such as complex lipids.

5.2.3 Sphingomyelin loading increases glycohydrolytic enzymes at the plasma membrane level

I evaluated the localization of the Transcription Factor EB (TFEB), recently described to play an important role in the regulation of lysosomal function, lysosomal biogenesis, autophagy and lysosomal exocytosis. As shown in Figure 45, TFEB nuclear localization was observed in SM loaded cells at 30 days after SM loading by Western Blot analysis. If compared to control cells, a 1.8 fold increase of TFEB is detected in the nuclear extracts from NPA SM loaded fibroblasts.

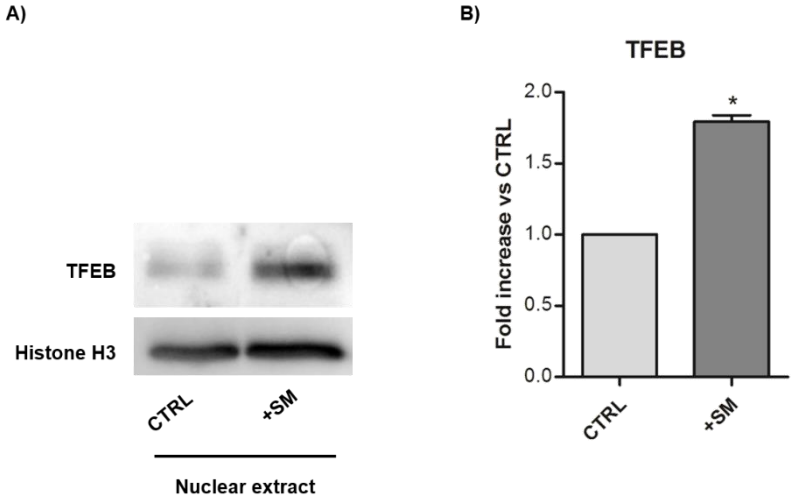

Figure 45 – Western Blot analysis of TFEB in Niemann-Pick Type A human fibroblasts loaded or not with 50 μM sphingomyelin (SM). A) Representative Western Blot image showing TFEB protein expression; Histone H3 was used as loading control. B) Semi-quantitative graph of normalized TFEB/Histone H3; *p<0.05 vs CTRL. CTRL: control cells; +SM: 30-day SM loaded cells.

Besides lysosomal biogenesis, TFEB can also promote lysosomal exocytosis. For this reason, I evaluated the activity of the main glycohydrolases associated with the cell plasma membrane in live cells. Among the evaluated enzymes, the lysosomal enzymes β-glucocerebrosidase GBA1, β-galactosidase and β-hexosaminidase can reach the cell surface after fusion between lysosomes and the cell plasma membrane. As shown in Figure 46, all the measured activities are increased in SM loaded cells with respect to control cells. Interestingly, also GBA2 activity, which is the non-lysosomal β-glucosylceramidase mainly associated with the cell surface, is augmented after SM loading. In particular, a 3.1 fold increase of GBA1 activity in sucrose loaded fibroblasts with respect to control cells (9.67 ± 0.40 nmoles/10^6 cells/h vs 3.17 ± 0.16 nmoles/10^6 cells/h, respectively); 2.1 fold increase of GBA2 (2.46 ± 0.01 nmoles/10^6 cells/h vs 1.16 ± 0.08 nmoles/10^6 cells/h); a 1.8 fold increase in the activity of β-galactosidase (1.04 ± 0.04 nmoles/10^6 cells/h vs 0.57 ± 0.13 nmoles/10^6 cells/h), and a 3 fold increase of β-hexosaminidase is (25.25 ± 3.49 nmoles/10^6 cells/h vs 8.34 ± 2.60 nmoles/10^6 cells/h).

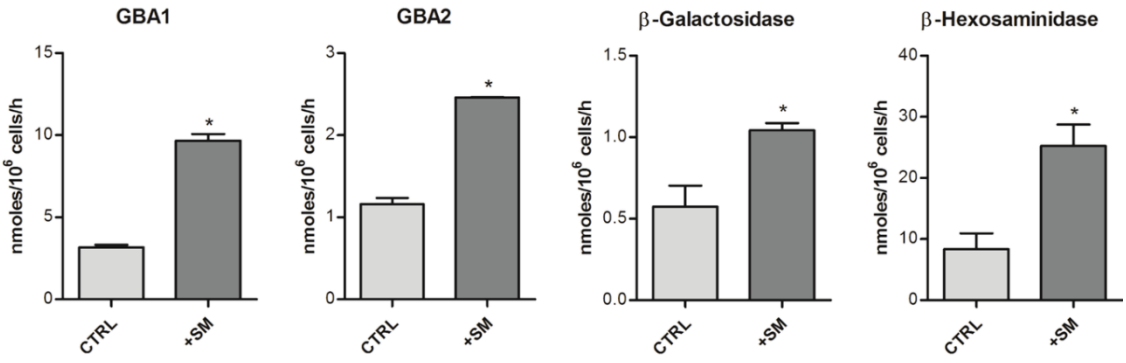

Figure 46 – SM loading induces increased activity of plasma membrane-associated glycohydrolases. Graphs represent the enzymatic activities of plasma membrane-associated β-glucocerebrosidase GBA1, non-lysosomal β-glucosylceramidase GBA2, β-galactosidase and β-hexosaminidase measured in live Niemann-Pick Type A human fibroblasts loaded or not with SM. Average value of triplicate analyses is expressed as nmoles/10^6 cells/h. *$p<0.05$ vs CTRL. CTRL: control cells; +SM: 30-day SM loaded cells.

The increased activity of glycohydrolytic enzymes at the plasma membrane level could result in the ectopic production of pro-apoptotic ceramide at this site, as previously demonstrated in sucrose loaded fibroblasts.

5.3 Acid Sphingomyelinase Knockout mice: the possible pathogenic role of Transcription Factor EB

Acid Sphingomyelinase Knockout (ASMKO) mice (Horinouchi K et al., 1995) represent the animal model of the human Niemann-Pick Type A disease (NPA). ASMKO mouse brains showed a 6-fold SM increase compared to wild type (WT) mouse brains (Scandroglio et al., 2008; Galvan C et al., 2008). Interestingly, ASMKO mouse brains are also characterized by 12 fold increase of the two monosialogangliosides GM2 and GM3 (Scandroglio et al., 2008).

I decided to further study ASMKO mouse brains using ASMKO mice at 3 months old age, age at which neurological symptoms occurred. Since ASKMO mouse brains accumulate SM, I evaluated the subcellular localization of the Transcription Factor EB (TFEB). As shown in Figure 47, a 3.2 fold increase of TFEB expression is detected in the nuclear extracts from ASMKO mouse brains compared to WT ones.

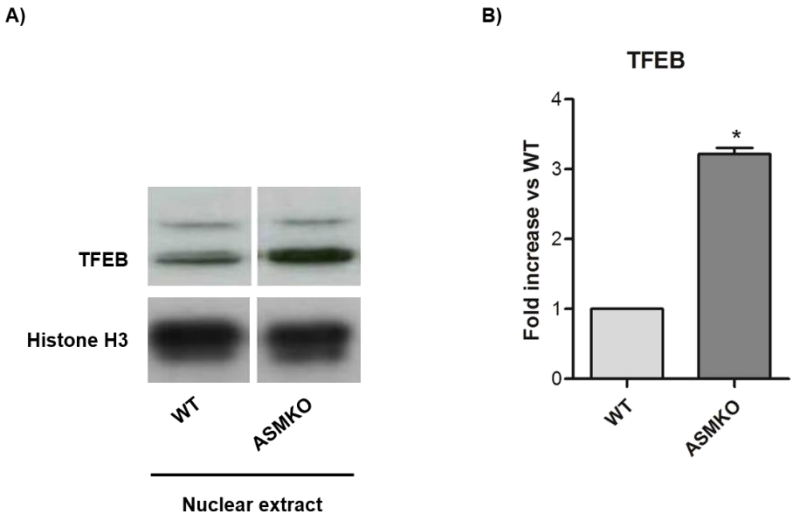

Figure 47 – TFEB nuclear localization in Acid Sphingomyelinase Knockout (ASMKO) mouse brain. A) Representative Western Blot image showing TFEB protein expression in nuclear extracts obtained from brain homogenates; Histone H3 was used as loading control. B) Semi-quantitative graph of normalized TFEB/Histone H3; *p<0.05 vs WT. WT: Wild Type mouse brain; ASMKO: ASMKO mouse brain.

I then evaluated the expression of the lysosomal marker Lamp-1 in ASMKO mouse brains. As shown in Figure 48, ASMKO mouse brains are characterized by a 2.6 fold increase of Lamp-1 protein expression compared to WT ones. This result suggests that in ASMKO mouse brain acid sphingomyelinase deficiency and the consequent SM accumulation determine an increased lysosomal biogenesis which is mediated by TFEB.

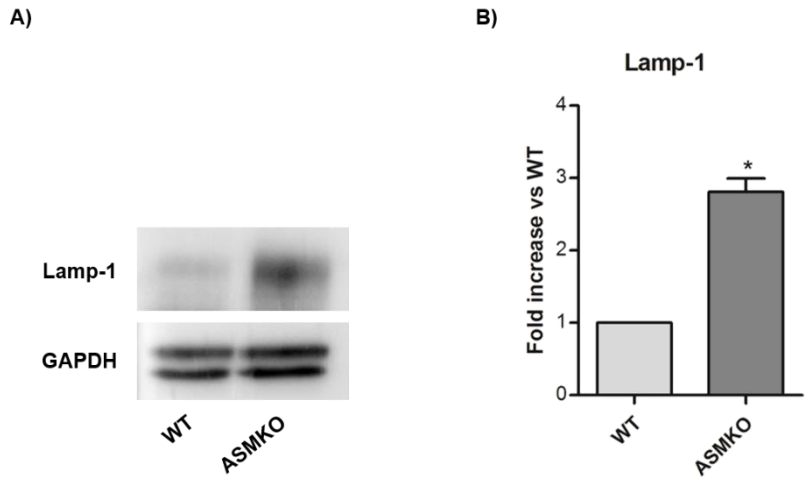

Figure 48 – Increased lysosomal biogenesis in Acid Sphingomyelinase Knockout (ASMKO) mouse brain. A) Representative Western Blot image showing Lamp-1 protein expression in brain homogenates; GAPDH was used as loading control. B) Semi-quantitative graph of normalized Lamp-1/GAPDH; *p<0.05 vs WT. WT: Wild Type mouse brain; ASMKO: ASMKO mouse brain.

I measured the activity of the main glycohydrolases in the homogenates from brains of ASMKO mice.

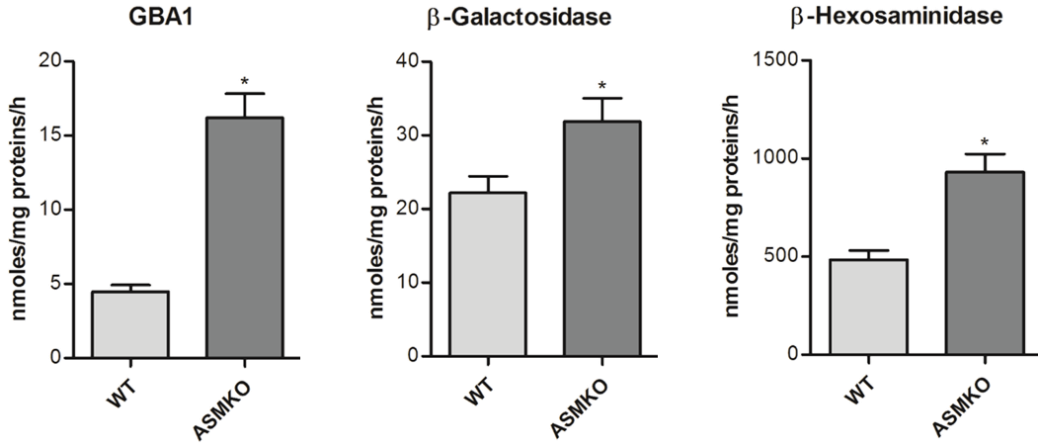

Figure 49 – Increase of glycohydrolase activities in Acid Sphingomyelinase Knockout (ASMKO) mouse brain. Graphs represent the enzymatic activities of β-glucocerebrosidase GBA1, β-galactosidase and β-hexosaminidase in the brain homegenates. Average value of triplicate analyses is expressed as nmoles/mg proteins/h. *p<0.005 vs WT. WT: Wild Type mouse brain; ASMKO: ASMKO mouse brain.

As shown in Figure 49, all the measured activities are increased in ASMKO mouse brain homogenates with respect to WT mouse brain homogenates. In particular, a 3.6 fold increase of GBA1 activity (16.20 ± 1.62 nmoles/mg proteins/h vs 4.48 ± 0.45 nmoles/mg proteins/h, ASMKO vs WT respectively); a 1.4 fold increase of β-galactosidase activity (31.87 ± 3.19 nmoles/mg proteins/h vs 22.23 ± 2.22 nmoles/mg proteins/h); a 1.9 fold increase of β-hexosaminidase (930.52 ± 93.10 nmoles/mg proteins/h vs 483.85 ± 4.84 nmoles/mg proteins/h).

To investigate the onset of tissue damage in ASMKO mouse brain, I analysed the protein expression of Caspase-3, main effector of both intrinsic and extrinsic apoptotic pathways, and LC3-II, well-known autophagic marker. As shown in Figure 50, I found an increase in both cleaved form of Caspase-3 and LC3-II levels in ASMKO mouse brains with respect to WT ones. In particular, a 5.3 and 6.6 fold increase of the cleaved form of Caspase-3 and LC3-II respectively are observed.

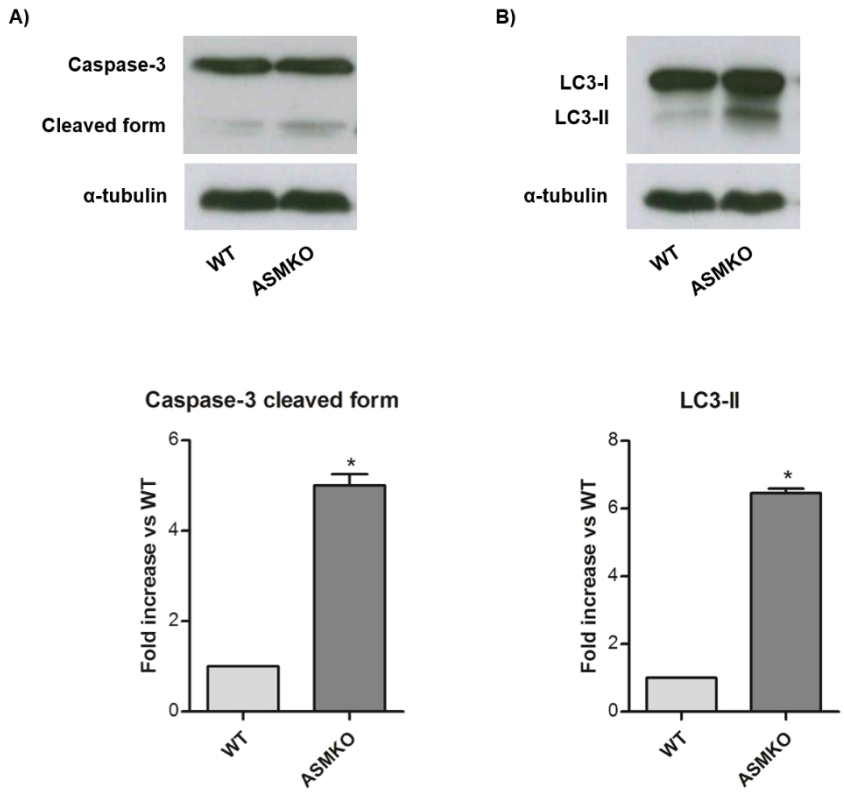

Figure 50 – Activation of both apoptosis and autophagy in Acid Sphingomyelinase Knockout (ASMKO) mouse brain. A) Representative Western Blot image showing the cleaved form of Caspase-3 protein expression; α-tubulin was used as loading control; semi-quantitative graph of normalized Caspase-3 cleaved form/α-tubulin. B) Representative Western Blot image showing LC3-I and LC3-II protein expression; α-tubulin was used as loading control; semi-quantitative graph of normalized LC3-II/α-tubulin. *p<0.05 vs WT. WT: Wild Type mouse brain; ASMKO: ASMKO mouse brain.

6. Discussion

Lysosomal accumulation of undegraded molecules is a common feature of several pathologies, such as Lysosomal Storage Diseases (LSDs) (Platt FM et al., 2012) and neurodegenerative diseases (i.e. Alzheimer's disease and Parkinson's disease) (Zhang L et al., 2009) as well as aging process (Carmona-Gutierrez D et al., 2016). In these pathological conditions, lysosomal storage and dysfunction are related to the onset of cell damage and cell death. Although numerous studies have addressed this relationship, no clear evidence of the molecular mechanisms linking these events has been described.

One of the main limitations in the study of LSDs, is the lack of suitable cellular models. In fact, despite the huge availability of fibroblasts derived from patients affected by diverse LSDs, these cells may not always represent an appropriate disease model. Usually, they show just a modest level of lysosomal storage with no effect on cell damage. Both these features are essential to address the objective of my PhD project aimed to investigate the relationship between lysosomal storage and cell injury.

Previous works have reported that in human healthy fibroblasts, the administration of 88 mM sucrose for 14 days results in a lysosomal storage phenotype. In fact, due to the absence of invertase, fibroblasts are not able to catabolize sucrose that is accumulated in lysosomes without inducing osmotic stress (Kato T et al., 1981; Karageorgos LE et al., 1997).

Interestingly, I found that sucrose loaded cells are characterized by a significant slowdown of cell growth and by the activation of apoptosis, as demonstrated by the presence of the cleaved form of Caspase-3, the main effector of both extrinsic and intrinsic apoptotic pathways. In addition, sucrose loading also induces an aberrant activation of the macroautophagic pathway.

In this scenario, sucrose loaded fibroblasts represent an excellent artificial model to investigate the molecular mechanisms linking lysosomal impairment with the onset of cell damage.

First, I found that the cellular response to sucrose-induced lysosomal accumulation involves an alteration of the endo-lysosomal compartment. Interestingly, by RNA-sequencing analysis I found that 37 genes encoding for lysosomal proteins are upregulated after sucrose loading.

Recently, several lines of evidence point out the crucial role of the Transcription Factor EB (TFEB) in the regulation of lysosomal function (Sardiello M et al. 2009). TFEB is normally localized to the cytosol but under stress conditions, such as lack of nutrients or lysosomal impairment, it moves into the nucleus leading to an augmented expression of lysosomal genes as well as to an increased lysosomal biogenesis.

As expected, sucrose loaded fibroblasts show a massive nuclear translocation of TFEB compared to untreated cells. However, only 8 of the 37 upregulated genes in response to sucrose loading are TFEB-regulated genes (ARSB, CTSA, GBA, GNS, HEXA, MCOLN1, NEU1, TPP1). This finding let me to speculate that transcription factors other than TFEB could also contribute to the control of cellular processes triggered by sucrose storage.

Among the upregulated genes, 6 genes encoding for enzymes involved in sphingolipid catabolism, such as ASAH1, GBA, HEXA, HEXB, NEU1 and SMPD1 have also been found. However, I demonstrated in live sucrose loaded cells that these enzymes are not able to work on their natural substrates within the lysosomes. This impaired lipid catabolism, as demonstrated by lipid analyses, induces a strong increase in the cell content of phospholipids, cholesterol, neutral glycosphingolipids and gangliosides. As known, secondary lipid storage is a common feature of many LSDs (Walkley SU and Vanier MT et al., 2009). For example, an increased content of gangliosides GM2 and GM3 is associated with neuropathology in multiple LSDs such as Niemann-Pick disease and mucopolysaccharidoses. The data obtained clearly indicated that the augmented lipid content is due to the loss of lysosomal catabolic function. Furthermore, I can exclude the possible contribute of the biosynthetic pathways since I did not find any changes in the expression of the enzymes involved in sphingolipid biosynthesis (RNA-sequencing analysis).

One of the proposed mechanisms that LSDs cells could use to reduce the storage of undegraded compounds into lysosomes is represented by lysosomal exocytosis (Samie MA and Xu H, 2014). This process consists in the fusion between lysosomes and the cell plasma membrane resulting in the release of undegraded materials in the extracellular milieu. Recently, TFEB has been demonstrated to play an important role in the regulation of lysosomal exocytosis. For this reason, TFEB has been suggested as a potential therapeutic target for LSDs (Medina DL et al. 2011). Considering this, I found that sucrose loading leads to an increased fusion between lysosomes and the cell plasma membrane. However, the release of toxic and harmful undegraded compounds in the extracellular milieu, which can be considered apparently as a favourable event, could compromise the integrity of the same cells as well as of neighbouring ones. Notably, while proteins can be degraded by proteases present in the extracellular environment, the release of vesicles enriched in uncatabolized lipids can lead to the alteration of the lipid composition of the plasma membranes. In fact, the shedding of complex lipids can alter the lipid pattern and content of the surrounding cell membranes (Chigorno V et al., 2006).

Another important consequence of lysosomal exocytosis is the strong increase of sphingolipid-hydrolases at the cell surface. As known, these enzymes are able to catabolize sphingolipids directly at the plasma membrane (Aureli M et al. 2009; Sonnino S et al., 2010; Aureli et al., 2011). Therefore, in these conditions,sphingolipid catabolism can be activated at the cell surface leading to an augmented production of ceramide. Over the past three decades, ceramide is considered a lipid second messenger involved in the onset of cell death (Obeid LM et al., 1993; Mullen TD and Obeid LM, 2012).

Despite the pioneering studies indicated that ceramide derived from sphingomyelin hydrolysis is pro-apoptotic (Obeid LM et al., 1993), some more recent findings suggest that also ceramide derived from glycosphingolipid catabolism could have a role in the activation of the apoptotic pathway. Valaperta et al. demonstrated that in human fibroblasts, the overexpression of the specific plasma membrane sialidase Neu3 hydrolyses ganglioside GM3 leading to ceramide production and activation of apoptosis (Valaperta R et al., 2006). The ectopic production of pro-apoptotic ceramide due to the activation of glycosphingolipid-hydrolases at the cell surface was also found in a breast cancer cell line treated with ionizing radiations (Aureli M et al., 2012). Despite these lines of evidence, the downstream pathways triggered by ceramide induced-cell death are still unknown. It has been suggested that ceramide accumulation within cell plasma membranes determines its spontaneous association to form small ceramide-enriched membrane microdomains (Zhang Y et al., 2009). These microdomains have the tendency to fuse together forming ceramide-enriched macrodomains also called ceramide-enriched platforms. These structures seem to play a role in protein sorting and signal transduction. For example, ceramide-mediated clustering of CD95 receptors (Schütze S et al., 2008) has been described to promote CD95 internalization thus activating the extrinsic apoptosis pathway. In this view, it can be argued that in sucrose loaded fibroblasts, the increased production of plasma membrane ceramide from glycosphingolipids may trigger a similar pathway.

To confirm the putative role of plasma membrane-associated ceramide in the onset of apoptosis, I administered specific β-glucosidases inhibitors to sucrose loaded cells. These enzymes are responsible for the last hydrolytic step of glycosphingolipid catabolism, yielding ceramide from glucosylceramide. As previously mentioned, lysosomes of these cells are not able to work properly, therefore the catabolism of complex glycosphingolipids can only occur at the cell surface. Interestingly, I found that the treatment with β-glucosidases inhibitors leads to a strong reduction of the cleaved form of Caspase-3 suggesting a possible reversion of the apoptotic phenotype. This result indicates that the ectopic ceramide production at the plasma membrane level could promote the onset of cell damage in sucrose loading fibroblasts. Remarkably, in these

experimental conditions, I also found a reduction of autophagy. Autophagy is an essential process in maintaining normal cell homeostasis. Nevertheless, recent evidence indicate that dysregulation of autophagy could contribute to cell damage (Ryter SW et al., 2013). Besides to promote lysosomal function, TFEB is also known as a master regulator of autophagy (Settembre C et al., 2011). In fact, I found that sucrose-induced TFEB nuclear translocation is associated with a strong activation of autophagy, as demonstrated by the increased level of the autophagic marker LC3-II. Interestingly, when I treated sucrose loaded cells with β-glucosidases inhibitors in conditions blocking ceramide production at the cell surface, I found a slight but significant reduction of LC3-II protein expression. This result also points out a possible contribution of ectopic plasma membrane ceramide in the promotion of a potentially harmful autophagic process, even if the precise role for ceramide as autophagy inducer has not fully unveiled. (Pattingre S et al., 2009).

Taken together, the results obtained indicate that sucrose loading represents a very powerful strategy to better understand the involvement of several cellular pathways in the onset of cell damage consequent to lysosomal accumulation and impairment. On the other hand, it may have some potential limitations since is an artificial model of lysosomal impairment. For this reason, I developed another *in vitro* model able to mimic the phenotypic features of Niemann-Pick Type A disease (NPA), one of the most common and widely studied LSDs.

NPA is a neurodegenerative sphingolipidosis characterized by deficit of the lysosomal enzyme acid sphingomyelinase (ASMase) resulting in sphingomyelin (SM) accumulation (Schuchman EH and Wasserstein MP, 2015). Human fibroblasts derived from NPA patients show a very low residual ASMase activity (<2% vs healthy cells); however, it is sufficient to prevent the accumulation of huge amounts of undegraded SM into the cells. For this reason, NPA fibroblasts cannot be considered a good model to study this pathology; therefore, I administered exogenous SM (50 μM) to these cells for 30 days. This condition allowed to obtain a significant accumulation of SM, like that occurring in NPA damaged tissues (Walkley SU and Vanier MT, 2009). It is noteworthy that in NPA fibroblasts the lysosomal impairment caused by SM accumulation activates the same molecular pathways described in healthy fibroblasts subjected to sucrose loading. These findings further support the hypothesis that cell damage is triggered by lysosomal accumulation and dysfunction.

Collectively, the results obtained with these two *in vitro* models of lysosomal impairment are very promising to better clarify the molecular mechanisms underlying the pathogenesis of multiple diseases such as LSDs. However, cellular models have an intrinsic limit represented by the lack of complexity characteristic of injured tissues. For this reason, with the purpose to translate my findings to a more complex system, I

performed preliminary studies on brain tissue homogenates of Acid Sphingomyelinase Knockout (ASMKO) mice (Horinouchi K et al., 1995). ASMKO mice are the most studied and extensively characterized animal model of NPA. I focused my attention on brains because central nervous system is the most seriously damaged tissue in ASMKO mice, which show a neurodegenerative phenotype starting from two months of age. Notably, ASMKO mouse brains are characterized not only by SM accumulation but also by storage of other lipids such as gangliosides GM2 and GM3 (Ledesma MD et al., 2011). Interestingly, in ASMKO mice brain homogenates I found: *i*) the nuclear translocation of TFEB; *ii*) an increased lysosomal biogenesis; *iii*) augmented glycohydrolytic activities and *iv*) the onset of cell damage. Of course, the analysis performed on total tissue homogenates provides only a general scenario on what really happens into damaged brains. In fact, in brain homogenates I cannot distinguish the different cellular populations such as neuronal, glial and endothelial cells. As known, neurons are the most affected cell type in neurodegenerative LSDs, including sphingolipidoses. In fact, neuronal cells are post-mitotic cells particularly enriched in sphingolipids; for these reasons, neurons are the best candidates for the establishment of my proposed hypothesis of the etiopathogenis of LSDs. Therefore, in brain homogenates I can underestimate the real damage occurring in neuronal cells. Moreover, I can speculate that the increased lysosomal exocytosis promoted by TFEB could lead to the release of toxic undegraded compounds in the extracellular matrix. In a tissue context, the release of uncatabolized molecules can damage other cell types such as glial cells, causing for example the onset of neuroinflammation which can contribute to neuronal cell death (Ransohoff RM, 2016). In conclusion, as schematized in Figure 51, the data obtained suggest that the primary accumulation of an undegraded substrate leads to a more general impairment of lysosomes resulting in the storage of other undigested materials. The lysosomal impairment causes the nuclear translocation of TFEB, which in turn determines an increased lysosomal biogenesis as well as an enhanced synthesis of lysosomal proteins, including catabolic enzymes. Furthermore, new lysosomes also accumulated undegraded compounds; therefore, they are not able to exert their catabolic activity. In addition, the enhanced fusion between lysosomes and the cell plasma membrane leads to: *i*) the release of toxic undegraded molecules in the extracellular environment, including complex lipids that can alter the plasma membrane lipid composition by a shedding mechanism; *ii*) the increase of plasma membrane sphingolipid-hydrolases. The coexistence of these enzymes and their substrates results in the ectopic production of pro-apoptotic ceramide at the cell surface leading to the onset of cell damage.

Thus, the findings of my research represent an initial excellent step to deeply investigate how the ectopic sphingolipid hydrolysis could mediate the onset of cell damage consequent to lysosomal storage.

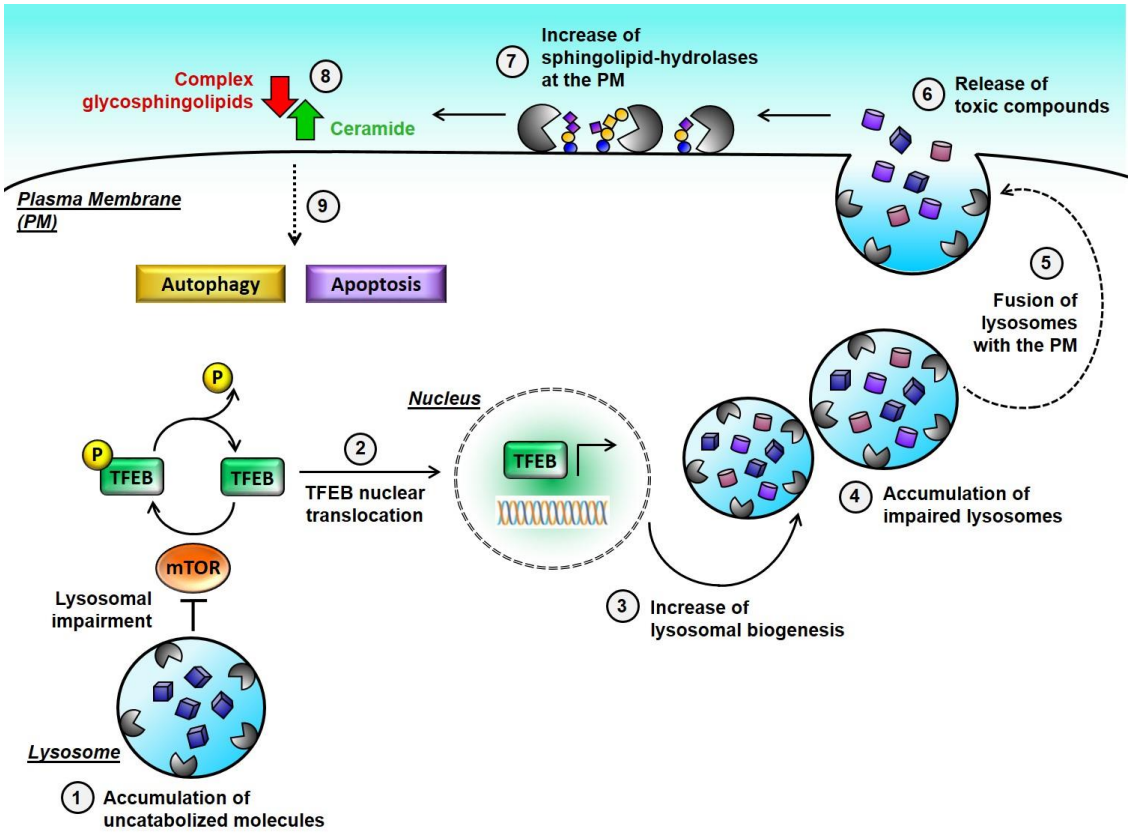

Figure 51 - Schematic representation of the suggested molecular mechanism linking lysosomal impairment and the alteration of plasma membrane sphingolipid composition to the cell damage.

7. Bibliography

Appelmans F, Wattiaux R, De Duve C, *Tissue fractionation studies. 5. The association of acid phosphatase with a special class of cytoplasmic granules in rat liver*, Biochem J., 1955 Mar;59(3):438-45

Appelqvist H, Wäster P, Kågedal K, Öllinger K, *The lysosome: from waste bag to potential therapeutic target*, J Mol Cell Biol. 2013 Aug;5(4):214-26

Aureli M, Bassi R, Prinetti A, Chiricozzi E, Pappalardi B, Chigorno V, Di Muzio N, Loberto N, Sonnino S, *Ionizing radiations increase the activity of the cell surface glycohydrolases and the plasma membrane ceramide content*, Glycoconj J. 2012 Dec;29(8-9):585-97

Aureli M, Loberto N, Chigorno V, Prinetti A, Sonnino S, *Remodeling of sphingolipids by plasma membrane associated enzymes*, Neurochem Res. 2011 Sep;36(9):1636-44

Aureli M, Loberto N, Lanteri P, Chigorno V, Prinetti A, Sonnino S, *Cell surface sphingolipid glycohydrolases in neuronal differentiation and aging in culture*, J Neurochem. 2011b Mar;116(5):891-9

Aureli M, Masilamani AP, Illuzzi G, Loberto N, Scandroglio F, Prinetti A, Chigorno V, Sonnino S, *Activity of plasma membrane beta-galactosidase and beta-glucosidase*, FEBS Lett. 2009 Aug 6;583(15):2469-73

Bongarzone ER, Escolar ML, Gray SJ, Kafri T, Vite CH, Sands MS, Insights into the Pathogenesis and Treatment of Krabbe Disease, Pediatr Endocrinol Rev. 2016 Jun;13 Suppl 1:689-96

Boot RG, Verhoek M, Donker-Koopman W, Strijland A, van Marle J, Overkleeft HS, Wennekes T, Aerts JM, *Identification of the non-lysosomal glucosylceramidase as beta-glucosidase 2*, J Biol Chem. 2007 Jan 12;282(2):1305-12

Bourbon NA, Yun J, Kester M, *Ceramide directly activates protein kinase C ζ to regulate a stress-activated protein kinase signaling complex*, J Biol Chem 2000;275:35617–23

Boya P and Kroemer G, *Lysosomal membrane permeabilization in cell death*, Oncogene. 2008 Oct 27;27(50):6434-51

Braulke T and Bonifacino JS, *Sorting of lysosomal proteins*, Biochim Biophys Acta. 2009 Apr;1793(4):605-14

Bremer EG, Schlessinger J, Hakomori S, *Ganglioside-mediated modulation of cell growth. Specific effects of GM3 on tyrosine phosphorylation of the epidermal growth factor receptor*, J Biol Chem. 1986 Feb 15;261(5):2434-40

Brunetti-Pierri N and Scaglia F, *GM1 gangliosidosis: review of clinical, molecular, and therapeutic aspects*, Mol Genet Metab. 2008 Aug;94(4):391-6

Carmona-Gutierrez D, Hughes AL, Madeo F, Ruckenstuhl C, *The crucial impact of lysosomes in aging and longevity*, Ageing Res Rev. 2016 Dec;32:2-12

Carter HE, Glick FJ, Norris WP, Phillips GE, *Biochemisrty of sphingolipides. III. Structure of sphingosine*, J Biol Chem., 1947;170:285-294

Chigorno V, Giannotta C, Ottico E, Sciannamblo M, Mikulak J, Prinetti A, Sonnino S, *Sphingolipid uptake by cultured cells: complex aggregates of cell sphingolipids with serum proteins and lipoproteins are rapidly catabolized*, J Biol Chem. 2005 Jan 28;280(4):2668-75

Chigorno V, Sciannamblo M, Mikulak J, Prinetti A, Sonnino S, *Efflux of sphingolipids metabolically labeled with [1-3H]sphingosine, L-[3-^{3}H]serine and [9,10-^{3}H]palmitic acid from normal cells in culture*, Glycoconj J. 2006 May;23(3-4):159-65

Coant N, Sakamoto W, Mao C, Hannun YA, *Ceramidases, roles in sphingolipid metabolism and in health and disease*, Adv Biol Regul. 2016 Oct 11. pii: S2212-4926(16)30058-6

Conzelmann E and Sandhoff K, *Partial enzyme deficiencies: residual activities and the development of neurological disorders*, Dev Neurosci. 1983-1984;6(1):58-71

Couet J, Li S, Okamoto T, Ikezu T, Lisanti MP, *Identification of peptide and protein ligands for the caveolin-scaffolding domain. Implications for the interaction of caveolin with caveolae-associated proteins*, J Biol Chem. 1997 Mar 7;272(10):6525-33

Crespo PM, Demichelis VT, Daniotti JL, *Neobiosynthesis of glycosphingolipids by plasma membrane-associated glycosyltransferases*, J Biol Chem. 2010 Sep 17;285(38):29179-90

Crocker AC, *The cerebral defect in Tay-Sachs disease and Niemann-Pick disease*, J Neurochem. 1961 Apr;7:69-80

Daniels LB, Coyle PJ, Chiao YB, Glew RH, Labow RS, *Purification and characterization of a cytosolic broad specificity beta-glucosidase from human liver*, J Biol Chem. 1981 Dec 25;256(24):13004-13

De Duve C, Pressman BC, Gianetto R, Wattiaux R, Appelmans F, *Tissue fractionation studies. 6. Intracellular distribution patterns of enzymes in rat-liver tissue*, Biochem J., 1955 Aug;60(4):604-17

Dobin A, Davis CA, Schlesinger F, Drenkow J, Zaleski C, Jha S, Batut P, Chaisson M, Gingeras TR, *STAR: ultrafast universal RNA-seq aligner*, Bioinformatics. 2013 Jan 1;29(1):15-21

Doherty GJ and McMahon HT, *Mechanisms of endocytosis*, Annu Rev Biochem. 2009;78:857-902

Ehlert K, Frosch M, Fehse N, Zander A, Roth J, Vormoor J, *Farber disease: clinical presentation, pathogenesis and a new approach to treatment*, Pediatr Rheumatol Online J. 2007 Jun 29;5:15

Farooqui T, Franklin T, Pearl DK, Yates AJ, *Ganglioside GM1 enhances induction by nerve growth factor of a putative dimer of TrkA*, J Neurochem. 1997 Jun;68(6):2348-55

Ferlinz K, Hurwitz R, Weiler M, Suzuki K, Sandhoff K, Vanier MT, *Molecular analysis of the acid sphingomyelinase deficiency in a family with an intermediate form of Niemann-Pick disease*, Am J Hum Genet. 1995 Jun;56(6):1343-9

Ferlinz K, Kopal G, Bernardo K, Linke T, Bar J, Breiden B, Neumann U, Lang F, Schuchman EH, Sandhoff K, *Human acid ceramidase: processing, glycosylation, and lysosomal targeting*, J Biol Chem. 2001 Sep 21;276(38):35352-60

Filocamo M and Morrone A, *Lysosomal storage disorders: molecular basis and laboratory testing*, Hum Genomics. 2011 Mar;5(3):156-69

Folch J, Lees M, Sloane Stanley GH, *A simple method for the isolation and purification of total lipides from animal tissues*, J Biol Chem. 1957 May;226(1):497-509

Galvan C, Camoletto PG, Cristofani F, Van Veldhoven PP, Ledesma MD, *Anomalous surface distribution of glycosyl phosphatidyl inositol-anchored proteins in neurons lacking acid sphingomyelinase*, Mol Biol Cell. 2008 Feb;19(2):509-22

Geeraert L, Mannaerts GP, van Veldhoven PP, *Conversion of dihydroceramide into ceramide: involvement of a desaturase*, Biochem J. 1997 Oct 1;327 (Pt 1):125-32

Ghosh P, Dahms NM, Kornfeld S, *Mannose 6-phosphate receptors: new twists in the tale*, Nat Rev Mol Cell Biol. 2003 Mar;4(3):202-12

Gieselmann V, *What can cell biology tell us about heterogeneity in lysosomal storage diseases?*, Acta Paediatr Suppl. 2005 Mar;94(447):80-6; discussion 79

Giri S, Khan M, Rattan R, Singh I, Singh AK, *Krabbe disease: psychosine-mediated activation of phospholipase A2 in oligodendrocyte cell death*, J Lipid Res. 2006 Jul;47(7):1478-92

Goldstein JL, Dana SE, Faust JR, Beaudet AL, Brown MS, *Role of lysosomal acid lipase in the metabolism of plasma low density lipoprotein. Observations in cultured fibroblasts from a patient with cholesteryl ester storage disease*, J Biol Chem. 1975 Nov 10;250(21):8487-95

Guirland C, Suzuki S, Kojima M, Lu B, Zheng JQ, *Lipid rafts mediate chemotropic guidance of nerve growth cones*, Neuron. 2004 Apr 8;42(1):51-62

Hallsson JH, Haflidadóttir BS, Stivers C, Odenwald W, Arnheiter H, Pignoni F, Steingrímsson E, *The basic helix-loop-helix leucine zipper transcription factor Mitf is conserved in Drosophila and functions in eye development*, Genetics. 2004 May;167(1):233-41

Hanada K, *Serine palmitoyltransferase, a key enzyme of sphingolipid metabolism*, Biochim Biophys Acta. 2003 Jun 10;1632(1-3):16-30

Hemesath TJ, Steingrímsson E, McGill G, Hansen MJ, Vaught J, Hodgkinson CA, Arnheiter H, Copeland NG, Jenkins NA, Fisher DE, *microphthalmia, a critical factor in melanocyte development, defines a discrete transcription factor family*, Genes Dev. 1994 Nov 15;8(22):2770-80

Holtzman E, *Lysosomes*, 1989, Plenum Press - New York

Horinouchi K, Erlich S, Perl DP, Ferlinz K, Bisgaier CL, Sandhoff K, Desnick RJ, Stewart CL, Schuchman EH, *Acid sphingomyelinase deficient mice: a model of types A and B Niemann-Pick disease*, Nat Genet. 1995 Jul;10(3):288-93

Huitema K, van den Dikkenberg J, Brouwers JF, Holthuis JC, *Identification of a family of animal sphingomyelin synthases*, EMBO J. 2004 Jan 14;23(1):33-44

Ichikawa S and Hirabayashi Y, *Glucosylceramide synthase and glycosphingolipid synthesis*, Trends Cell Biol. 1998 May;8(5):198-202

Ikeda M, Kihara A, Igarashi Y, *Lipid asymmetry of the eukaryotic plasma membrane: functions and related enzymes*, Biol Pharm Bull. 2006 Aug;29(8):1542-6

Jakóbkiewicz-Banecka J, Gabig-Cimińska M, Banecka-Majkutewicz Z, Banecki B, Węgrzyn A, Węgrzyn G, *Factors and processes modulating phenotypes in neuronopathic lysosomal storage diseases*, Metab Brain Dis. 2014 Mar;29(1):1-8

Kakugawa Y, Wada T, Yamaguchi K, Yamanami H, Ouchi K, Sato I, Miyagi T, *Up-regulation of plasma membrane-associated ganglioside sialidase (Neu3) in human colon cancer and its involvement in apoptosis suppression*, Proc Natl Acad Sci U S A. 2002 Aug 6;99(16):10718-23

Karageorgos LE, Isaac EL, Brooks DA, Ravenscroft EM, Davey R, Hopwood JJ, Meikle PJ, *Lysosomal biogenesis in lysosomal storage disorders*, Exp Cell Res. 1997 Jul 10;234(1):85-97

Kato T, Okada S, Oshima T, Inui K, Yutaka T, Yabuuchi H, *Lysosomal hydrolase induction in cultures human skin fibroblasts: the effects of sucrose*, Biochem Int. 1981; 3,551-556

Kaur J and Debnath J, *Autophagy at the crossroads of catabolism and anabolism*, Nat Rev Mol Cell Biol. 2015 Aug;16(8):461-72

Kishimoto Y, Hiraiwa M, O'Brien JS, *Saposins: structure, function, distribution, and molecular genetics*, J Lipid Res. 1992 Sep;33(9):1255-67

Kitatani K, Idkowiak-Baldys J, Hannun YA, *The sphingolipid salvage pathway in ceramide metabolism and signalling*, Cell Signal. 2008 Jun;20(6):1010-8

Kolter T and Sandhoff K, *Glycosphingolipid degradation and animal models of GM2-gangliosidoses*, J Inherit Metab Dis. 1998 Aug;21(5):548-63

Kuiper RP, Schepens M, Thijssen J, Schoenmakers EF, van Kessel AG, *Regulation of the MiTF/TFE bHLH-LZ transcription factors through restricted spatial expression and alternative splicing of functional domains*, Nucleic Acids Res. 2004 Apr 26;32(8):2315-22

Lannert H, Gorgas K, Meissner I, Wieland FT, Jeckel D, *Functional organization of the Golgi apparatus in glycosphingolipid biosynthesis. Lactosylceramide and subsequent glycosphingolipids are formed in the lumen of the late Golgi*, J Biol Chem. 1998 Jan 30;273(5):2939-46

Lapierre LR, De Magalhaes Filho CD, McQuary PR, Chu CC, Visvikis O, Chang JT, Gelino S, Ong B, Davis AE, Irazoqui JE, Dillin A, Hansen M, *The TFEB orthologue HLH-30 regulates autophagy and modulates longevity in Caenorhabditis elegans*, Nat Commun. 2013;4:2267

Ledeen RW and Wu G, *The multi-tasked life of GM1 ganglioside, a true factotum of nature*, Trends Biochem Sci. 2015 Jul;40(7):407-18

Ledeen RW, *Biology of gangliosides: neuritogenic and neuronotrophic properties*, J Neurosci Res. 1984;12(2-3):147-59

Ledesma MD, Prinetti A, Sonnino S, Schuchman EH, *Brain pathology in Niemann Pick disease type A: insights from the acid sphingomyelinase knockout mice*, J Neurochem. 2011 Mar;116(5):779-88

Leinekugel P, Michel S, Conzelmann E, Sandhoff K, *Quantitative correlation between the residual activity of beta-hexosaminidase A and arylsulfatase A and the severity of the resulting lysosomal storage disease*, Hum Genet. 1992 Mar;88(5):513-23

Levade T, Tempesta MC, Moser HW, Fensom AH, Harzer K, Moser AB, Salvayre R, *Sulfatide and sphingomyelin loading of living cells as tools for the study of ceramide turnover by lysosomal ceramidase--implications for the diagnosis of Farber disease*, Biochem Mol Med. 1995 Apr;54(2):117-25

Levental I, Lingwood D, Grzybek M, Coskun U, Simons K, *Palmitoylation regulates raft affinity for the majority of integral raft proteins*, Proc Natl Acad Sci U S A. 2010 Dec 21;107(51):22050-4

Levy M and Futerman AH, *Mammalian ceramide synthases*, IUBMB Life. 2010 May;62(5):347-56

Love MI, Huber W, Anders S, *Moderated estimation of fold change and dispersion for RNA-seq data with DESeq2*, Genome Biol. 2014;15(12):550

Luzio JP, Pryor PR, Bright NA, *Lysosomes: fusion and function*, Nat Rev Mol Cell Biol. 2007 Aug;8(8):622-32

Maceyka M, Harikumar KB, Milstien S, Spiegel S, *Sphingosine-1-phosphate signaling and its role in disease*, Trends Cell Biol. 2012 Jan;22(1):50-60

Marchesini N and Hannun YA, *Acid and neutral sphingomyelinases: roles and mechanisms of regulation*, Biochem Cell Biol. 2004 Feb;82(1):27-44

Martina JA, Chen Y, Gucek M, Puertollano R, *MTORC1 functions as a transcriptional regulator of autophagy by preventing nuclear transport of TFEB*, Autophagy. 2012 Jun;8(6):903-14

Medina DL, Di Paola S, Peluso I, Armani A, De Stefani D, Venditti R, Montefusco S, Scotto-Rosato A, Prezioso C, Forrester A, Settembre C, Wang W, Gao Q, Xu H, Sandri M, Rizzuto R, De Matteis MA, Ballabio A, *Lysosomal calcium signalling regulates autophagy through calcineurin and TFEB*, Nat Cell Biol. 2015 Mar;17(3):288-99

Medina DL, Fraldi A, Bouche V, Annunziata F, Mansueto G, Spampanato C, Puri C, Pignata A, Martina JA, Sardiello M, Palmieri M, Polishchuk R, Puertollano R, Ballabio A, *Transcriptional activation of lysosomal exocytosis promotes cellular clearance*, Dev Cell. 2011 Sep 13;21(3):421-30

Mego JL, *The ATP-dependent proton pump in lysosome membranes: still a valid hypothesis*, FEBS Lett. 1979 Nov 1;107(1):113-6

Mencarelli S, Cavalieri C, Magini A, Tancini B, Basso L, Lemansky P, Hasilik A, Li YT, Chigorno V, Orlacchio A, Emiliani C, Sonnino S, *Identification of plasma membrane associated mature beta-hexosaminidase A, active towards GM2 ganglioside, in human fibroblasts*, FEBS Lett. 2005 Oct 24;579(25):5501-6

Merrill AH Jr, *Sphingolipid and glycosphingolipid metabolic pathways in the era of sphingolipidomics*, Chem Rev. 2011 Oct 12;111(10):6387-422. doi: 10.1021/cr2002917. Epub 2011 Sep 26

Michel C, van Echten-Deckert G, Rother J, Sandhoff K, Wang E, Merrill AH Jr, *Characterization of ceramide synthesis. A dihydroceramide desaturase introduces the 4,5-trans-double bond of sphingosine at the level of dihydroceramide*, J Biol Chem. 1997 Sep 5;272(36):22432-7

Milhas D, Clarke CJ, Hannun YA, *Sphingomyelin metabolism at the plasma membrane: implications for bioactive sphingolipids*, FEBS Lett. 2010 May 3;584(9):1887-94

Monti E, Bonten E, D'Azzo A, Bresciani R, Venerando B, Borsani G, Schauer R, Tettamanti G, *Sialidases in vertebrates: a family of enzymes tailored for several cell functions*, Adv Carbohydr Chem Biochem. 2010;64:403-79

Morales A, Lee H, Goñi FM, Kolesnick R, Fernandez-Checa JC, *Sphingolipids and cell death*, Apoptosis. 2007 May;12(5):923-39

Mullen TD and Obeid LM, *Ceramide and apoptosis: exploring the enigmatic connections between sphingolipid metabolism and programmed cell death*, Anticancer Agents Med Chem. 2012 May;12(4):340-63

Mullen TD, Hannun YA, Obeid LM, *Ceramide synthases at the centre of sphingolipid metabolism and biology*, Biochem J. 2012 Feb 1;441(3):789-802

Mutoh T, Hamano T, Tokuda A, Kuriyama M, *Unglycosylated Trk protein does not co-localize nor associate with ganglioside GM1 in stable clone of PC12 cells overexpressing Trk (PCtrk cells)*, Glycoconj J. 2000 Mar-Apr;17(3 -4):233-7

Nagral A, *Gaucher disease*, J Clin Exp Hepatol. 2014 Mar;4(1):37-50

Neufeld EF, *Lysosomal storage diseases*, Annu Rev Biochem. 1991;60:257-80

Nishi T and Forgac M, *The vacuolar (H+)-ATPases--nature's most versatile proton pumps*, Nat Rev Mol Cell Biol. 2002 Feb;3(2):94-103

Obeid LM, Linardic CM, Karolak LA, Hannun YA, *Programmed cell death induced by ceramide*, Science. 1993 Mar 19;259(5102):1769-71

Overkleeft HS, Renkema GH, Neele J, Vianello P, Hung IO, Strijland A, van der Burg AM, Koomen GJ, Pandit UK, Aerts JM, *Generation of specific deoxynojirimycin-type inhibitors of the non-lysosomal glucosylceramidase*, J Biol Chem. 1998 Oct 9;273(41):26522-7

Parenti G, Andria G, Ballabio A, *Lysosomal storage diseases: from pathophysiology to therapy*, Annu Rev Med. 2015;66:471-86

Pattingre S, Bauvy C, Levade T, Levine B, Codogno P, *Ceramide-induced autophagy: to junk or to protect cells?*, Autophagy. 2009 May;5(4):558-60

Perera RM and Zoncu R, *The Lysosome as a Regulatory Hub*, Annu Rev Cell Dev Biol. 2016 Oct 6;32:223-253

Perry RJ and Ridgway ND, *Molecular mechanisms and regulation of ceramide transport*, Biochim Biophys Acta. 2005 Jun 1;1734(3):220-34

Pike LJ, *Growth factor receptors, lipid rafts and caveolae: an evolving story*, Biochim Biophys Acta. 2005 Dec 30;1746(3):260-73

Platt FM, Boland B, van der Spoel AC, *The cell biology of disease: lysosomal storage disorders: the cellular impact of lysosomal dysfunction*, J Cell Biol. 2012 Nov 26;199(5):723-34

Powis K and De Virgilio C, *Conserved regulators of Rag GTPases orchestrate amino acid-dependent TORC1 signaling*, Cell Discov. 2016 Mar 8;2:15049

Rabin SJ, Bachis A, Mocchetti I, *Gangliosides activate Trk receptors by inducing the release of neurotrophins*, J Biol Chem. 2002 Dec 20;277(51):49466-72

Ramstedt B and Slotte JP, *Membrane properties of sphingomyelins*, FEBS Lett. 2002 Oct 30;531(1):33-7

Ransohoff RM, *How neuroinflammation contributes to neurodegeneration*, Science. 2016 Aug 19;353(6301):777-83

Rao SK, Huynh C, Proux-Gillardeaux V, Galli T, Andrews NW, *Identification of SNAREs involved in synaptotagmin VII-regulated lysosomal exocytosis*, J Biol Chem. 2004 May 7;279(19):20471-9

Reczek D, Schwake M, Schröder J, Hughes H, Blanz J, Jin X, Brondyk W, Van Patten S, Edmunds T, Saftig P, *LIMP-2 is a receptor for lysosomal mannose-6-phosphate-independent targeting of beta-glucocerebrosidase*, Cell. 2007 Nov 16;131(4):770-83

Reddy A, Caler EV, Andrews NW, *Plasma membrane repair is mediated by Ca(2+)-regulated exocytosis of lysosomes*, Cell. 2001 Jul 27;106(2):157-69

Roczniak-Ferguson A, Petit CS, Froehlich F, Qian S, Ky J, Angarola B, Walther TC, Ferguson SM, *The transcription factor TFEB links mTORC1 signaling to transcriptional control of lysosome homeostasis*, Sci Signal. 2012 Jun 12;5(228):ra42

Ryter SW, Cloonan SM, Choi AM, *Autophagy: a critical regulator of cellular metabolism and homeostasis*, Mol Cells. 2013 Jul;36(1):7-16

Saftig P and Klumperman J; *Lysosome biogenesis and lysosomal membrane proteins: trafficking meets function*, Nat Rev Mol Cell Biol., 2009 Sep;10(9):623-35

Samie MA and Xu H, *Lysosomal exocytosis and lipid storage disorders*, J Lipid Res. 2014 Jun;55(6):995-1009

Sandhoff K and Harzer K, *Gangliosides and gangliosidoses: principles of molecular and metabolic pathogenesis*, J Neurosci. 2013 Jun 19;33(25):10195-208

Sandhoff K, *Sphingolipidoses*, J Clin Pathol Suppl (R Coll Pathol). 1974;8:94-105

Sangiorgio V, Pitto M, Palestini P, Masserini M, *GPI-anchored proteins and lipid rafts*, Ital J Biochem. 2004 Jul;53(2):98-111

Sardiello M, Palmieri M, di Ronza A, Medina DL, Valenza M, Gennarino VA, Di Malta C, Donaudy F, Embrione V, Polishchuk RS, Banfi S, Parenti G, Cattaneo E, Ballabio A, *A gene network regulating lysosomal biogenesis and function*, Science. 2009 Jul 24;325(5939):473-7

Scandroglio F, Venkata JK, Loberto N, Prioni S, Schuchman EH, Chigorno V, Prinetti A, Sonnino S, *Lipid content of brain, brain membrane lipid domains, and neurons from acid sphingomyelinase deficient mice*, J Neurochem. 2008 Oct;107(2):329-38

Schiffmann R, *Fabry disease*, Handb Clin Neurol. 2015;132:231-48

Schuchman EH and Wasserstein MP, *Types A and B Niemann-Pick Disease*, Pediatr Endocrinol Rev. 2016 Jun;13 Suppl 1:674-81

Schuchman EH and Wasserstein MP, *Types A and B Niemann-Pick disease*, Best Pract Res Clin Endocrinol Metab. 2015 Mar;29(2):237-47

Schulze H, Kolter T, Sandhoff K, *Principles of lysosomal membrane degradation: Cellular topology and biochemistry of lysosomal lipid degradation*, Biochim Biophys Acta. 2009 Apr;1793(4):674-83

Schütze S, Tchikov V, Schneider-Brachert W, *Regulation of TNFR1 and CD95 signalling by receptor compartmentalization*, Nat Rev Mol Cell Biol. 2008 Aug;9(8):655-62

Schwake M, Schröder B, Saftig P, *Lysosomal membrane proteins and their central role in physiology*, Traffic. 2013 Jul;14(7):739-48

Settembre C and Medina DL, *TFEB and the CLEAR network*, Methods in Cell Biology, 2015;Vol. 126,Chapter 3

Settembre C, Di Malta C, Polito VA, Garcia Arencibia M, Vetrini F, Erdin S, Erdin SU, Huynh T, Medina D, Colella P, Sardiello M, Rubinsztein DC, Ballabio A, *TFEB links autophagy to lysosomal biogenesis*, Science. 2011 Jun 17;332(6036):1429-33

Settembre C, Fraldi A, Medina DL, Ballabio A, *Signals from the lysosome: a control centre for cellular clearance and energy metabolism*, Nat Rev Mol Cell Biol. 2013 May;14(5):283-96

Simons K and Ikonen E, *Functional rafts in cell membranes*, Nature. 1997 Jun 5;387(6633):569-72

Simons K and Sampaio JL, *Membrane organization and lipid rafts*, Cold Spring Harb Perspect Biol. 2011 Oct 1;3(10):a004697

Simons K and Toomre D, *Lipid rafts and signal transduction*, Nat Rev Mol Cell Biol. 2000 Oct;1(1):31-9

Sonnino S, Aureli M, Loberto N, Chigorno V, Prinetti A, *Fine tuning of cell functions through remodeling of glycosphingolipids by plasma membrane-associated glycohydrolases*, FEBS Lett. 2010 May 3;584(9):1914-22

Sonnino S, Mauri L, Chigorno V, Prinetti A, *Gangliosides as components of lipid membrane domains*, Glycobiology. 2007 Jan;17(1):1R-13R

Spassieva S and Bieberich E, *Lysosphingolipids and sphingolipidoses: Psychosine in Krabbe's disease*, J Neurosci Res. 2016 Nov;94(11):974-81

Spector AA and Yorek MA, *Membrane lipid composition and cellular function*, J Lipid Res. 1985 Sep;26(9):1015-35

Stoffel W, *Studies on the biosynthesis and degradation of sphingosine bases*, Chem Phys Lipids. 1970 Oct;5(1):139-58

Subramanian K and Balch WE, *NPC1/NPC2 function as a tag team duo to mobilize cholesterol*, Proc Natl Acad Sci U S A. 2008 Oct 7;105(40):15223-4

Suzuki S, Numakawa T, Shimazu K, Koshimizu H, Hara T, Hatanaka H, Mei L, Lu B, Kojima M, BDNF-induced recruitment of TrkB receptor into neuronal lipid rafts: roles in synaptic modulation, J Cell Biol. 2004 Dec 20;167(6):1205-15

Tagami S, Inokuchi Ji J, Kabayama K, Yoshimura H, Kitamura F, Uemura S, Ogawa C, Ishii A, Saito M, Ohtsuka Y, Sakaue S, Igarashi Y, *Ganglioside GM3 participates in the pathological conditions of insulin resistance*, J Biol Chem. 2002 Feb 1;277(5):3085-92

Tan MA, Fuller M, Zabidi-Hussin ZA, Hopwood JJ, Meikle PJ, *Biochemical profiling to predict disease severity in metachromatic leukodystrophy*, Mol Genet Metab. 2010 Feb;99(2):142-8

Tani M, Ito M, Igarashi Y, *Ceramide/sphingosine/sphingosine 1-phosphate metabolism on the cell surface and in the extracellular space*, Cell Signal. 2007 Feb;19(2):229-37

Tanida I, Ueno T, Kominami E, *LC3 and Autophagy*, Methods Mol Biol. 2008;445:77-88

Tsujimoto Y and Shimizu S, *Another way to die: autophagic programmed cell death*, Cell Death Differ. 2005 Nov;12 Suppl 2:1528-34

Valaperta R, Chigorno V, Basso L, Prinetti A, Bresciani R, Preti A, Miyagi T, Sonnino S, *Plasma membrane production of ceramide from ganglioside GM3 in human fibroblasts*, FASEB J. 2006 Jun;20(8):1227-9

Valaperta R, Valsecchi M, Rocchetta F, Aureli M, Prioni S, Prinetti A, Chigorno V, Sonnino S, *Induction of axonal differentiation by silencing plasma membrane-associated sialidase Neu3 in neuroblastoma cells*, J Neurochem. 2007 Feb;100(3):708-19

van Meer G and Lisman Q, *Sphingolipid transport: rafts and translocators*, J Biol Chem. 2002 Jul 19;277(29):25855-8

van Meer G, Voelker DR, Feigenson GW, Membrane lipids: where they are and how they behave, Nat Rev Mol Cell Biol. 2008 Feb;9(2):112-24

van Rappard DF, Boelens JJ, Wolf NI, *Metachromatic leukodystrophy: Disease spectrum and approaches for treatment*, Best Pract Res Clin Endocrinol Metab. 2015 Mar;29(2):261-73

Vanier MT, *Niemann-Pick disease type C*, Orphanet J Rare Dis. 2010 Jun 3;5:16

Verheij M, Bose R, Lin XH, Yao B, Jarvis WD, Grant S, Birrer MJ, Szabo E, Zon LI, Kyriakis JM, Haimovitz-Friedman A, Fuks Z, Kolesnick RN, *Requirement for ceramide-initiated SAPK/JNK signalling in stress-induced apoptosis*, Nature. 1996 Mar 7;380(6569):75-9

Vitner EB, Platt FM, Futerman AH, *Common and uncommon pathogenic cascades in lysosomal storage diseases*, J Biol Chem. 2010 Jul 2;285(27):20423-7

Walkley SU and Vanier MT, *Secondary lipid accumulation in lysosomal disease*, Biochim Biophys Acta. 2009 Apr;1793(4):726-36

Walkley SU, *Secondary accumulation of gangliosides in lysosomal storage disorders*, Semin Cell Dev Biol. 2004 Aug;15(4):433-44

Wang RY, Bodamer OA, Watson MS, Wilcox WR; ACMG Work Group on Diagnostic Confirmation of Lysosomal Storage Diseases, *Lysosomal storage diseases: diagnostic confirmation and management of presymptomatic individuals*, Genet Med. 2011 May;13(5):457-84

Wang XQ, Sun P, Paller AS, *Ganglioside induces caveolin-1 redistribution and interaction with the epidermal growth factor receptor*, J Biol Chem. 2002 Dec 6;277(49):47028-34

Weiss B and Stoffel W, *Human and murine serine-palmitoyl-CoA transferase--cloning, expression and characterization of the key enzyme in sphingolipid synthesis*, Eur J Biochem. 1997 Oct 1;249(1):239-47

Westwick JK, Bielawska AE, Dbaibo G, Hannun YA, Brenner DA, *Ceramide activates the stress-activated protein kinases*, J Biol Chem. 1995 Sep 29;270(39):22689-92

Wolff RA, Dobrowsky RT, Bielawska A, Obeid LM, Hannun YA, *Role of ceramide-activated protein phosphatase in ceramide-mediated signal transduction*, J Biol Chem. 1994 Jul 29;269(30):19605-9

Xiong J and Zhu MX, *Regulation of lysosomal ion homeostasis by channels and transporters*, Sci China Life Sci. 2016 Aug;59(8):777-91

Yu RK, Tsai YT, Ariga T, Yanagisawa M, *Structures, biosynthesis, and functions of gangliosides--an overview*, J Oleo Sci. 2011;60(10):537-44

Zhang L, Sheng R, Qin Z, *The lysosome and neurodegenerative diseases*, Acta Biochim Biophys Sin (Shanghai). 2009 Jun;41(6):437-45

Zhang Y, Li X, Becker KA, Gulbins E, *Ceramide-enriched membrane domains--structure and function*, Biochim Biophys Acta. 2009 Jan;1788(1):178-83